공학박사학위논문

분산발전을 위한 용융탄산염 연료전지와 예혼합압축착화 엔진 하이브리드 시스템 설계

Design of Molten Carbonate Fuel Cell (MCFC) and Homogeneous Charge Compression Ignition (HCCI) Engine Hybrid System for Distributed Power Generation

2017 년 2 월

서울대학교 대학원

기계항공공학부

김 선 엽

Abstract

Design of Molten Carbonate Fuel Cell (MCFC) and Homogeneous Charge Compression Ignition (HCCI) Engine Hybrid System for Distributed Power Generation

Seonyeob Kim
School of Mechanical and Aerospace Engineering
The Graduate School
Seoul National University

Recently, various energy issues, e.g. depletion of natural resources and growing environmental concerns, have been encountered year by year. For the reason, the demand for renewable power source increases, and fuel cell technology draws interest as a good applicant in the field due to high efficiency and low pollutant. In the previous work, a new MCFC hybrid system integrated with HCCI engine was developed. In the hybrid system, the HCCI engine replaces the catalytic combustor in the original fuel cell system and yields additional power by using the left-over fuel in the anode off-gas. In this thesis,

the engine design is performed for the 250 kW-class MCFC system. For the thermodynamic analysis, thermodynamic modeling is performed and the parametric study is conducted with design options variation. With the determined engine specification, the hybrid system is analyzed at the design point and part-load operation. The hybrid system efficiency can achieve 57.1 %, which is 9.8 % higher than the standalone system efficiency at the design point operation. And the systematic control strategies are developed at the part-load conditions, and thus the hybrid system can operate at the various fueling levels. An economic assessment is also conducted for comparison between the standalone system and the hybrid system. The analysis is performed by calculating the levelized cost of electricity (LCOE) with total revenue requirement (TRR) method. The LCOE of the hybrid system is ~5.4 % lower than that of the standalone system, thus the economic feasibility of the hybrid system was verified. Based on the simulation results, the engine experiment is conducted to demonstrate the possibility of the HCCI engine operation in the system. As a result, the engine net indicated efficiency is measured to be ~17 %. Considering the small displacement volume of the tested engine with its relatively un-favorable heat transfer characteristic, the engine performances in the hybrid system are shown to be quite promising. It is anticipated that the results of this thesis would be considered the study leading up to the

commercialization of the new MCFC-HCCI engine hybrid system for distributed power generation in near-future.

Keywords: MCFC, HCCI engine, Hybrid system design, Efficiency, Economic analysis, Engine experiment

***Identification Number*: 2013-30945**

Contents

List of Figures

List of Tables

Nomenclature

A_{seg}	area of each segment (cm^2)	R	specific heat ratio
CI	compression ignition	T	temperature (K)
ΔF	change in molar flow rate (mol h^{-1})	V_{opn}	operating cell voltage (V)
ΔG	gibbs free energy change (J mol^{-1})	W	work output (J)
ΔH	apparent activation energy for resistance parameters (J mol^{-1})	X	conversion degree
E_{rev}	maximum reversible potential (V)	***Greek Letter***	
f	faraday's constant (96487 C mol^{-1})	η	loss
F	molar flow rate (mol h^{-1})		
H	frequency factor for resistance	***Subscripts***	
F	parameters (J mol^{-1})	and	anode
i	current (A)	and, i	species at anode
j	current density (A cm^{-2})	cat	cathode
K_p	equilibrium constant	cat, i	species at cathode
M	molar fraction	CO	carbon monoxide
NO_x	oxides of nitrogen	CO_2	carbon dioxide
$ODEs$	ordinary differential equations	H_2	hydrogen molecule
P	partial pressure (bar)	H_2O	water
Q	energy required (J)	i	species
R	universal gas constant (J mol^{-1} K^{-1})	Nern	Nernst
R_{and}	irreversible loss at anode (Ω cm^{-2})	X	Gas
R_{cat}	irreversible loss at cathode (Ω cm^{-2})	c	compressor
R_{int}	internal cell resistance (Ω cm^{-2})	t	turbine
R_{total}	total irreversible loss (Ω cm^{-2})	comb	combustion

Chapter 1. Introduction

1.1 Research background

Recently, various energy related problems have been encountered year after year like rapid depletion of natural resources and growing environmental concerns such as global warming. And the demand for reliability of power supply increases as energy usage rises. By 2015 IEA report, the demand for energy grows about 20% higher than 2013 levels in 2030 [1]. In Figure 1.2, IRENA report says energy use causes over two-thirds of total annual greenhouse gas emissions, and especially, power generation sector accounts for most these emissions [2]. If the energy sources are not changed and energy usage increase, environmental problems would be worse. Thus, in the Paris conference, the representatives of 195 countries discussed the environmental concerns, and then they drew the Paris Agreement. The Kyoto Protocol, which was implemented in 2008 to reduce greenhouse gas emissions, applies only developed countries. However, the Paris Agreement will be applied to all countries attending the conference. The goal of the treaty is holding the global temperature increase below 2 ^{o}C [3].

As energy usage increases rapidly, there are many issues with unbalanced energy supplies, like power outages. Power supplies fall short of urban demand. So market movements are changed to a small-scale system like uninterrupted power supply (UPS) from a large-scale system. Fuel cell technology satisfies these demands, which are eco-friendlier and more stable power supply. The fuel

cell system has been drawing attention for its higher efficiency and lower pollutant emissions over conventional power generation technologies [4, 5].

Among various types of fuel cell systems, there are two major categories, which are high temperature fuel cell (HTFC) and low temperature fuel cell (LTFC). HTFC generally show higher efficiency than LTFC [6]. Molten carbonate fuel cell (MCFC) and solid oxide fuel cell (SOFC) belong to the HTFC due to their high operating temperature (~600-1000 ^{o}C) [7]. The latter is still under active research and development stage, but the former is already commercialized for various power ranges [6]. In this thesis, new hybrid system of the molten carbonate fuel cell for distributed power generation is suggested.

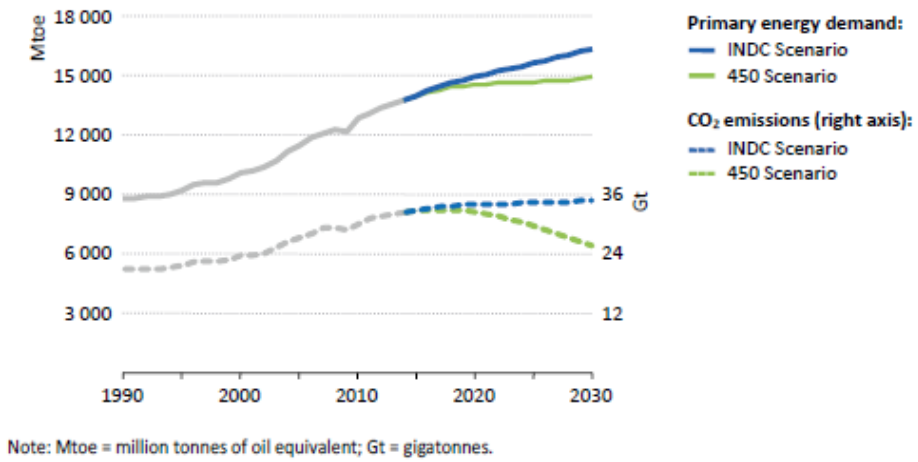

Note: Mtoe = million tonnes of oil equivalent; Gt = gigatonnes.

Figure 1.1 Global primary energy demand and related CO_2 emissions [1]

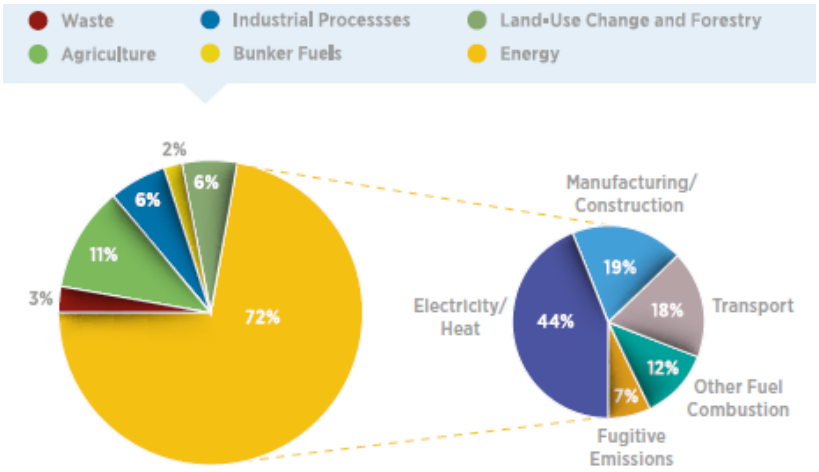

Figure 1.2 Global GHG emissions by sectors [2]

1.2 Literature survey

In order to improve system performance, several studies have attempted to hybridize MCFC with other power generating sources. Specially, a number of researchers have studied MCFC system integrated with gas turbine for the increase in overall plant efficiency [8-18]. Wee investigated the MCFC and GT hybrid systems as distributed energy resources. He explained the worth of the MCFC-GT hybrid system as distributed generation. And he discussed the two kinds of MCFC-GT hybrid system. He suggested that the indirect system is suitable to the small-scale [8]. Oh et al. proposed various types of the ambient pressure MCFC-GT hybrid system. They analyzed the performances of the systems. As a result, they showed the directly fired system is more efficient than indirectly fired system [9]. El-Emam et al. performed the thermodynamic analysis of the MCFC-GT hybrid system. They analyzed the hybrid system in aspects of energy and exergy. The system is about 314 kW capacity, and achieves 42.89 % of energy efficiency and 37.75 % of exergy efficiency [10]. Lunghi et al. analyzed a hybrid MCFC–GT power plant. They used the MCFC with internal reforming and operating at ambient pressure, and the gas turbine (GT) is a PGT-2 produced by GE-Nuovo Pignone. The fuel cell efficiency is 47.3% and the hybrid system efficiency is 57.0%, thus the system efficiency is increased by 9.7% [11]. Kimijima et al. studied a mircro GT and MCFC hybrid system for distributed power generation. They analyzed the system at design parameters variation. The hybrid system efficiency is 62% at a pressure ratio of 3.0–3.5 [12]. Liu et al. show a performance analysis of a pressurized MCFC–

μGT hybrid system. They analyzed the hybrid system at design and part-load operation. The MCFC efficiency is ~50% and the hybrid system efficiency is increased by ~8% due to additional power generation of GT [13]. Leto et al. conducted a sensitivity analysis for an MCFC–microturbine hybrid system. They analyzed the system under the working pressure and S/C ratio variation, and at partial load operation. The system efficiency is about 60% at nominal load [14]. Milewski et al. studied a control strategy for an MCFC–GT hybrid system. The hybrid system efficiency is ~58%, and they show that the hybrid system has control flexibility keeping the performance [15]. Zhang et al. suggested a new model of a syngas MCFC–GT hybrid system, and they evaluated a performance of the hybrid system and conducted parametric optimum design based on the simulation model. They show that a maximum power output of the hybrid system is achieved under the fuel utilization of 0.78 [16]. Lorenzo et al. also studied an optimization of an MCFC–GT hybrid system. They developed a zero-dimensional simulation model for the system, and optimized the system efficiency by changing values of air excess factor, current density, fuel utilization factor and recirculation temperature [17]. Huang et al. presents a performance of an MCFC–MGT hybrid system bi-fueled by city gas and biogas, experimentally and numerically. They confirmed that the hybrid system can be operated stably and the efficiency range is 39.0% to 42.0% with biogas flow rate which is 50% of the overall input heat value [18]. For higher system efficiency, an organic Rankine cycle (ORC) could be also integrated with an MCFC system [19-21]. Angelino et al. studied ORC system for using waste heat from MCFC system. They simulated the ORC cycle for

various working fluids, and then they presented that the system efficiency is about 58% [19]. Vatani et al. performed a thermodynamic analysis of ORC cycle for heat recovery from an MCFC system. They also studied various working fluids, and then the total system efficiency can be about 60% when the working fluid is toluene [20]. Mamaghani et al. introduced an integrated MCFC–GT plant and ORC system for achieving high electrical and exergetic efficiencies. They performed an optimization for the system, considering the exergetic and economic factors. As a results, they presented that the system exergetic efficiency is ~55% [21]. Stirling engine has been also studied for yielding additional power output from an MCFC system [22-24]. Sanchez et al. suggested an MCFC-Stirling hybrid system. They compared the Stirling engine to Rankine and Brayton system, and then presented that the Stiling hybrid system is more efficient than others. The MCFC-Stirling hybrid system efficiency is about 60.8% [22]. De Escalona et al. compared a Stirling engine to SCO_2 cycle for bottoming cycle of an MCFC system. They present the MCFC-SCO_2 hybrid system is more efficient than the MCFC-Stirling hybrid system [23]. Chen et al. also studied MCFC-Stirling engine hybrid system. They performed parametric studies of the hybrid system, thus they proposed the optimal operating condition [24].

Academic researches of the MCFC hybrid systems have been referred until now. However, various MCFC systems have been already commercialized and hybrid systems were demonstrated. First of all, the MCFC standalone systems of various power range were commercialized by Fuel Cell Energy (FCE). FCE's systems are DFC300, DFC1500, DFC3000, DFC4000. DFC300

is a sub-megawatt 300 kW power generation system with 47% electrical efficiency. DFC 1500, DFC 3000, and DFC 4000 provide 1.4 MW, 2.8 MW and 3.7 MW of power, respectively [25, 26]. With this DFC300, DFC/T hybrid system was demonstrated. This system integrated MCFC with an unfired gas turbine. The gas turbine is a C60 micro-turbine of Capstone [27, 28]. And the system efficiency is about 56%. FCE suggested MW-scale (1-3 MW) and 40 MW DFC/T power plant design [29]. Ansaldo Fuel Cells (AFCo) validated integration of stack-microturbine, and Figure 1.5 shows AFCo's MCFC-GT hybrid system installation in Milan, Italy [30]. For the 2005 EXPO in Aichi, a MCFC-GT hybrid system were installed by Ishikawajima-Harima Heavy Industries (IHI). The system power output is 300 kW [30]. Likewise, SOFC hybrid systems, which are belong to same high-temperature category, were also demonstrated. Siemens demonstrated a pressurized micro turbine generator (MTG)-SOFC hybrid system with National Fuel Cell Research Center (NFCRC), as shown in Figure 1.6. The system consists of a Siemens Westinghouse SOFC and an Ingersoll-Rand Energy Systems MTG. The system was designed to yield 220 kW, and the system efficiency is 53 % [31, 32]. Mitsubishi Hitachi Power Systems (MHPS) have developed a SOFC-MGT hybrid system for commercialization. Figure 1.7 shows the hybrid system. MHPS setup the prototype of the system in Kyushu university. The target rated output of the system is 250 kW and the target efficiency is 55 %. They also planned the load variation test [33, 34]. In addition, LG Fuel Cell Systems, which are originated from Rolls Royce Fuel Cell Systems, have also studied a pressurized SOFC-MGT hybrid system [35].

Figure 1.3 DFC300 fuel cell power plant [25]

Figure 1.4 Alpha DFC/T unit installed at the billings clinic, Montana demonstration site [27]

Figure 1.5 AFCo's hybrid MCFC-GT installation in Milan [30]

Figure 1.6 Pressurized MTG-SOFC hybrid system [31]

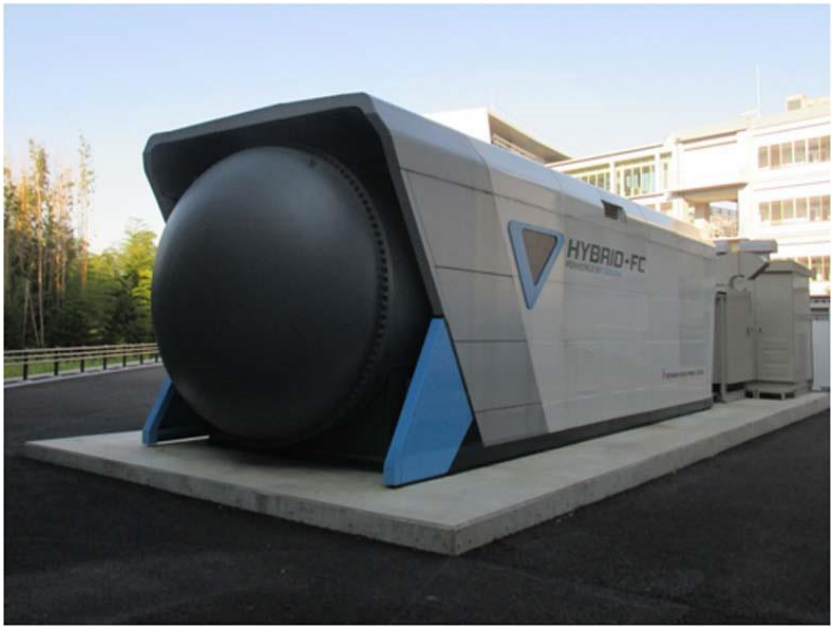

Figure 1.7 SOFC-MGT hybrid system demonstration in Kyushu university [33]

1.3 Development of hybrid system concept

In Chapter 1.1, previous academic researches and industrial demonstration, which are focused on MCFC hybrid system, were discussed. For combining fuel cell and other component, there are two major options, which are using leftover fuel of anode off-gas and using waste-heat of the system. In this thesis, the former option is chosen, and the hybrid system is combined MCFC with Homogeneous charge compression ignition (HCCI) engine. Recently, we suggested a new MCFC-HCCI engine hybrid system concept for distributed power generation [36-41]. This section presents the new MCFC-HCCI engine hybrid system concept referencing previous papers [36-41].

Figure 1.8 shows typical MCFC standalone system schematic. In typical MCFC operation, to prevent the fuel cell from fuel starving, fuel gas is supplied to the anode in excess of the amount that is actually reacted to generate electricity. The leftover fuel in the anode off-gas is oxidized in a separate catalytic combustor to generate heat and carbon dioxide, which are fed back into the cathode of the fuel cell with fresh oxidizer. However, this anode off-gas still contains noteworthy portion of initial fuel chemical energy -20-30% of initial heating values- that can be utilized to yield additional power. The anode off-gas has characteristics which is highly diluted, high temperature. Thus if the hybrid system uses conventional engines like spark ignition (SI) or compression ignition (CI) engine, the following problems may occur due to the features of the anode off-gas. In the case of SI engine, it is possible that the flame is not propagated in cylinder due to a lean fuel condition. In case of CI engine, it is

inefficient that the high temperature gaseous fuel is compressed to a typical injection pressure. However, the anode off-gas can readily be exploited by the HCCI engine. Hence, in the present hybrid system, the HCCI engine replaces the catalytic combustor to generate additional power by oxidizing the leftover fuel, and thus it could increase overall system power output and efficiency.

In an HCCI engine, a homogeneous mixture of fuel, oxidizer, and diluents is compressed to the point of auto-ignition, without the need of the spark ignition or high-pressure fuel injection used in conventional engines. Therefore, the combustion timing in an HCCI engine is solely dependent on the thermodynamic states of the in-cylinder mixture and chemical reaction kinetics. The one of the advantages using HCCI is high efficiency, which is typically 20-30% (relative) higher as compared to the one of a conventional spark ignition engine. And the HCCI engine produce the low emissions of oxides of nitrogen (NO_X) and almost no soot due to low combustion temperature and the homogenous characteristics of combustion process, respectively [42].

Finally, the MCFC-HCCI engine hybrid system configuration is suggested. The left-over fuel of anode off-gas is mixed with fresh air, and then, the gas mixture enters the HCCI engine. After combusting in HCCI engine, the exhaust gas is mixed with preheated air. The gas mixture enters the cathode of fuel cell. There is more detail process of the hybrid system in Chapter 2.

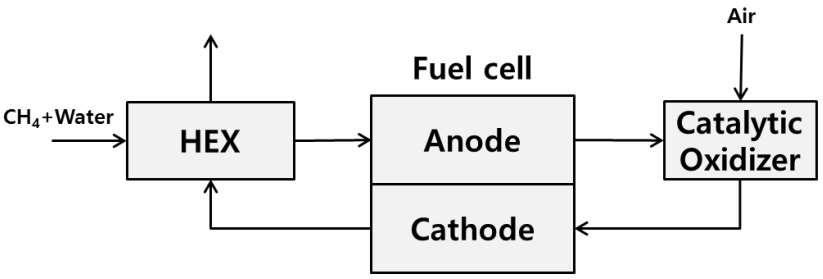

Figure 1.8 Typical MCFC system schematic

1.4 Summary

In this chapter, it is introduced why new energy resource technology, fuel cell, is needed. Fuel cell technology has been studied by academy, industry and research institutes. They proposed various hybrid system concepts, which are the systems integrated with a gas turbine, an ORC or a Stirling engine for higher efficiency. Some of them demonstrated the systems by experimental setup.

In previous papers, new hybrid system concept was proposed. The new hybrid system is composed of MCFC and HCCI engine. The HCCI engine is newly added to the original MCFC system, replacing the catalytic combustor. The left-over fuel of the anode off-gas is combusted in the HCCI engine, and then the engine yields additional power output and hot exhaust gas which is composed of carbon dioxide and nitrogen. Hence, the total electrical system efficiency can be higher than that of the MCFC standalone system.

In this thesis, the engine design, economic assessments and experiments about the MCFC-HCCI engine hybrid system would be performed. The main body of this thesis consists of five chapters—Chapter 2 Hybrid system thermodynamic modeling, Chapter 3 Hybrid system engine design, Chapter 4 Hybrid system operation, Chapter 5 Economic analysis of the hybrid system, Chapter 6 Hybrid system feasibility verification. In Chapter 2, details for the component-level modeling of an MCFC and HCCI engine are given, which are followed by descriptions on hybrid system integration and model validation. In Chapter 3, based on the modeling of Chapter 2, engine specification is designed by considering some design options, and then the proper engine size range is

suggested. After all, one of the engine size is chosen, and a design point condition of the system is determined. In Chapter 4, the component-level modeling results are presented first and then the hybrid system performance is analyzed at design point operation and part-load operation. In Chapter 5, economic analysis is conducted about fuel cell standalone system and the hybrid system. The analysis is performed by the total revenue requirement (TRR) method. By the method, levelized cost of electricity (LCOE) factor is evaluated, and then the economic worth of the hybrid system would be discussed. In Chapter 6, the experiment is conducted to demonstrate the possibility of the HCCI engine operation in the hybrid system. Finally, in Chapter 7, the new hybrid system characteristics and feasibility for commercialization are discussed. Specially, the remaining issues are discussed for the proposed hybrid system to be commercialized.

Chapter 2. Hybrid system thermodynamic analysis methods

2.1 Introduction

In a previous chapter, the concept of the new hybrid system is proposed and the hybrid system configuration is introduced briefly. To evaluate the feasibility and performance of the hybrid system, thermodynamic modeling was performed by using the Mathworks MATLAB and Cantera thermochemistry toolbox. In this chapter, the modeling descriptions of components are discussed. Most of components models were previously developed in the past studies [36-39]. Thus the descriptions are reproduced, referencing the papers, except some sub-sections. Firstly, for an MCFC stack, a one-dimensional fuel cell model that incorporates non-isothermal behavior was developed. This model includes various loss mechanisms and allows temperature variation as reaction proceeds along the channel in the fuel cell. Secondly, for an HCCI engine, a zero-dimensional HCCI engine model, previously developed in past study, was adopted. Thirdly, for blower and pump, simple models were developed. In this thesis, the system pressure is just 1 bar, and thus these BOP models are used in Chapter 5 due to calculate the equipment costs. Finally, a complete system was configured by combining fuel cell stack, heat exchangers, mixers, and either catalytic burner or HCCI engine.

2.2 MCFC stack modeling description

In this study, a non-isothermal fuel cell model with reforming channel model integrated was developed for analyzing the performance of the MCFC stack in either standalone or hybrid system configuration. The MCFC stack model was developed in past study of authors [36, 37] and the following contents reference master's theses of author [38] and Abid [39]. Thus the followings are almost reproduced from the references [36-39] and some contents are revised in this thesis. In this chapter, the stack modeling is briefly described. There would be the detailed modeling description in Ref. [36-39] or Appendix A.

The stack model took a similar approach as shown in Ref. [43], although we newly added reforming channel and non-isothermal fuel cell operations in the model. By using the developed model, stack performances, e.g. electrical efficiency, power output, and losses, would be evaluated and temperature change would be also depicted.

Figure 2.1 depicts the algorithm flow chart of the stack model [37, 38]. Firstly, the operating voltage is assumed to be the proper value. Based on the voltage, the fuel cell losses and the current density are evaluated, and then the gross power output is calculated. And then the heat balance is computed and the temperature change is evaluated. The stack model is divided into 25 segments along the gas flow direction. Thus, this process is iterated for the 25 segments. After all the evaluations, MCFC gross power output is calculated and fuel utilization factor is determined on basis of flow rate of CO and H_2 [44]. If

the evaluated utilization factor doesn't match the designed one, the operating voltage is newly assumed, and then all the process is repeated. At the end of this process, the fuel cell gross efficiency and gross power output are obtained. The net power output and efficiency of the fuel cell are evaluated, considering the BOP power output and inverter efficiency. The BOP model will be explained in Chapter 2.4. Detailed modeling process for the fuel cell is obtained in Ref. [36-39] or Appendix A.

The data of a commercialized DFC 300 model from Fuel Cell Energy Corp. is used to validate the MCFC stack model. Generally, it is known that the FCE's DFC 300 generates a power output of about 250 kW with net efficiency of about 47 %. These numbers are closely compared to 237 kW and 47.3 % from the present standalone MCFC system model, especially considering those simplifying assumptions above. Furthermore, the composition of anode off-gas in simulation is almost same with that in DFC 300 model. Table 2.1 lists the composition of anode off-gas in DFC 300 model and the simulation result [45]. The compositions are slightly different between the DFC 300 and the simulation about H_2O and CO_2 concentrations, but overall trend is almost same, specially, about H_2 and CO concentrations.

Table 2.1 Anode off-gas composition at fuel utilization of 65%

Composition	**DFC 300 (%)**	**Simulation (%)**
H_2	10	11
H_2O	40	44
CO	5	5
CO_2	45	40

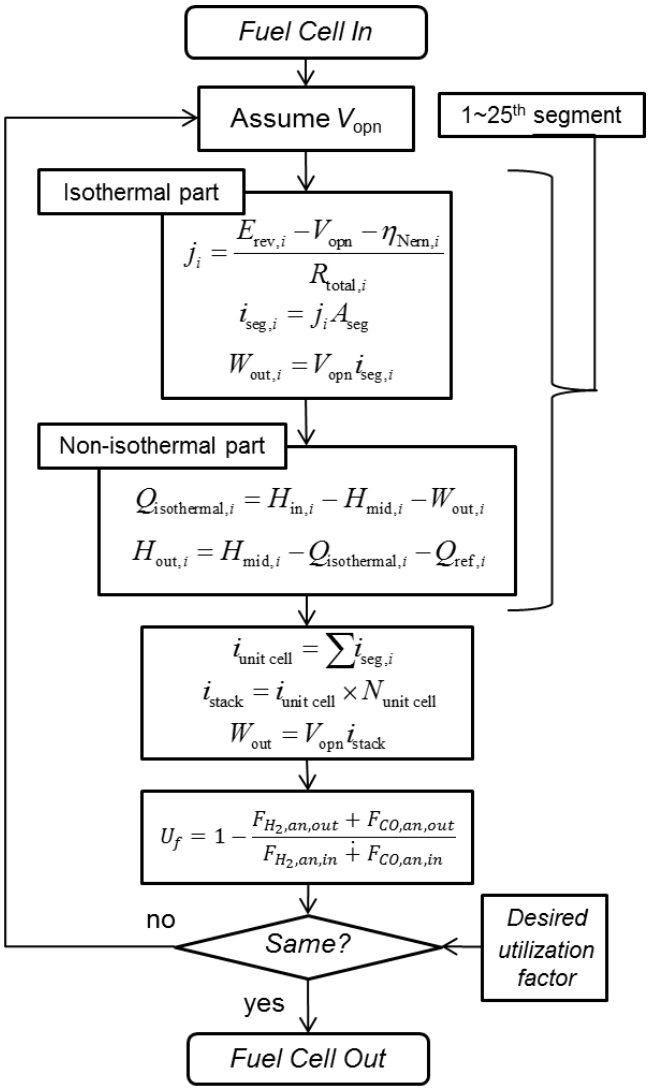

Figure 2.1 MCFC stack modeling flow chart [37, 38]

2.3 HCCI engine modeling description

The HCCI engine model was previously developed and validated by the past study [46, 47]. This model was developed by using MATALB and Cantera toolbox. The toolbox helps us to calculate the thermodynamic properties and chemical reaction kinetics. In a typical HCCI operation, well-mixed reactant mixture is introduced during the intake process. During the main compression stroke, the reactant mixture is compressed up to the point where the volumetric self-ignition occurs throughout the cylinder, without any external ignition source, such as, a spark-plug in spark-ignition engine (a.k.a. gasoline engine) or a direct-fuel-injection-system in compression-ignition engine (a.k.a. diesel engine). Therefore, the combustion timings are largely dependent on the thermodynamic states of the reactants and chemical reaction kinetics. In typical HCCI operation, the temperature and composition of the intake mixture become the major control variables in combustion timings. In this model, the combustion timing is defined as CA50, which is the point of 50 % of total heat release.

In HCCI engine, combustion timing is one of the most determining factors in efficiency. Firstly, too early combustion timing, near or before the top dead center (TDC), has a negative effect on the efficiency by increased heat transfer, because high-temperature post-combustion gas is exposed to the relatively cold cylinder wall with the highest surface-to-volume ratio near TDC. Secondly, too late combustion timing may also degrade the cycle efficiency by possible incomplete combustion or even misfire. As the piston moves down after the top

dead center, the mixture expands and cools down to the level when the mixture is no more reactive enough to complete the combustion reactions. Therefore, the proper combustion timing should be maintained to maximize the efficiency of the HCCI engine.

Due to the nearly homogenous nature of the mixture preparation and combustion phenomena in HCCI engine, our engine model assumes a homogeneous thermodynamic state for the in-cylinder mixture during the closed parts of the engine cycle, i.e. compression and expansion strokes. In order to predict the combustion timing, GRI-Mech 3.0, including 53 species and 325 reactions, is adopted, which was developed for natural gas application [48]. The detailed modeling descriptions can be found in Appendix B.

This model omits intake and exhaust strokes, and thus doesn't consider the pumping losses from gas exchange processes. Intake throttling is not adapted in typical HCCI operation, thus intake and exhaust manifold pressures are almost 1 bar, thus the pumping loss is usually zero. Although the model omits the gas exchange processes, heat transfer to the cylinder wall during the gas exchange processes is considered due to more accurate prediction about the amount of heat transfer. The heat transfer to the cylinder wall is evaluated by using the Woschni model [49]. Engine friction is calculated by Chen-Flynn model, which uses maximum pressure and mean piston speed [50, 51].

Finally, the combustion efficiency is evaluated to determine the degree of completeness of the combustion and defined as in Eqn. 2.1.

$$\eta_c = 1 - \frac{LHV_{out}}{LHV_{in}} \qquad (2.1)$$

where LHV_{in} is the lower heating value of the inlet fuel, and LHV_{out} is the lower heating value of the exhaust gas. In this study, the combustion efficiency over 98% is assumed to be complete combustion.

2.4 Blower and pump modeling description

In this thesis, the system is assumed to be under atmospheric condition, and not considered pressure drop. So the blower and pump models are only used to calculate BOP power consumption in simulation analysis of Chapter 3 and 4. On the other hand, in Chapter 5, economic analysis needs to use these models for estimating the blower and pump costs.

To evaluate the costs of blower and pump, simple thermodynamic blower and pump models are used, which are isentropic models. All the blowers, which are fuel blower, cathode air blower, and catalytic burner blower, are using the isentropic efficiency value of 0.5 and mechanical efficiency value of 0.9. Pump components, which are water pump and heat recovery water pump, use also same isentropic and mechanical efficiencies with blowers.

2.5 System integration

Figure 2.2 shows a schematic for MCFC hybrid systems. It is noted that the state numbering in Figure 2.2 is in the ascending order for the flow direction. At the inlet of the system (state 1), methane is mixed with water in a mole ratio of 1:2.5, which is to ensure sufficient conversion of methane to the reformed

gas in the reforming channel of the fuel cell. Before entering the reforming channel of the fuel cell, this mixture of methane and water is preheated by cathode off-gas (state 17) and anode off-gas (state 4) at HEX1 and HEX2, sequentially. The heat exchangers HEX1 and HEX2 are added to finally achieve the reforming channel (anode side) inlet temperature. The anode off-gas after HEX2 (state 5) still has a high temperature and is used to preheat intake air (state 11) in heat exchanger HEX4.

For engine operation, a stoichiometric amount of air (state 7) is mixed with the anode off-gas (state 6) and the resultant mixture (state 8) is combusted in the HCCI engine to exhaust high-temperature product gas (state 9).

Ambient air (state 10) is supplied and mixed with combustion products from the engine (state 9) for supplying sufficient CO_2 and O_2 flows to the cathode channel. To achieve typical cathode inlet temperature (580^{o}C), the incoming air is preheated at HEX3, HEX4 and HEX5 by anode off-gas and cathode off-gas. The flow rate of ambient air is determined to achieve certain air utilization factor in the fuel cell stack. Here, the air utilization factor refers to the ratio of O_2 mass flow rate consumed in the MCFC to O_2 mass flow rate supplied to the cathode of MCFC, which is fixed at 0.4 in this study.

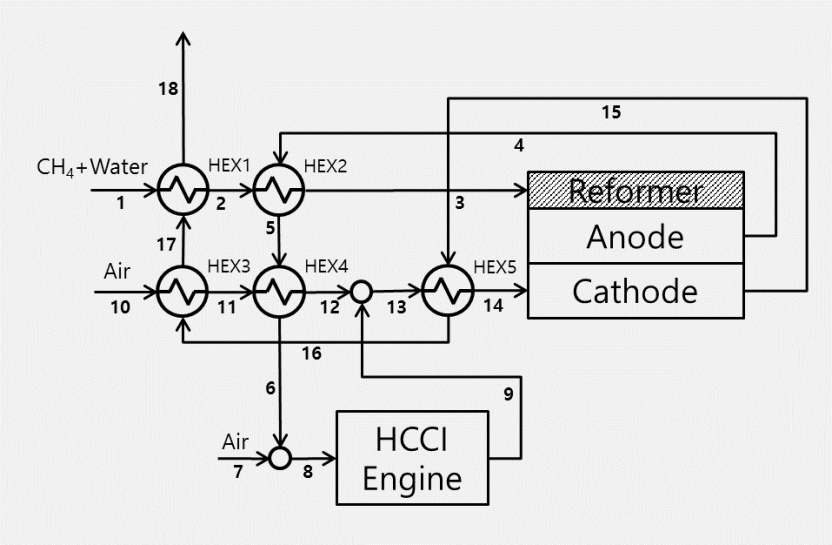

Figure 2.2 MCFC-HCCI engine hybrid system configuration

2.6 Summary

In this chapter, there are the thermodynamic modeling descriptions of various components of the hybrid system. The modeling was performed by using the Mathworks MATLAB and Cantera tool box which provides chemical reaction kinetics as a thermochemistry tool box. Firstly, the MCFC stack modeling description was introduced. The model includes electro-chemical reactions, and temperature variation. For using the model, it can evaluate the MCFC power output, the efficiency, outlet temperature, and other thermodynamic statuses. Secondly, there is the HCCI engine modeling description. The model solves ODEs to simulate the engine cycle, and then shows the temperature and pressure profiles during the engine cycle. Using these information, it can evaluate the engine power output and efficiency. The model can also evaluate the composition and thermodynamic properties of the engine exhaust gas. Thirdly, simple blower and pump models are developed, which are isentropic models. For using these models, it can be possible that the system is analyzed in aspect of economics. Finally, the system integration was conducted with various components' models, as shown in Figure 2.2. In next chapter, the hybrid system would be designed by using these thermodynamic models.

Chapter 3. Hybrid system engine design

3.1 Introduction

In Chapter 1, a newly developed MCFC-HCCI engine hybrid system concept is introduced. The hybrid system adds the engine component to the original fuel cell system. Thus, this hybrid system needs to adopt the proper engine specification for the fuel cell capacity. In this chapter, especially, it is discussed focusing the engine size. The HCCI engine, which is newly added to the MCFC system, uses the anode off-gas of MCFC for a fuel. If the concentration or the mass flow rate of the anode off-gas is changed at other operating condition, the engine, of which size is fixed, has to combust the anode off-gas with the proper amount of air. Therefore, in this chapter, the appropriate specification range of the engine would be suggested as various decision variables for design are changed. The MCFC system capacity is chosen to 250 kW-class, which is motivated by DFC300 model of FCE. To propose the engine size for the system capacity, firstly, it is discussed what the decision variables are for engine design. Secondly, when the variables are changed, it is analyzed how the system performance is affected. Finally, the engine specification is decided from the simulation results.

3.2 System operation with design options variation

3.2.1 System decision variables

In the system, there are various factors of each component. For the fuel cell, the fuel utilization factor is one of the most important factor. The factor means how much the fuel is used in the fuel cell, that is, it affects the fuel cell efficiency and the composition of the anode off-gas which is the fuel of the HCCI engine. In this thesis, the fuel cell system is motivated by DFC300 model of FCE. FCE announced DFC300 operates generally at the fuel cell utilization factor of 70% or 70%-80% ranges [45]. Thus, in this chapter, the system characteristics, especially the engine size, is analyzed at the fuel utilization factor of 70-80% ranges. And other fuel cell parameters are a voltage, a current, an S/C ratio, an O_2 utilization factor, and so on. However, the voltage and the current are subordinated to the fuel utilization factor. The S/C ratio is 2.5, which is generally used in the fuel cell system, and the O_2 utilization factor is also chosen to general value of 0.4.

For the HCCI engine, there are also various factors, e.g. RPM, equivalence ratio, intake charge temperature, compression ratio, and so on, which affect the system characteristics. The intake charge temperature is decided by calculating the minimum temperature requirement at the combustion timing near 5^o aTDC for the reasons discussed in Chapter 2.2, and at the combustion efficiency over 98%. The equivalence ratio of unity means intake air has just enough oxygen to completely oxidize the fuel. And the equivalence ratio under 1 means the

over-supply of air, and the equivalence ratio over 1 is the opposite of that under 1. Therefore, the value changes the composition of the intake charge, and then influences the combustion characteristics in the engine and the engine size. The compression ratio and RPM affect also the engine size. In this chapter, the engine size is discussed at various operating conditions of the variables, i.e. compression ratio, equivalence ratio, RPM, and fuel utilization factor of the fuel cell.

3.2.2 Engine compression ratio variation

In this chapter, it is discussed how the HCCI engine compression ratio affects the system operation. The compression ratio is not a variable which can be changed during the operation, but should be designed when the engine is manufactured. So the compression ratio should be chosen carefully. For this purpose, the simulation is conducted with different compression ratio by using Matlab, based on the thermodynamic model in Chapter 2. In this thesis, the compression ratio is changed from 10 to 20 at fixed equivalence ratio of unity. The low limit is chosen to match the value near the typical compression ratio of the gasoline-fueled HCCI engine, and the upper limit corresponds to the typical upper limit of the conventional diesel-fueled CI engine.

Figure 3.1 depicts the downsizing ratio in the engine displacement volume, where the 100% corresponds to the engine size at the compression ratio of 10. When the compression ratio increases, the engine size decreases due to the lower volume flow rate. At the higher compression ratio, the intake charge

temperature requirement is lower, keeping the proper combustion timing shown in Figure 3.4. The volume flow rate for a given mass flow is also decreased, and thus it leads to smaller engine volume requirement. Figure 3.3 shows that the combustion timing is kept almost same near 5^{o} aTDC under the compression ratio variation.

As shown in Figure 3.2, the system efficiency and engine efficiency increase when the compression ratio increases. The power output and efficiency of the MCFC are nearly constant due to same fuel utilization while those of the HCCI engine gradually escalates. But the amount of increase is very low, so the efficiency is not a big part for selecting an engine size in this chapter.

Because the fuel cell system is known for lower pollutant emissions, it is desirable that the added HCCI engine has also low harmful emissions. Major pollutants of internal combustion engines are unburned hydrocarbons (UHC), carbon monoxide (CO) and oxides of nitrogen (NO_X). In our engine model, the first two pollutants are difficult to be estimated exactly due to limitation of 0-d model. But it is known that the production of NO_X is determined by the peak temperature during engine cycle, and the pollutant increases exponentially above 1800 K. Figure 3.5 shows the peak temperature during engine cycle. The temperature is always under 1800 K due to the diluted nature of the anode off-gas, and thus it is anticipated that the NO_X emission doesn't produce.

The peak pressure during combustion process is shown in Figure 3.6. As the compression ratio increases, the peak pressure is also escalated linearly. At the high compression ratio of 20, the peak pressure is even under 60 bar, thus the mechanical issues due to the peak pressure could be not considered.

Until now, the results of the analysis say that a specific compression ratio should be chosen considering the downsizing ratio in the engine displacement volume. That is, the highest compression ratio is the best condition due to the lowest engine displacement volume. But there is the upper limit of the compression ratio due to heat effectiveness of some heat exchanger. As the compression ratio is higher, the intake charge temperature (state 8 in Figure 2.2) is lower, and then the exhaust gas temperature also decreases. It requires that the temperature of stream 12 should be higher, and then the HEX3 should work more. At the compression ratio of 20, especially, the heat effectiveness of HEX4 is over 85%, that is, the heat exchanger could be difficult to operate. Thus operating the system might be not possible at the condition.

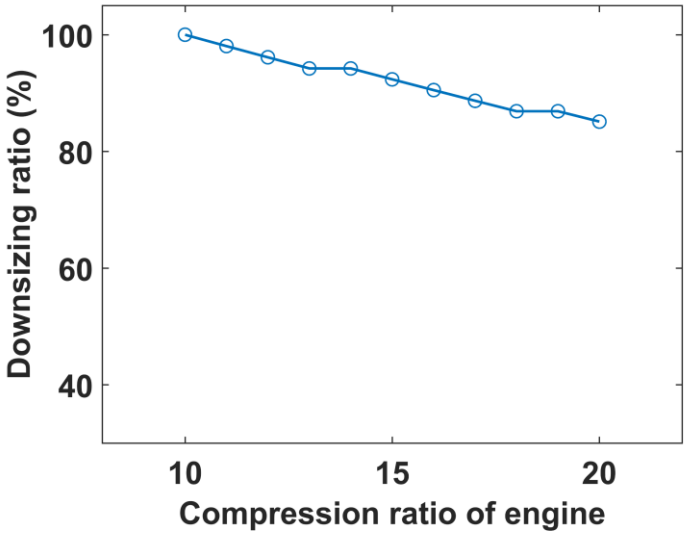

Figure 3.1 HCCI engine downsizing ratio under compression ratio variation

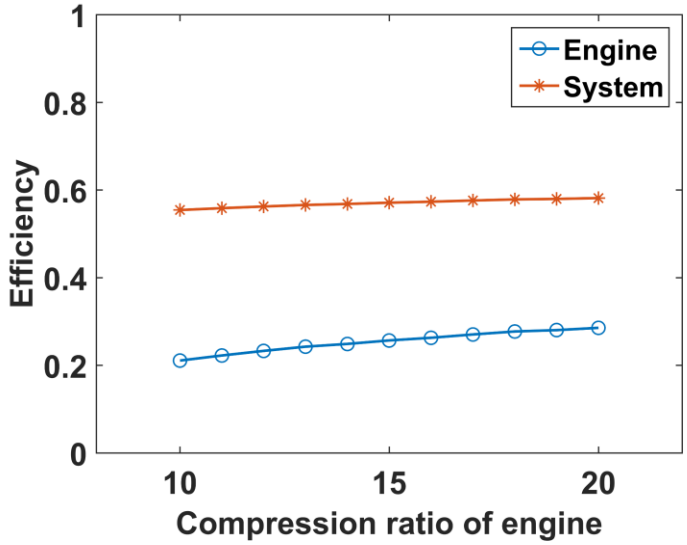

Figure 3.2 Engine and system efficiency under compression ratio variation

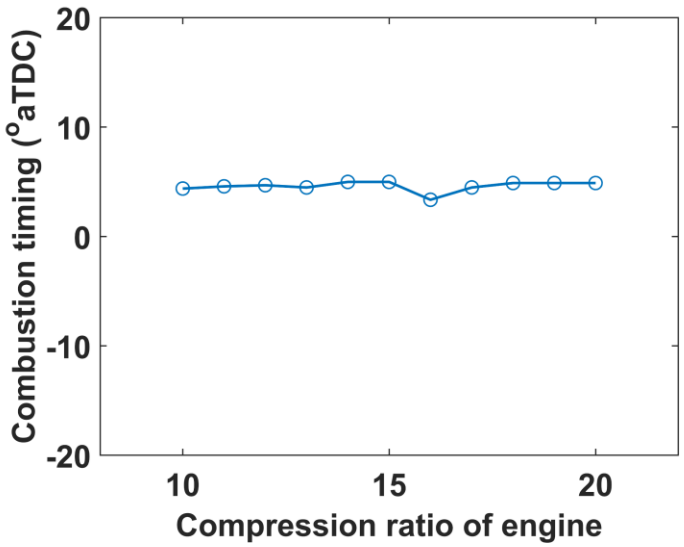

Figure 3.3 HCCI engine combustion timing under compression ratio variation

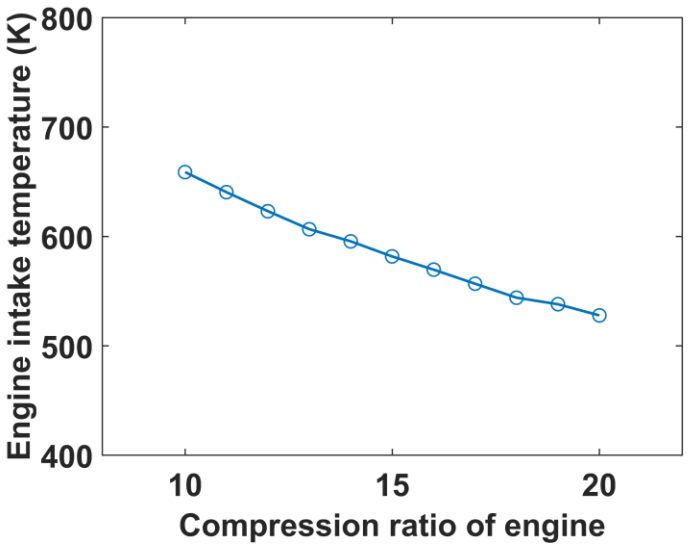

Figure 3.4 HCCI engine intake charge temperature under compression ratio variation

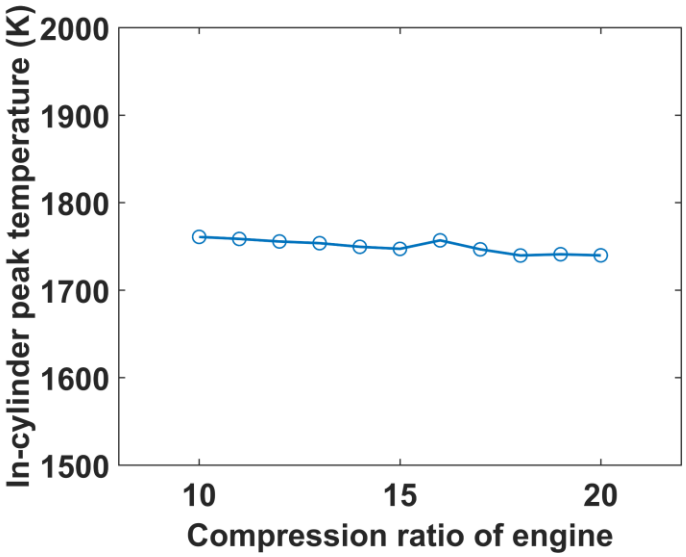

Figure 3.5 HCCI engine in-cylinder peak temperature under compression ratio variation

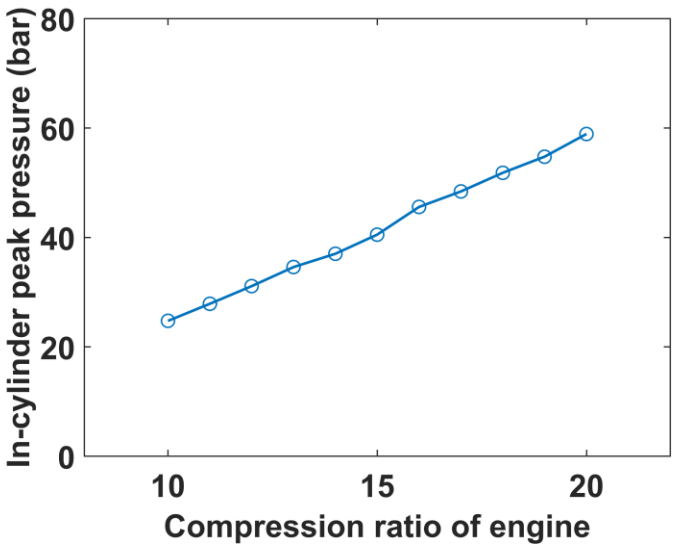

Figure 3.6 HCCI engine in-cylinder peak pressure under compression ratio variatio

3.2.3 Engine intake charge equivalence ratio variation

As mentioned earlier, the equivalence ratio is an important factor for combustion characteristics and engine displacement volume. In this chapter, it is discussed about the equivalence ratio variation.

Figure 3.7 depicts the downsizing ratio of the engine displacement volume under the equivalence ratio variation, where the 100% corresponds to the engine size at the equivalence ratio of unity. As the equivalence ratio decreases, the downsizing ratio increases due to oversupplying air with a same amount of fuel. And it is affected by decrease of the intake charge temperature, as shown in Figure 3.10. At the lower equivalence ratio, the intake charge temperature requirement is also lower, but the gas mixture can achieve comparable post-compression temperature due to higher specific heat ratio. Thus the combustion timings are almost same like Figure 3.9.

When the equivalence ratio is also reduced, the peak temperature during engine cycle decreases due to oversupplying air shown in Figure 3.11. The peak temperature, however, is always under 1800 K, thus NO_X emission would be not produced at all the analyzed equivalence ratio conditions. The peak pressure in the engine is almost same under the equivalence ratio variation, as shown in Figure 3.12. Figure 3.8 shows the efficiency variation of both the system and the HCCI engine. Although the equivalence ratio is changed, the both efficiency is kept almost same. When the equivalence ratio is reduced, the air flow rate entering the engine is increased. Therefore, the engine gross efficiency is slightly increased due to specific heat ratio increase of the intake gas mixture. But the engine friction loss is increased due to increase of the engine size, thus

the engine and system net efficiency is kept almost same. Consequently, it can be not considered to design the engine.

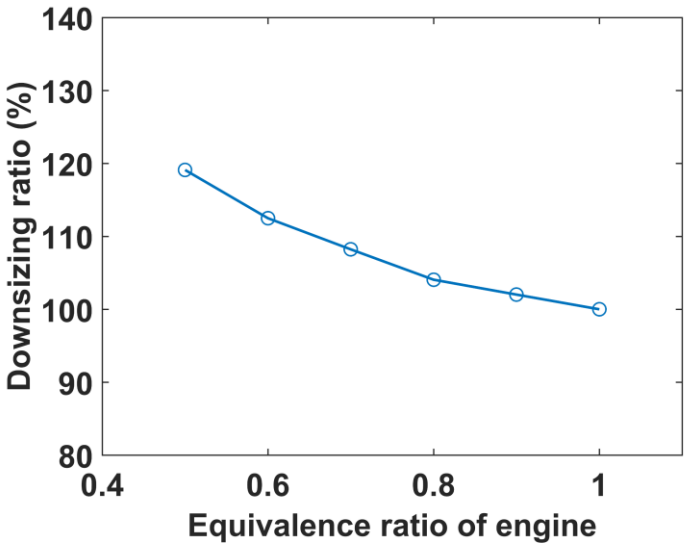

Figure 3.7 HCCI engine downsizing ratio under equivalence ratio variation

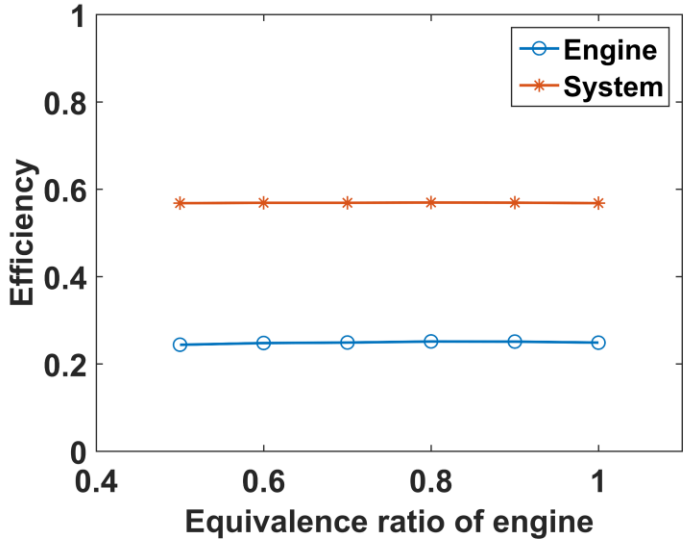

Figure 3.8 Engine and system efficiencies under equivalence ratio variation

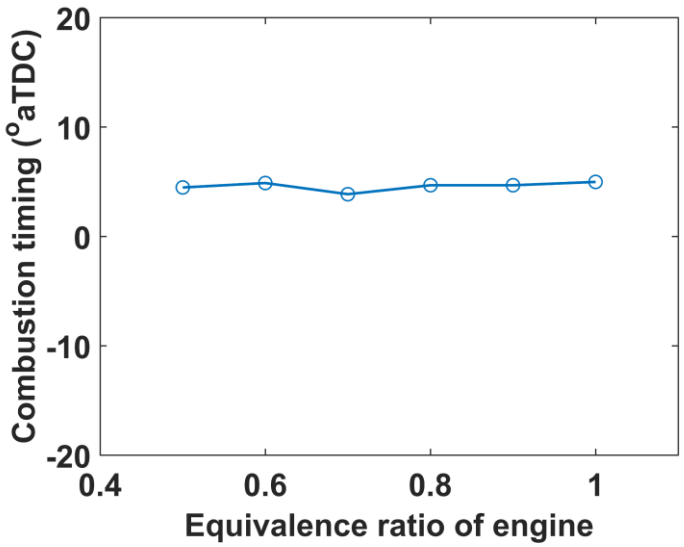

Figure 3.9 HCCI engine combustion timing under equivalence ratio variation

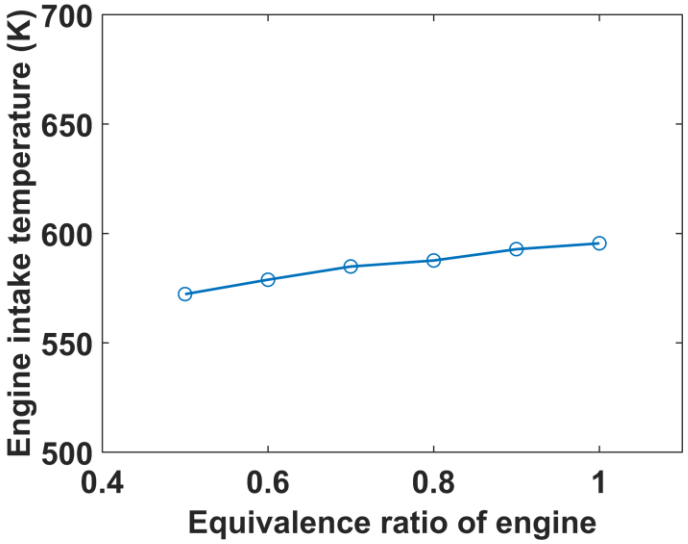

Figure 3.10 HCCI engine intake charge temperature under equivalence ratio variation

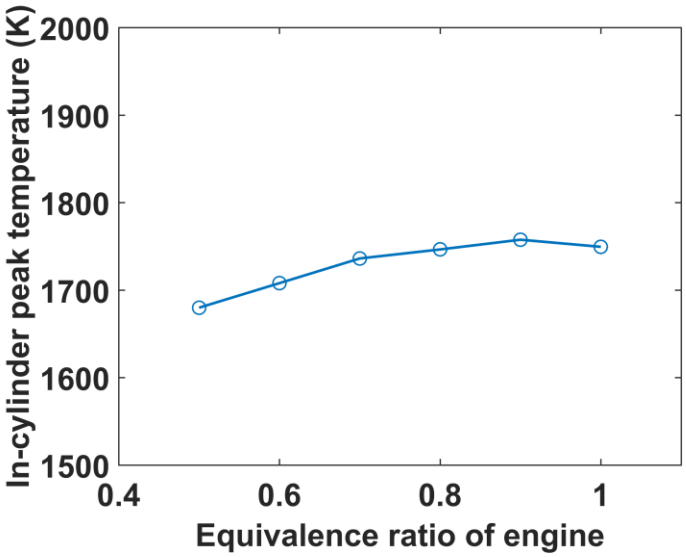

Figure 3.11 HCCI engine in-cylinder peak temperature under equivalence ratio variation

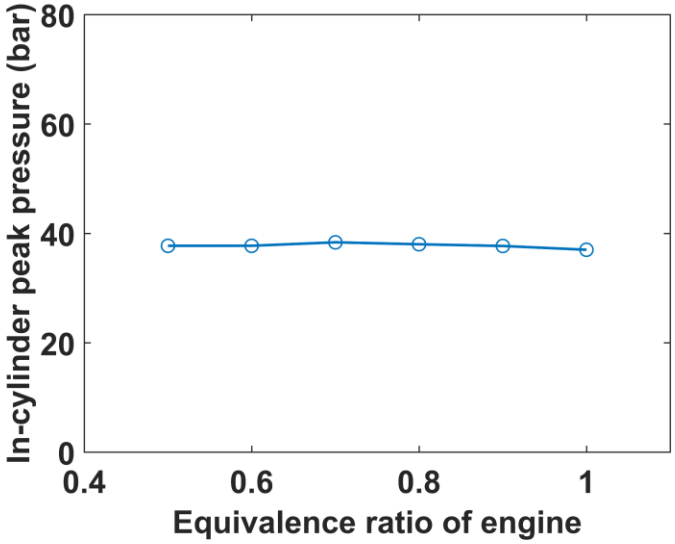

Figure 3.12 HCCI engine in-cylinder peak pressure under equivalence ratio variation

3.2.4 Engine RPM variation

In this chapter, the system is analyzed under the engine RPM variation. The engine for power generation generally doesn't operate at the high rpm, thus it is analyzed under the 2000 RPM in this thesis. Figure 3.13 depicts the downsizing ratio in the engine displacement volume under the engine RPM variation, where the 100% corresponds to the engine size at 1500 RPM. As the RPM increases, the engine size is reduced. Because the engine speed is faster, the mass flow rate of the intake charge is more. But, the mass flow rate of the anode off-gas is fixed, and thus the size of the engine can be less although the temperature of the intake charge increases a bit like Figure 3.14. The system efficiency is almost same under the RPM variation. The RPM variation doesn't affect the peak temperature and pressure during the engine cycle largely, and the temperature is under 1800 K. Therefore, it is considered to design the engine in the aspect of engine size. And if the power of the engine is connected to power grid of the plant, the frequency of generating power should be also considered. The frequency of 50 Hz (at 1500 RPM) or 60 Hz (at 1800 RPM) is generally used in the power generation.

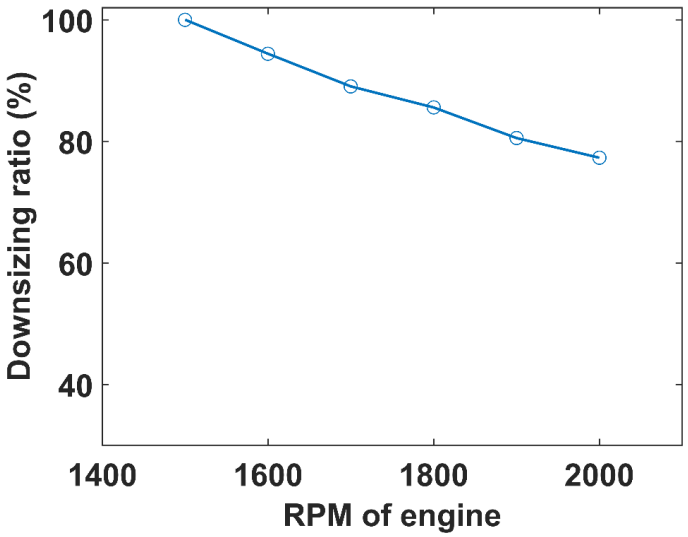

Figure 3.13 HCCI engine downsizing ratio under RPM variation

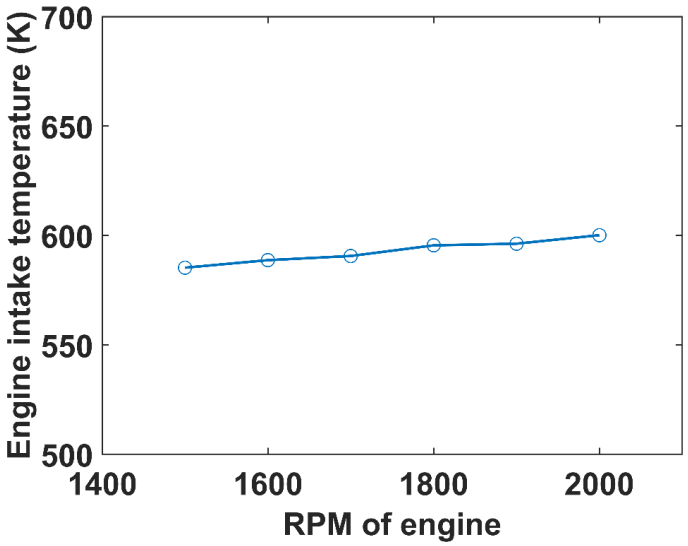

Figure 3.14 HCCI engine intake charge temperature under RPM variation

3.2.5 MCFC fuel utilization factor variation

In this chapter, the system is analyzed under the various fuel utilizations of the MCFC which are general operating range in the fuel cell system. In this thesis, starting and stopping of the system are not considered, but steady-state condition is only considered. DFC 300 system normally operates under the fuel utilization of 70-80 % range [45]. Therefore, in this chapter, it is analyzed under the fuel utilization of 70-80 %.

Figure 3.15 shows the downsizing ratio in the engine displacement volume under the MCFC fuel utilization variation, where the 100% corresponds to the engine size at the fuel utilization of 70%. As the fuel utilization is changed, the downsizing ratio is almost same. At the higher fuel utilization, the mass flow rate of the anode off-gas increases due to reacting more amount of fuel in the anode. The mass flow rate of the engine intake charge, however, is reduced due to decreasing the amount of air for stoichiometric condition, as shown in Figure 3.18. The intake charge temperature rises as the utilization factor increase, which is due to combusting the much more diluted gas, shown in Figure 3.19. To sum up the effects, the engine size is kept almost same under the utilization variation.

Figure 3.17 shows the power output of the MCFC, HCCI engine and the overall system. As the utilization rises, the MCFC power output obviously increases, but the engine power output decreases due to reacting the lower amount of fuel in the engine. Thus the overall system efficiency is kept almost same under the utilization variation. Figure 3.20 and 3.21 show that there are not possibilities that the engine produces the NO_X emission and may suffer

mechanical problems due to high peak pressure.

At various fuel utilization conditions, the hybrid system could operate and the efficiency is even same mostly. Therefore, when the engine size is chosen, the MCFC fuel utilization may be not concerned under the normal operating range.

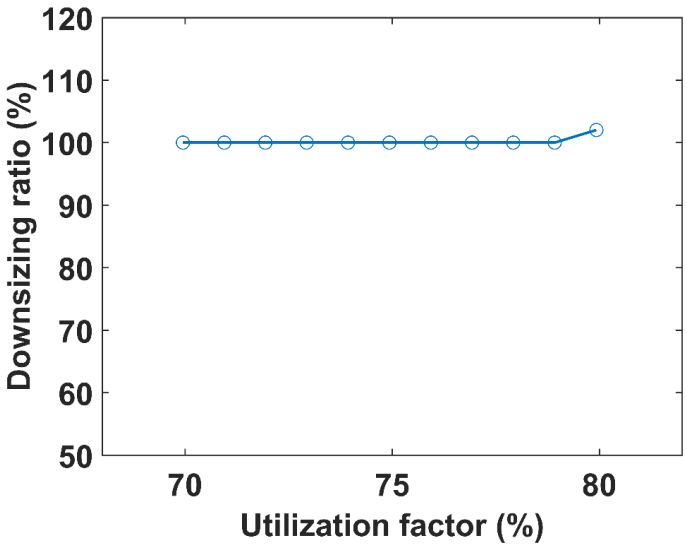

Figure 3.15 HCCI engine downsizing ratio
under MCFC fuel utilization variation

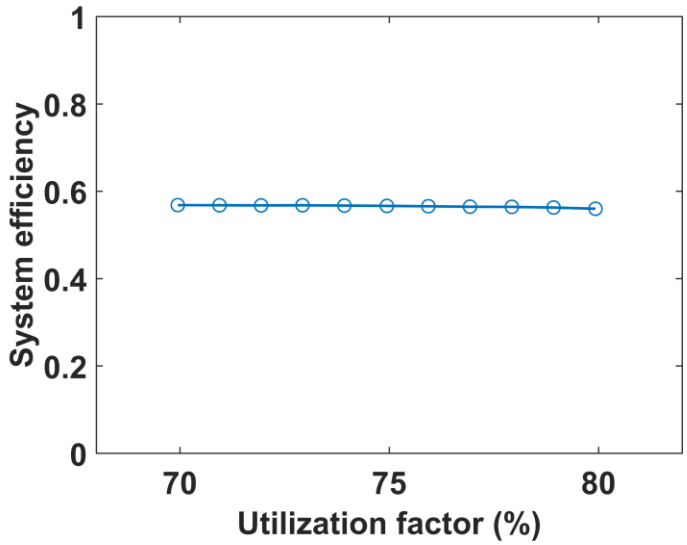

Figure 3.16 System efficiency under MCFC fuel utilization variation

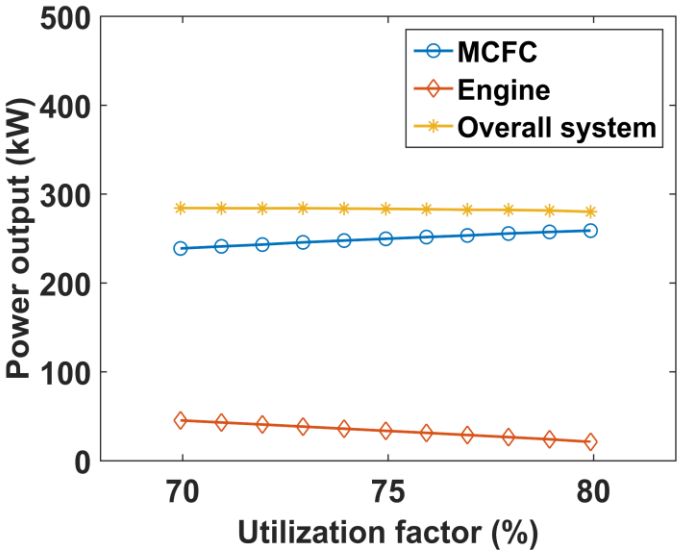

Figure 3.17 Power output under MCFC fuel utilization variation

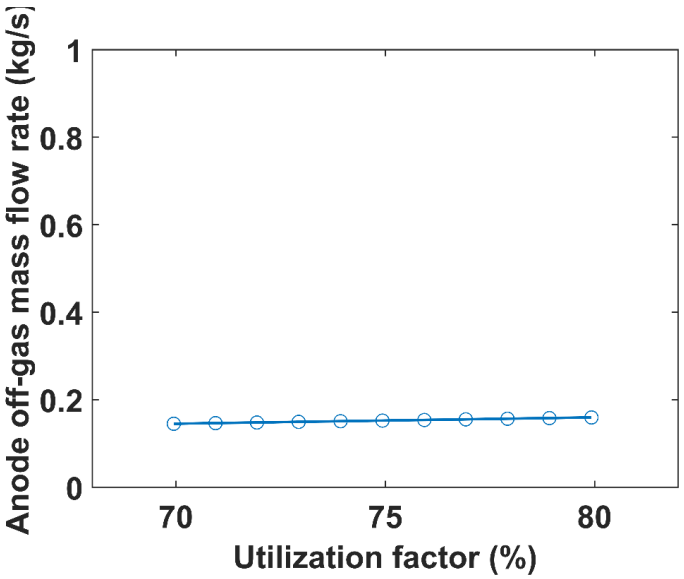

Figure 3.18 Mass flow rate of anode off-gas
under MCFC fuel utilization variation

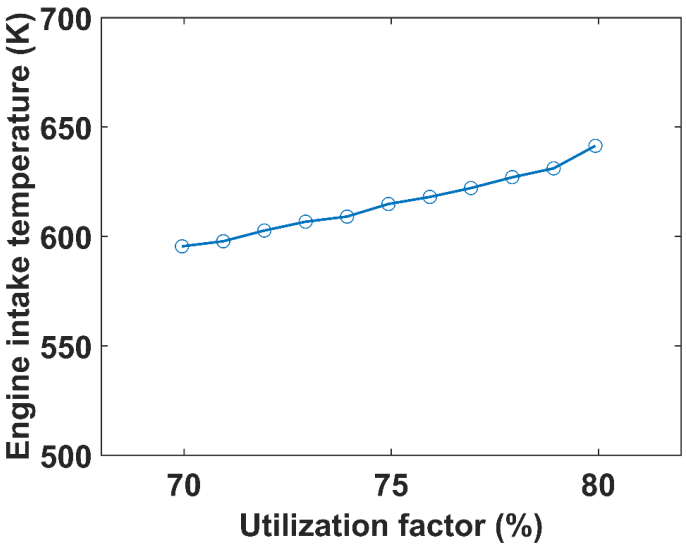

Figure 3.19 HCCI engine intake charge temperature under MCFC fuel utilization variation

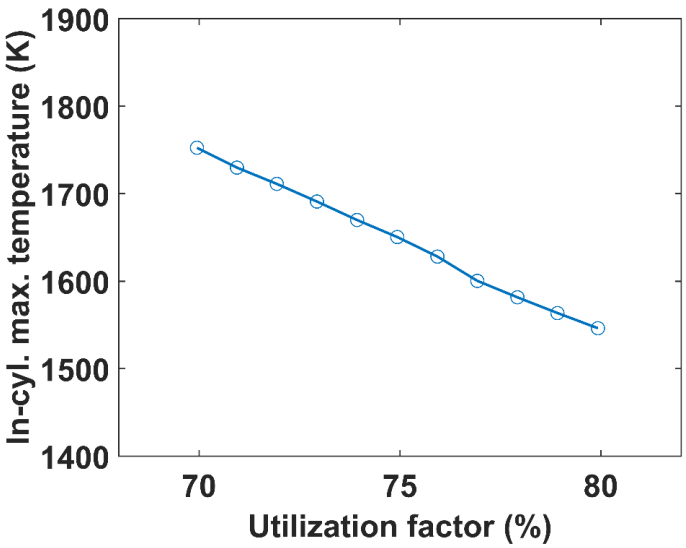

Figure 3.20 HCCI engine in-cylinder peak temperature under MCFC fuel utilization variation

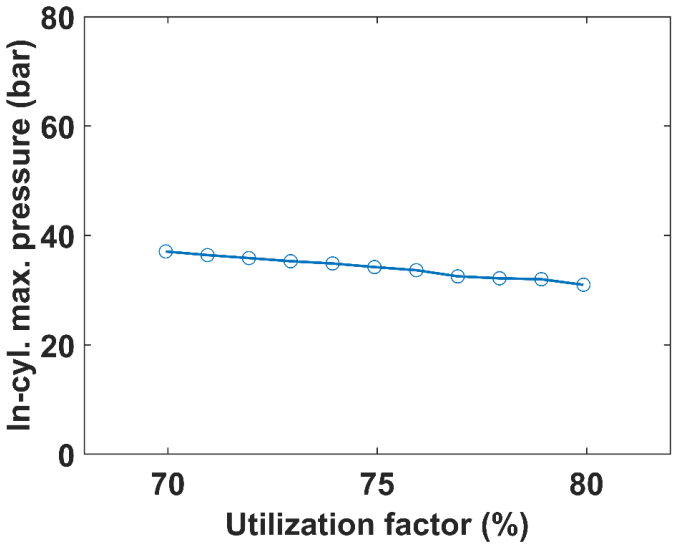

Figure 3.21 HCCI engine in-cylinder peak pressure under MCFC fuel utilization variation

3.3 Engine size decision

Based on the results of the previous simulation, engine size would be decided in this chapter. For determining the HCCI engine size, various criteria are considered. Firstly, for the lower NO_X emission, in-cylinder peak temperature need to be under 1800 K. Secondly, the condition of the higher system efficiency is favorable. Thirdly, the smaller size of the engine is better due to the system footprint and the cost. Besides those, various criteria are applied to the decision.

Under the previous conditions, in-cylinder peak temperature is mostly under 1800 K, due to combustion of the diluted intake gas mixture. Therefore, the NOx emission wouldn't be concerned in this system. In the intake gas mixture, there are the air and the anode off-gas, which is composed of CO_2, H_2O (steam), CO and H_2. But the amount of CO_2 and H_2O (steam) is much more than that of CO and H_2, so the operating condition is extremely diluted condition for combustion in the engine. It is very diluted condition in comparison with general syn-gas, which is also composed of CO_2, H_2O (steam), CO and H_2 mostly. CO_2 and H_2O (steam) don't participate in the chemical reaction. But the thermal energy for the combustion is also distributed to the non-reacting gas, and then more dilution causes less peak temperature in the engine. In the previous results, the in-cylinder peak pressure is under 100 bar at most conditions. Thus there wouldn't be a possibility that the HCCI engine may suffer mechanical issues by the high pressure.

In Chapter 3.2.4, when the RPM of the engine is higher, the engine size is

less. The system efficiency is almost same under the engine rpm variation. Based on the results, the engine is chosen with 1800 RPM although the engine size is less at the 2000 RPM. Because there is not much difference between the engine sizes of two RPM, i.e. 1800 and 2000 RPM. But with 1800 RPM, the generating power of the engine could be connected to the power grid of the plant due to the frequency of 60 Hz.

In Chapter 3.2.5, the engine size is almost same under the fuel utilization factor variation, which is general operating range. When the fuel utilization factor increases, the system efficiency decrease, but there is not much difference. Higher fuel utilization factor means more using the fuel in the fuel cell, thus the anode off-gas doesn't have much left-over heating value. That is, in the engine, the intake charge is more diluted gas. But, the engine still can operate in that hard condition, and in-cylinder peak temperature is less at the higher fuel utilization condition. The results show the hybrid system can be operated at the general range of the fuel utilization with almost same engine size.

In Chapter 3.2.2, when the compression ratio is higher, the engine size is lower, and the system efficiency is also higher due to increase of the engine efficiency. But there is not much impact in the efficiency. In Chapter 3.2.3, when the equivalence ratio decreases, the engine size is higher due to over-supply of air. But the system efficiency is almost same under the equivalence ratio variation.

For the detail comprehension about the two variables, i.e. the compression ratio and the equivalence ratio, it is simultaneously analyzed under the various

compression ratio and equivalence ratio. Figure 3.22 shows the downsizing ratio of the engine under the two factors variation. The equivalence ratio variation is more influenced to the engine size than the compression ratio variation. And Figure 3.23 depicts the system efficiency is not changed largely. At the lower equivalence ratio, it is difficult to operate the heat exchanger (HEX3) due to higher heat effectiveness. Figure 3.24 shows operation at the lower equivalence ratio needs the higher effectiveness of HEX3, especially, the effectiveness of the HEX3 is over 85% at most compression ratio condition with equivalence ratio of 0.4. Thus, if the equivalence ratio is closer to unity, it is more advantage in point of the engine cost and system operation. And if the engine drives at the equivalence ratio of unity, it is possible to use an ad-hoc three-way catalytic converter. It is an after-treatment device which could eliminate harmful emissions to be fed into MCFC.

The heat effectiveness of HEX4 is analyzed with keeping the heat effectiveness of HEX5 almost same when the compression ratio and the equivalence ratio are changed. When the compression ratio increases, the effectiveness of HEX4 rises over the compression ratio of 15. If the compression ratio increases, the intake charge temperature requirement of the engine is reduced with keeping proper HCCI combustion timing and combustion efficiency. When the compression ratio increases, the exhaust gas temperature also decreases due to more expansion. Therefore, higher temperature of the state 12 is needed for reaching the cathode inlet temperature, and thus the effectiveness of HEX4 increases. In case of the lower compression ratio, the intake charge temperature requirement increases due to keeping the

proper combustion timing and combustion efficiency. That is, the temperature of cooled anode off-gas (state 6) needs to be higher. However, the temperature has a margin of increase due to the limit of the temperature of anode off-gas (state 4), which is decided by reacting in fuel cell. In this case, the fuel utilization of the fuel cell is fixed at 0.7, and then the temperature of the anode off-gas is almost same under the compression ratio of the engine variation. Thus, at the low compression ratio, it can be possible that the temperature of state 6 doesn't satisfy the requirement of the intake charge temperature. Figure 3.25 depicts the low operability under the compression ratio of 13. Although the equivalence ratio of unity is recommended, it is not proposed when the part-load operation of the system is considered. At the part-load operation, the engine operation at the lower equivalence ratio is needed due to a decrease of mass flow rate of the anode off-gas with the fixed engine size. Therefore, the compression ratio of 13-16 is recommended. Under the conditions, the system operating range can be wider than that under other conditions.

According to the recommended operating point, the design decision variables are the 1800 RPM, the equivalence ratio of unity and the compression ratio of 13-16 range under the 70% fuel utilization of the fuel cell. For the 300 kW-class fuel cell hybrid system, the engine size satisfying the recommended operating point is 21.2 L from 20.4 L. If a 250 kW-class fuel cell standalone system uses the one among this engine size range for hybridization, the system has a higher efficiency and still creates low NO_X emission.

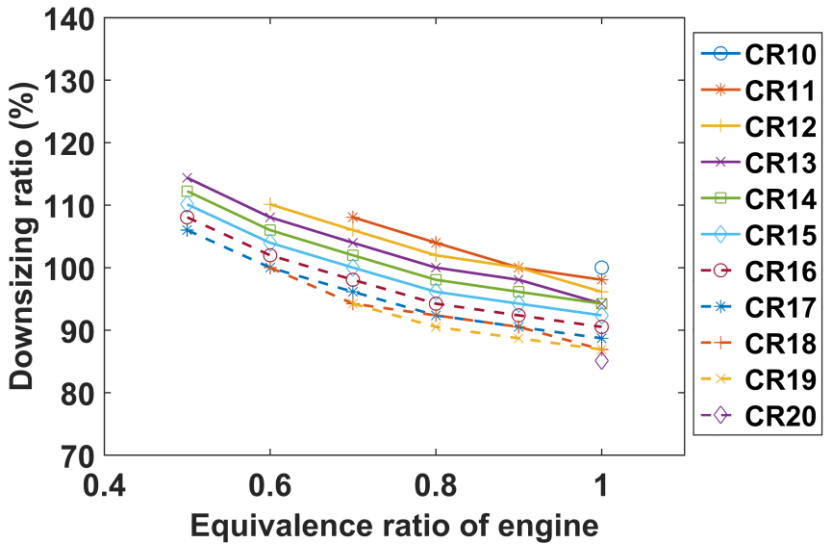

Figure 3.22 HCCI engine downsizing ratio

under Engine equivalence ratio and compressio ratio variation

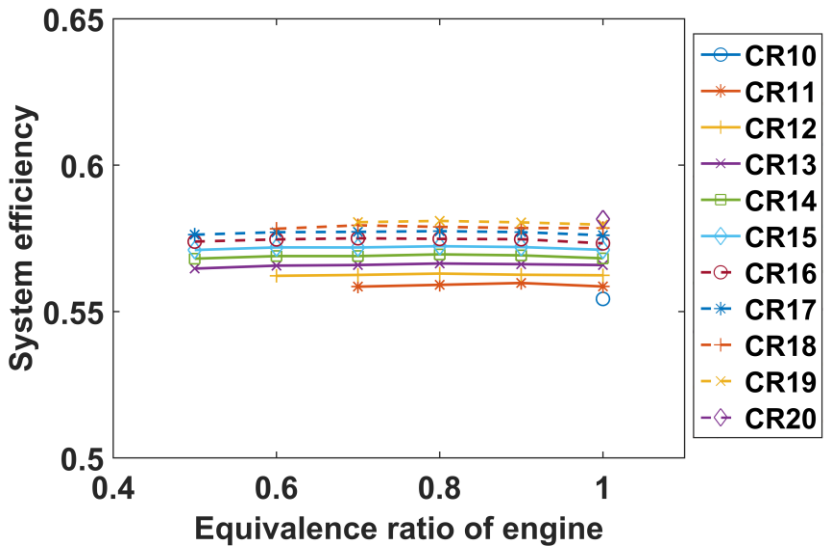

Figure 3.23 System efficiency

under Engine equivalence ratio and compression ratio variation

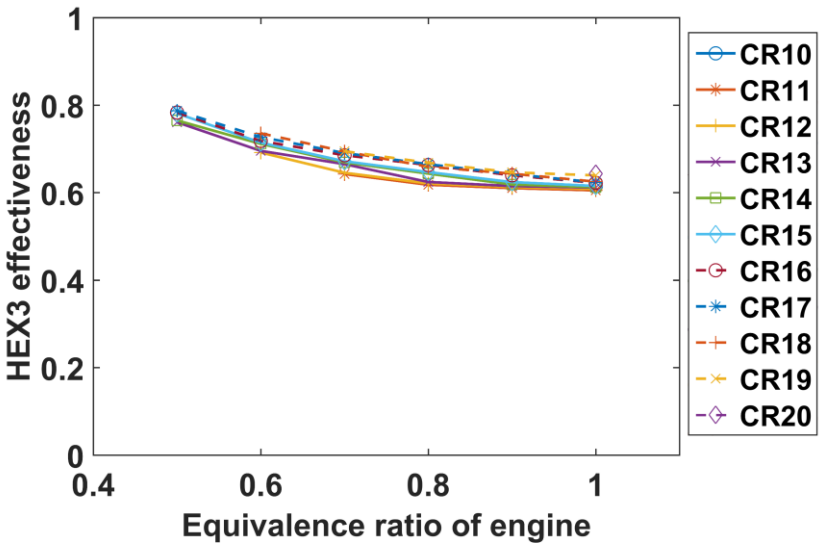

Figure 3.24 Heat effectiveness of HEX3

under Engine equivalence ratio and compressio ratio variation

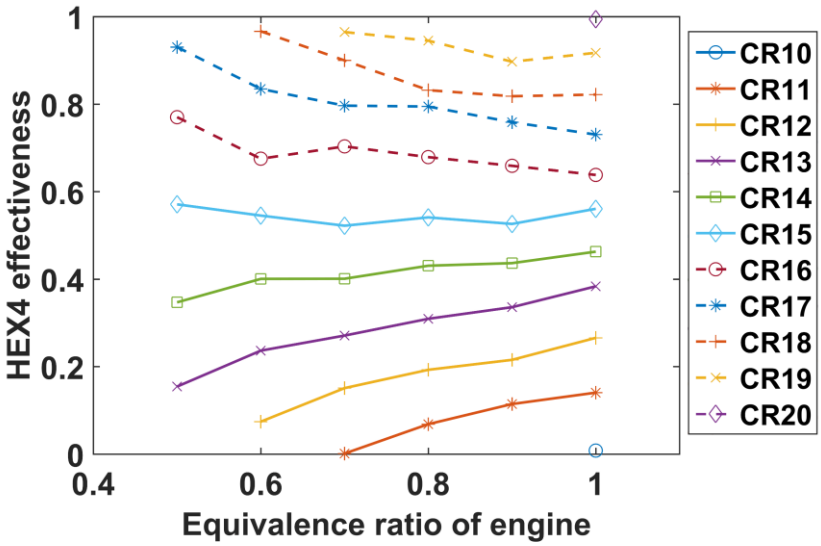

Figure 3.25 Heat effectiveness of HEX4

under Engine equivalence ratio and compression ratio variation

3.4 Summary

In this chapter, the engine size design is determined by conducting various simulations. The engine RPM and the fuel utilization of the fuel cell is discussed. For the engine RPM, 1800 RPM is recommended due to connecting to the power grid. Fuel utilization is chosen to be 70% which is general operating condition. The fuel utilization factor is changed from 70% to 80%, and then it is verified that the variation doesn't have a strong influence on the engine size. The effect of the compression ratio variation is also discussed, and then there is a discussion about the equivalence ratio variation. The engine equivalence ratio is chosen to be unity, which means a stoichiometric condition, and the compression ratio is recommended to be 13-16 range. For the 70% fuel utilization of the fuel cell, the engine size range is 21.2 L from 20.4 L under the conditions, as shown in Table 3.1. In that condition, it is expected that the hybrid system efficiency is higher and the NO_X emission is still low. For other power capacity system, the proper engine size could be selected by using the method suggested in this chapter. In the following chapter, the engine compression ratio is chosen among the range, and then the one of the engine size range is determined for analyzing the system operation at the design point operation and part-load operation.

Table 3.1 Proposed system design point

	Value
Fuel cell	
Fuel utilization (%)	70
Engine	
Speed (rpm)	1800
Equivalence ratio	1.0
Compression ratio	13-16
Displacement (L)	21.2-20.4

Chapter 4. Hybrid system operation

4.1 Introduction

In previous chapter, the engine specification is designed for a 250 kW-class MCFC system. For the engine design, various simulations, e.g. engine compression ratio, equivalence ratio variation and so on, are conducted, and then the engine specification is determined. The suggested engine specification range is shown in Table 3.1.

In this chapter, the hybrid system is analyzed at the design point and the off-design point operations. For the purpose, one engine specification is decided among the range of the suggested engine specification. In this thesis, the engine compression ratio of 15, which is a median value at the recommended range, is chosen, and thus the engine displacement size is 20.8 L. In Chapter 4.2, The hybrid system integrated the engine is analyzed at the design point operation. And the system is simulated at the off-design point, which means part-load operation in Chapter 4.3. The fueling level of 100 % means the level at the design point operation. A power plant is generally operated at constant power output for most of lifetime. But it still needs to run at various power levels under certain conditions. Thus it is important to verify the capability to cover various operating conditions for the new hybrid system. Therefore, in Chapter 4.3, the strategy to operate the hybrid system at part-load conditions is discussed.

4.2 System performances with design point operation

In this chapter, the hybrid system is analyzed at the design point operation. The main components characteristics, i.e. MCFC and HCCI engine, are discussed and the performance of the hybrid system is compared to the one of the standalone system.

4.2.1 System characteristics

MCFC

Table 4.1 shows the operating conditions for the MCFC stack at design point operation. The fuel utilization factor is 0.7 and the air utilization factor is 0.4. The inlet mixture temperatures of cathode and reforming channel (anode side) are chosen as 580 ^{o}C and 570 ^{o}C, which are typical values for MCFC operation. In the reforming channel, the fuel gas is reformed and preheated to the same temperature as the cathode (580 ^{o}C), before it enters the anode channel of the fuel cell.

Figure 4.1 shows the temperature change along the segments (1-25) within the unit cell. Here, each index corresponds to the inlet of the designated segment and, thus, there is the index of "26," which is the outlet of the 25th segment, or the outlet of the unit cell. Overall electrochemical reaction in the fuel cell is an oxidation reaction, which is net exothermic and, thus, will increase mixture temperature. However, it should be reminded that uniform heat transfer ($Q_{ref,i}$) to the reforming channel is assumed throughout the segments and the balance

between exothermicity from the electrochemical reaction and this heat transfer determines whether the mixture temperature will increase or decrease through each segment. As shown in Figure 4.1, temperature increases almost linearly in the earlier half of the segments, while it decreases in the later segments. This is because the electrochemical reaction is more vigorous with higher reactant concentrations in the former segments and the resultant exothermicity compensates the reformer heat requirement, but the reduced exothermic energy in the latter segments is not enough to cover the requirement. This is a small caveat from the assumption of uniform heat transfer for the reforming process, which, however, does not alter the overall conclusion in this study.

HCCI engine

Table 4.2 lists the operating conditions for HCCI engine at design point operation. The compression ratio is 15 and the engine speed is fixed at 1800 rpm. Inlet temperature is 308 ^{o}C, which is chosen to ensure proper HCCI combustion timing as explained below.

Figures 4.2 and 4.3 show the in-cylinder temperature and pressure profiles as a function of crank angle degree (CAD). As mentioned in Chapter 3, the maximum temperature during the engine cycle is under 1800 K shown in Figure 4.2. Therefore, it is expected that the NO_X emission doesn't produce in the engine. The combustion timing is near 5 ^{o} aTDC. In an HCCI engine, too early combustion timings at or before TDC can result in high peak combustion temperature and, thus, high NO_X emission with accompanying heat transfer

increase. On the other hand, significantly delayed combustion into the expansion stroke can lead to incomplete combustion due to the cooling effect from the expansion of in-cylinder mixture and thus unstable cycle with increased pollutant emissions such as carbon monoxide and unburned hydrocarbons.

Table 4.1 Operating conditions of MCFC stack at design point operation

		Value
Fuel utilization (%)		70
O_2 utilization (%)		40
Anode	Inlet mass flow rate (kg/s)	0.0381
	Inlet temperature (°C)	570
Cathode	Inlet mass flow rate (kg/s)	0.4933
	Inlet temperature (°C)	580

Table 4.2 Operating conditions of HCCI engine at design point operation

	Value
Displacement (L)	20.8
Compression ratio	15
Engine speed (rpm)	1800
Equivalence ratio	1
Intake temperature (°C)	308.5
Intake mass flow rate (kg/s)	0.1939

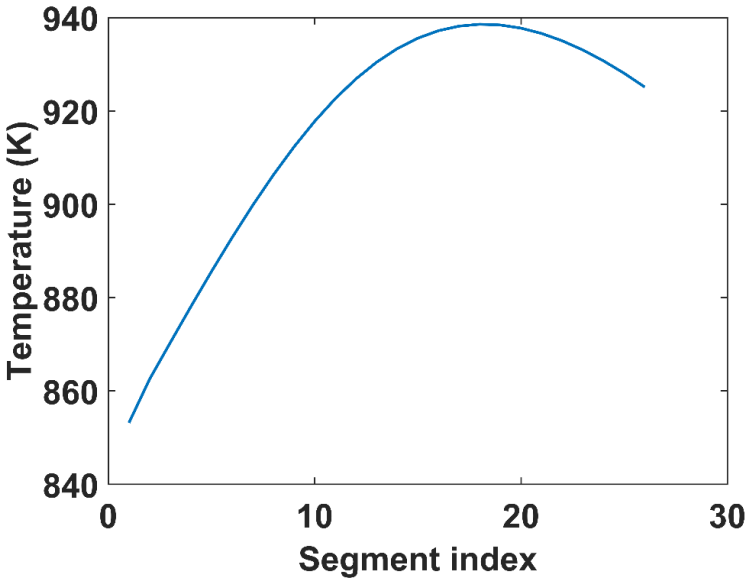

Figure 4.1 Temperature change in fuel cell

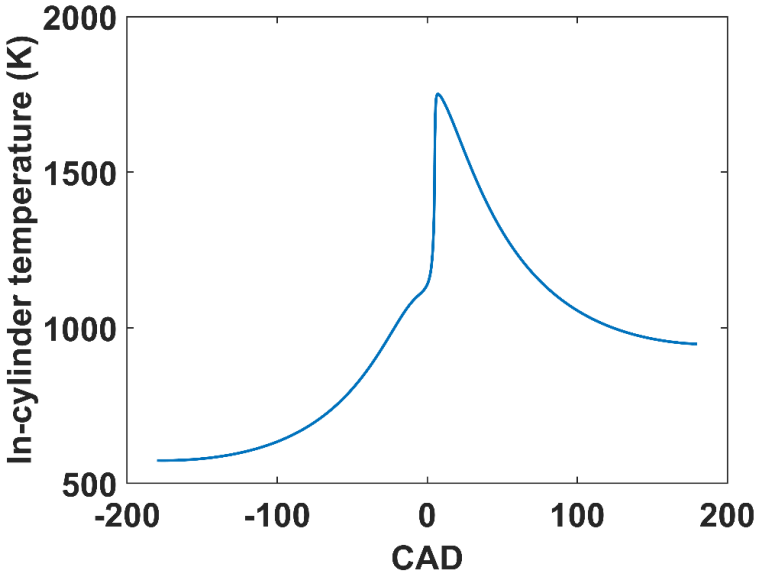

Figure 4.2 Engine in-cylinder temperature profile

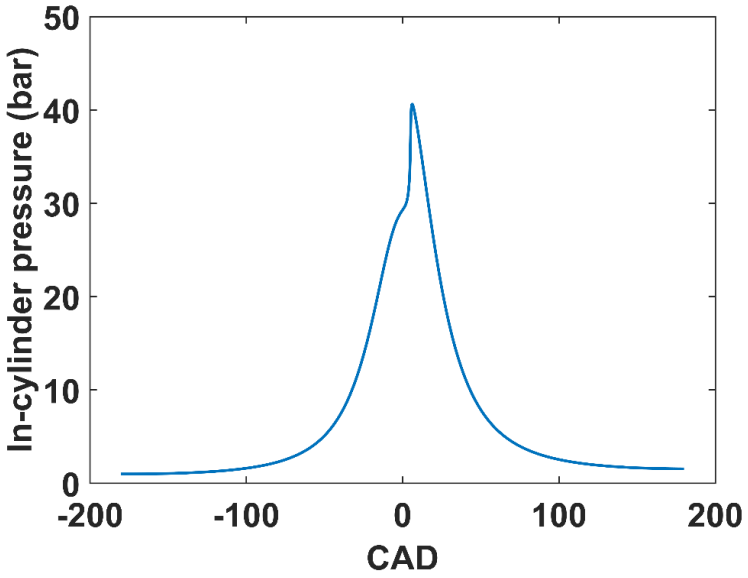

Figure 4.3 Engine in-cylinder pressure profile

4.2.2 Comparison between standalone and hybrid system performances

In this chapter, the configurations of the MCFC standalone system and the hybrid system are compared, and then the system performances at design point operation will be presented.

System configuration comparison

Figure 4.4 and 4.5 depict the MCFC standalone system and the MCFC-HCCI engine hybrid system configuration. And Table 4.3 and 4.4 show the thermodynamic stream properties for both systems. The standalone system is composed of MCFC, catalytic combustor, heat recovery steam generator (HRSG), and 4 heat exchanger (HEX). On the other hand, the hybrid system comprises MCFC, HCCI engine, and 5 HEX.

For both systems, all heat exchangers are considered to have counter-flow configuration so the cold fluid is allowed to approach the inlet temperature of the hot fluid. The highest effectiveness is limited at 85 % for all heat exchangers to consider more realistic operation. For the standalone system, the heat loss of the catalytic combustor is considered 2 % of the LHV of the inlet fuel. As the main purpose of this study is to understand the feasibility of the hybrid system and the performance relative to the standalone counterpart, we apply the same boundary conditions with S/C ratio of 2.5, fixed fuel flow rate, and oxidizer flow rates and their thermodynamic states for both systems. To elucidate the effect of introducing the HCCI engine instead of the catalytic burner, the inlet

conditions for the fuel cell stack are the same for both systems, which effectively isolate the effect of the fuel cell from two different configurations.

There are several stream properties to be pointed out. The inlet temperatures for the catalytic combustor and the HCCI engine (state 8 and state 10, respectively) are significantly different by ~100 ^{o}C. The inlet temperature for the catalytic combustor uses a general value of the standalone MCFC system, and the inlet temperature for the HCCI engine is adjusted to the higher temperature to keep the combustion timing and combustion efficiency as discussed in Chapter 3. The hybrid system yields more power output than the standalone system, thus the exhaust gas temperature of the system is about 115 ^{o}C. But the exhaust gas temperature of the standalone system is almost 393 ^{o}C, and thus the steam of 5 bar could be produced for using the waste heat of the standalone system.

Performance comparison

Table 4.5 shows the standalone and hybrid system performances at the design point operation. MCFC output is based on the modeling calculation by considering inverter efficiency of 96.5 %, and MCFC net output is evaluated by subtracting the balance of plant (BOP) power consumption. The MCFC power output is kept almost the same in both systems, but the HCCI engine in the hybrid system significantly increases the total system power by producing additional 46.8 kW, with an overall system efficiency of 57.1 %. Although the absolute efficiency number itself may not correspond to the figure that can be

achieved in the real system, it is important to note that around 20 % relative increase in system power and efficiency can be realized, which demonstrates the potential of the suggested new hybrid system.

Table 4.3 Thermodynamic stream properties of MCFC standalone system

				Mass concentration (%)						
State	T(°C)	P(bar)	ṁ(kg/s)	CH_4	CO	CO_2	H_2	H_2O	N_2	O_2
1	25	1	0.0381	26.3	-	-	-	73.7	-	-
2	120	1	0.0381	26.3	-	-	-	73.7	-	-
3	570	1	0.0381	26.3	-	-	-	73.7	-	-
4	652	1	0.1449	-	4.67	65.7	0.66	29.0	-	-
5	412	1	0.1449	-	4.67	65.7	0.66	29.0	-	-
6	244	1	0.1449	-	4.67	65.7	0.66	29.0	-	-
7	25	1	0.0490	-	-	-	-	-	76.7	23.3
8	200	1	0.1939	-	3.49	49.1	0.49	21.7	19.4	5.89
9	857	1	0.1939	-	-	54.6	-	26.1	19.4	-
10	25	1	0.3054	-	-	-	-	-	76.7	23.3
11	179	1	0.3054	-	-	-	-	-	76.7	23.3
12	497	1	0.4993	-	-	21.2	-	10.1	54.4	14.2
13	580	1	0.4993	-	-	21.2	-	10.1	54.4	14.2
14	652	1	0.3925	-	-	6.98	-	12.9	69.3	10.9
15	550	1	0.3925	-	-	6.98	-	12.9	69.3	10.9
16	393	1	0.3925	-	-	6.98	-	12.9	69.3	10.9
17	103	1	0.3925	-	-	6.98	-	12.9	69.3	10.9
18	25	5	0.0500	-	-	-	-	100	-	-
19	157	5	0.0500	-	-	-	-	100	-	-

Table 4.4 Thermodynamic stream properties
of MCFC-HCCI engine hybrid system

				Mass concentration (%)						
State	T(°C)	P(bar)	ṁ(kg/s)	CH_4	CO	CO_2	H_2	H_2O	N_2	O_2
1	25	1	0.0381	26.3	-	-	-	73.7	-	-
2	120	1	0.0381	26.3	-	-	-	73.7	-	-
3	570	1	0.0381	26.3	-	-	-	73.7	-	-
4	652	1	0.1449	-	4.67	65.7	0.66	29.0	-	-
5	472	1	0.1449	-	4.67	65.7	0.66	29.0	-	-
6	377	1	0.1449	-	4.67	65.7	0.66	29.0	-	-
7	25	1	0.0490	-	-	-	-	-	76.7	23.3
8	308	1	0.1939	-	3.49	49.1	0.49	21.7	19.4	5.89
9	508	1	0.1939	-	-	54.6	-	26.1	19.4	-
10	25	1	0.3054	-	-	-	-	-	76.7	23.3
11	300	1	0.3054	-	-	-	-	-	76.7	23.3
12	363	1	0.3054	-	-	-	-	-	76.7	23.3
13	429	1	0.4993	-	-	21.2	-	10.1	54.4	14.2
14	580	1	0.4993	-	-	21.2	-	10.1	54.4	14.2
15	652	1	0.3925	-	-	6.98	-	12.9	69.3	10.9
16	465	1	0.3925	-	-	6.98	-	12.9	69.3	10.9
17	282	1	0.3925	-	-	6.98	-	12.9	69.3	10.9
18	115	1	0.3925	-	-	6.98	-	12.9	69.3	10.9

Table 4.5 Performance results of Standalone system and Hybrid system

Parameter	Standalone system	Hybrid system
LHV CH_4 (kW)	500	500
Fuel utilization (%)	70	70
*MCFC output (kW)	251	251
BOP power consumption (kW)	14.9	12.6
**MCFC net output(kW)	237	239
MCFC net efficiency (%)	47.3	47.7
***Engine output (kW)	-	46.8
Engine efficiency (%)	-	25.7
Net power output (kW)	237	286
System electrical efficiency (%)	47.3	57.1

→ For standalone system, heat recovery is 133 kW, and the thermal efficiency is 26.6 %.

*MCFC output = MCFC gross output × Inverter efficiency

**MCFC net output = MCFC output – BOP power consumption

***Engine output = (Engine gross output – Friction loss) × Generator efficiency

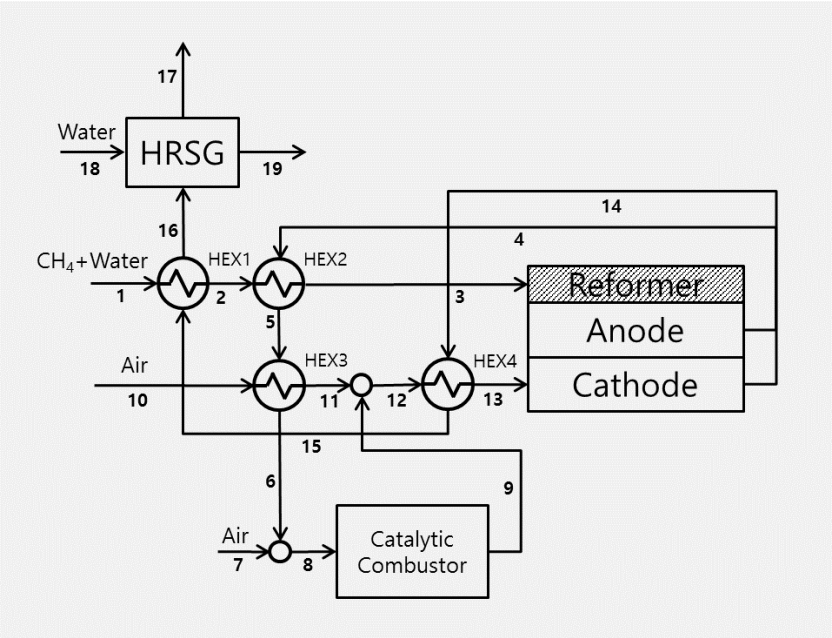

Figure 4.4 MCFC standalone system configuration

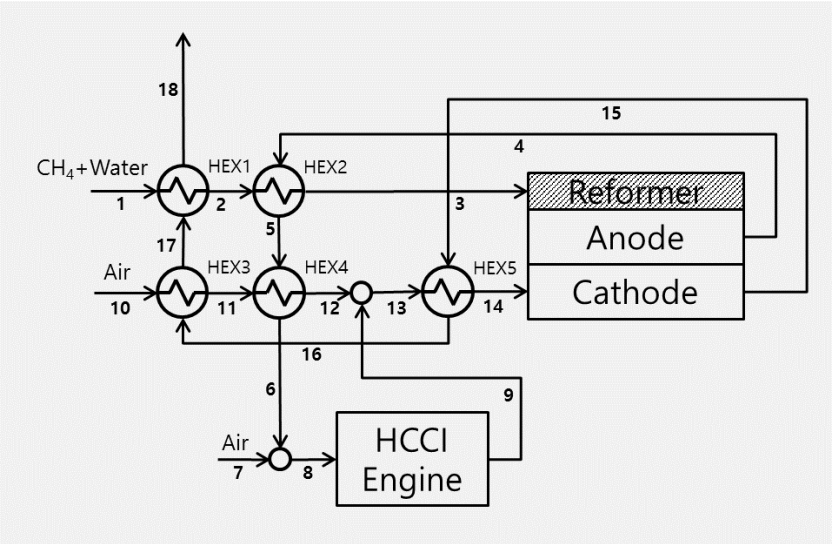

Figure 4.5 MCFC-HCCI engine hybrid system configuration

4.3 System performances with part-load operation

In this chapter, the hybrid system is analyzed at the off-design point operation, which means part-load operation in this thesis. For the part-load operation, the system fueling level is changed 75 % to 100 % which is a fueling level of the design point operation. The fueling level is based on the methane flow rate. The reason for choosing the fueling level, instead of the power output level at the part-load conditions, is for convenience purpose in conducting simulation. But the power output level variation is almost same with fueling level change in this simulation, due to the similar efficiencies.

4.3.1 Operating strategy for part-load operation

For operating the system at the part-load, the systematic control strategy is required. The hybrid system has MCFC and HCCI engine which are operable independently. Thus, when the operating condition is changed, new control strategy is needed for driving the two components harmoniously.

If the fuel flow rate of the system is reduced, the air flow rates of the cathode inlet and engine inlet need to be changed. Figure 4.6 shows the flow rates under the fueling level variation. Firstly, when the fueling level is reduced for part-load operation, the fuel mass flow rate (state 1) decreases with fixed S/C ratio of 2.5 and fuel utilization of 70 %. Secondly, air mass flow rate (state 10) of the cathode inlet is also reduced due to fixed O_2 utilization of 40 %. Thirdly, the mass flow rate of air entering the engine increases as the fueling level is down. The engine size is determined at the design point operation, but

the fuel mass flow rate entering the engine, i.e. the mass flow rate of the anode off-gas, is reduced as the fueling level decreases. Therefore, the mass flow rate of air entering the engine should be increased for preventing negative pressure of the engine intake charge, which could cause the engine efficiency drop.

The part-load operation is conducted at the fueling level range of 75-100 %. As the fueling level falls down, the absolute amount of reaction in the fuel cell also decreases, thus the temperature rise in the fuel cell is also reduced. The shortage of the temperature rise causes an excessive operation of heat exchangers. As mentioned earlier, the heat effectiveness of HEX is under 85 % in this thesis. But, the heat effectiveness of ~90 % is required for operating at the fueling level of 85 %, the effectiveness of ~95% is needed at the fuel level of 75 % and 80 % conditions.

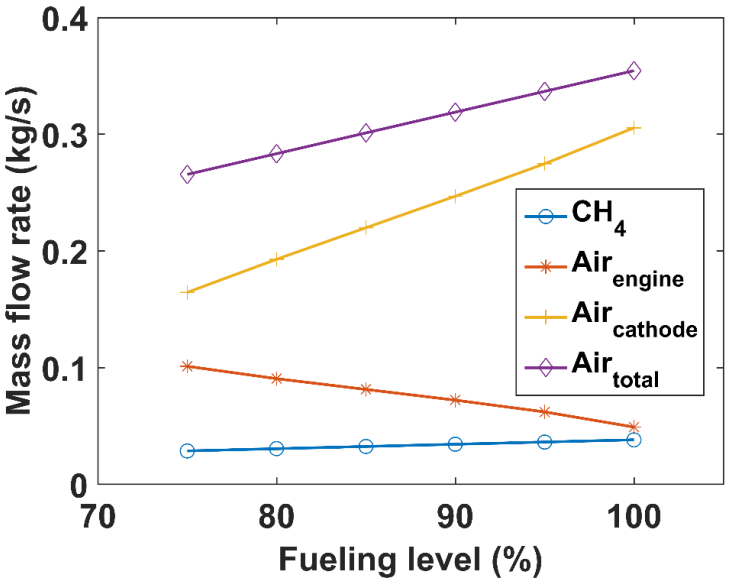

Figure 4.6 Mass flow rate of fuel and air at the part-load operation

4.3.2 System performances

Figure 4.7 shows the system power output and efficiency under the fueling level variation. As fueling level decreases, the system power output is also reduced, but the efficiency of the system increases a little. At the lower fueling level, the fuel cell operates at higher voltage and lower current density, which induces lower fuel cell losses and slightly increased efficiency. The gross efficiency of HCCI engine also increases a bit due to increased specific heat ratio. At the lower fueling level, the engine needs more air flow rate, which means that the equivalence ratio is lower, and thus specific heat ratio of the intake gas mixture rises. However, the friction work of the engine is almost same under the fueling level variation. Thus, the engine net efficiency decreases when the fueling level is reduced. Nevertheless, the MCFC net efficiency increase has more influence on the total system net efficiency than the engine net efficiency, hence the system net efficiency is slightly increased when the fueling level is reduced.

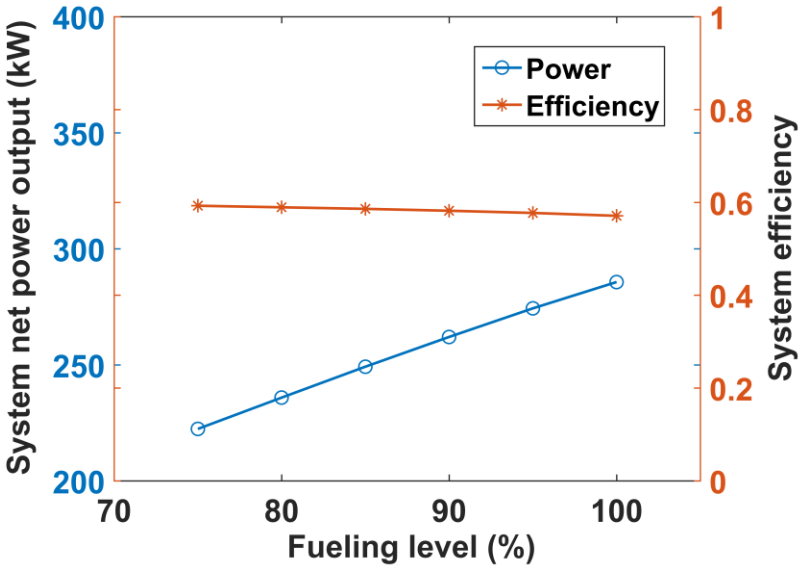

Figure 4.7 System power output and efficiency at the part-load operation

4.4 Summary

In this chapter, the proposed hybrid system is analyzed at the design point and off-design point operation. At the design point operation, the engine produces additional power output of 46.8 kW, and thus the hybrid system efficiency is increased 9.8 % compared to the standalone system efficiency. For operating the system at part-load conditions, some systematic control strategies are required. By using the strategies, the fueling level could be down to 75 % of the designed level although the heat exchangers need to operate excessively. In the end, it is confirmed that the system efficiency increases a bit as the fueling level is reduced. It is confirmed that the hybrid system operates with higher efficiency than the standalone system at the design point operation, and the system can still drive at the off-design operation. Consequently, it is known that the hybrid system is promising. In the next chapter, the system feasibility will be also verified with an economic assessment.

Chapter 5. Economic analysis

5.1 Introduction

In previous chapter, the MCFC-HCCI engine hybrid system design is conducted and the feasibility of the hybrid system is verified by thermodynamic analysis. In this chapter, the economics feasibility of the system would be discussed. The economic analysis is conducted by calculating levelized cost of electricity (LCOE) which is the total costs, including the plant construction cost, fuel cost, operating & maintenance cost, and so on, divided by energy production. The value is good to compare various power generating technologies easily although the lifetime or capacity of the technologies are different each other. In this thesis, however, the economic evaluation is conducted for comparing between fuel cell standalone system and the suggested hybrid system, not for comparing other technologies, e.g. solar, wind, geothermal power generation, and so on.

In this thesis, the LCOE value is calculated by using total revenue requirement (TRR) method, which is suggested by Electric Power Research Institute (EPRI) and explained in Ref. [52]. By using this method, various studies performed the economic analysis [53-57]. Xicoy Almirall analyzed the economic analysis about the wet sulfuric acid plants [53]. Lee performed the economic analysis of SOFC hybrid system [54, 55]. He studied life cycle assessment (LCA) of the SOFC standalone system, gas turbine hybrid system, and engine hybrid system, respectively. Park also analyzed thermodynamic and economic evaluation about SOFC hybrid system [56, 57]. He presented that the

hybrid system is better than the SOFC standalone system in point of efficiency and economics. Besides the aforementioned researches, there are various literatures referenced by using the TRR method.

5.2 Economic analysis methodology

As mentioned previously, the TRR method is adopted by calculating the LCOE value. The method evaluates the annual revenue requirement adding up the capital recovery cost including the depreciation cost, return on investment, carrying charge including tax and insurance, fuel cost, and operating & maintenance cost. And then the value is divided by the annual power production.

The TRR method can be conducted by the following 3 steps [52].

Step 1. Estimate the total capital investment (TCI).

Step 2. Calculate the total revenue requirement (TRR) based on the assumptions about the economic and financial parameters.

Step 3. Calculate the levelized cost (LCOE).

In this chapter, firstly, total capital investment cost is evaluated. The cost is composed of fixed-capital investment and other outlays. The fixed-capital investment (FCI) cost includes purchased-equipment costs, installation cost, land cost, and so on. Besides the costs, there are startup cost, working capital, and allowance for funds used during construction in other outlays. Secondly, fuel costs and operating & maintenance cost are calculated, and then the total

revenue requirement is evaluated based on the assumptions about the economic and financial parameters. Finally, levelized cost of electricity is calculated by using TRR value and the amount of power production. Most of cost evaluation is conducted with base year of 2014, and the lifetime of power-generation plant is assumed to be 20 years.

5.2.1 Cost of equipment

The MCFC standalone system and the suggested hybrid system are composed of MCFC stack, blower, pump, inverter, heat exchanger, heat recovery steam generator (HRSG), catalytic combustor (CC), HCCI engine, and other components. Purchase cost of each component are evaluated by using cost functions which are referenced by various bibliographies [52-65]. Table 5.1 shows the equipment cost functions. Each costs functions are made in other year, and thus the evaluated costs should be converted to the values based on reference year. In this study, 2014 is used for the reference year, so all the evaluated costs are recalculated in 2014-year dollars by using chemical engineering plant cost indices (CECPI), shown in Eqn. 5.1.

$$PEC_{ref} = PEC_{source} \frac{CECPI_{ref}}{CECPI_{source}} \qquad (5.1)$$

In this study, the lifetime of power-generation plant and most of equipment is assumed to be 20 years, but the lifetime of MCFC stack is assumed as 5 years due to the limit of present technology level. Thus the stack cost should be

considered about the cost of replacing the stack every 5 years.

Stack

MCFC stack cost cites the NREL's report's function and Korner's report [58, 59]. NREL estimates price changes of MCFC system year by year due to the potential of cost reduction as developing technology [58]. Korner mentions that the MCFC stack price is about 60 % of the system cost [59]. Thus, in this thesis, the MCFC stack cost is determined the NREL's function multiplying by 0.6. But the price fluctuation of the MCFC could be greater than the one of NREL's estimation due to the speed of development. Therefore, it might be desirable that the LCOE value, which is calculated in this study, is just for comparing between standalone and hybrid system of this thesis.

Reformer and catalytic combustor

The MCFC system of this study adopts the internal reforming, but the cost should be still considered. The reformer cost is calculated by using Lee's modified function [54, 55]. The function is based on the cost function of Calise et al. and Oyarzabal, and reflects the recent market trend of catalyst [54, 55, 60, 61]. The cost function of catalytic combustor also adopts the same function. The catalyst cost is a lot of portion in total cost of the catalytic combustor like a reformer.

Engine

The HCCI engine cost is evaluated by using the cost function reflecting market price of diesel generators and manufacturing cost. The costs of diesel generators are investigated, and then the cost function is developed by considering manufacturing cost for remodeling to perform HCCI operation. Lee also investigated the diesel generator price, and then developed engine cost function for relatively smaller size [54, 55]. But in this thesis, the engine size is about 20 L, thus the cost function is not matched with the engine. For the reason, the engine cost is investigated for large-size engine generator of which range is 10 L to 40L, and then the cost function is made, shown in table 5.1, and Figure 5.1.

Other components

For the inverter, the cost is evaluated by using the function of Chan et al., which calculates the cost of inverter based on the power output of the fuel cell stack [62]. The cost function of Calise et al. is used to calculate the cost of heat exchangers [50]. Based on the area of the HEX, the cost is evaluated. For blower and pump costs, functions, made by Chieasa et al. and Frangopolous, respectively, are used [63, 64]. Finally, heat recovery steam generator cost is evaluated by using the function of Nikhil et al. [65].

Table 5.1 Equipment cost functions

Component	Cost function	Reference year		Source
		Year	CECPI	
MCFC stack	$0.6 \times 15908 \times e^{-0.096\times(year-1992)} \times \dot{W}_{MCFC}$ (5.2)	2005	468.2	[58,59]
Reformer	$130 \times \left(\frac{A_R}{0.093}\right) + 3240 \times V_R + 21280.5 \times V_R$ (5.3)	2001	394.3	[54,55, 60,61]
Inverter	$10^5 \times \left(\frac{\dot{W}_{MCFC}}{500}\right)^{0.7}$ (5.4)	2002	395.6	[62]
Catalytic combustor	$130 \times \left(\frac{A_{CC}}{0.093}\right) + 3240 \times V_{CC} + 21280.5 \times V_{CC}$ (5.5)	2005	468.2	[54,55, 60,61]
HCCI engine	$1.1 \times \left(3984.5 \times V_{engine}^{0.7601}\right)$ (5.6)	2016 (April)	537.5	
Heat exchanger	$130 \times \left(\frac{A_{HEX}}{0.093}\right)$ (5.7)	2005	468.2	[60]
Fuel blower	$91562 \times \left(\frac{\dot{W}_{FB}}{455}\right)^{0.67}$ (5.8)	2003	402.3	[63]
Air blower	$91562 \times \left(\frac{\dot{W}_{AB}}{455}\right)^{0.67}$ (5.9)	2003	402.3	[63]
Pump	$442 \times \dot{W}_P^{0.71} \times 1.41 f_n \quad f_n = 1 + \frac{1-0.8}{1-\eta_P}$ (5.10)	1991	362.3	[64]
Heat recovery steam generator	$6750 \times \left[\left(\frac{Q_{ec}}{\Delta T_{lm,ec}}\right)^{0.8} + \left(\frac{Q_{ev}}{\Delta T_{lm,ev}}\right)^{0.8}\right] + 21276 \times \dot{m}_{steam} + 1184.4 \times \dot{m}_{gas}^{1.2}$ (5.11)	2002	395.6	[65]

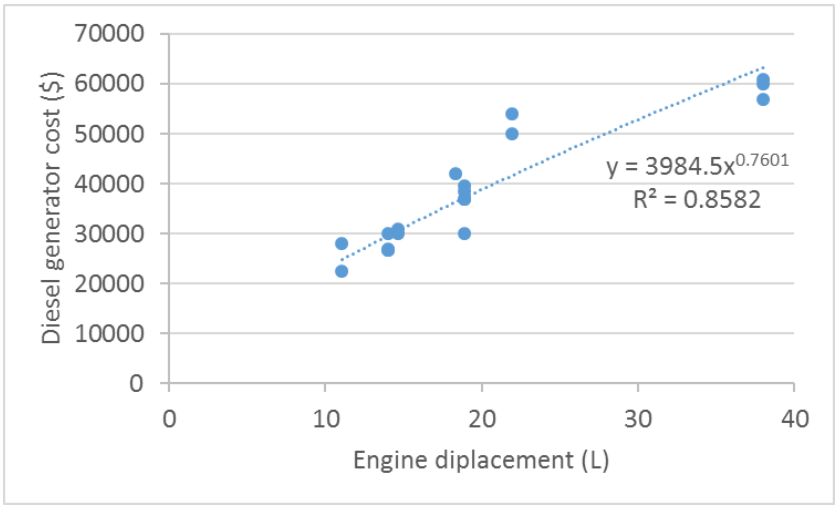

Figure 5.1 Investigated diesel generator costs

5.2.2 Total capital investment

In Chapter 5.2.1, purchased-equipment costs are evaluated by using various equations. For estimating total capital investment of the plant, various costs, which includes installation, piping, land, startup costs and so on, should be also calculated. Thus, in this thesis, the costs are estimated based on the purchased-equipment cost, multiplying by proper factors. The factor is shown in Table 5.2.

It should need financing plan and economic assumptions for calculating allowance for funds used during construction (AFUDC). The economic assumptions and financing plan are shown in Table 5.3, which includes construction, financing plans, operating, interest, and tax parameters. The AFUDC is a sort of interest, thus it means the time value of money. It is important to organize the time for each expenses, which is shown in Table 5.4. The working cost is disbursed at the end of 2017, which is not paid in construction period. Thus, the working cost is not considered for calculating the AFUDC. For evaluating this time value, it uses the Eqn. 5.12. *F* means future value of money, and *P* means present value of money.

$$F = P \times (1 + i_{eff})^n \qquad (5.12)$$

Table 5.2 Estimation of total capital investment [52, 54, 55]

I. Fixed capital investment	
Direct costs	
Onsite costs	
Purchased-equipment costs	
Equipment 1	
Equipment 2	
…	
Equipment N	
Total purchased-equipment cost (PEC)	
Purchased-equipment installation	33% of PEC
Piping	35% of PEC
Instrumentation and controls	12% of PEC
Electrical equipment and materials	13% of PEC
Total onsite costs	
Offsite costs	
Land	4.55% of PEC
Civil, structural, and architectural work	21% of PEC
Service facilities	35% of PEC
Total offsite costs	
Total direct costs (DC)	
Indirect costs	
Engineering and supervision	8% of DC
Construction costs and contractor's profit	15% of DC
Sum	123% of DC
Contingency	15% of above sum
Total indirect costs (IC)	
Total fixed-capital investment (FCI)	

Plant facility investment (PFI)	FCI-Land cost
II. Other outlays	
Startup costs	10% of FCI
Working capital	15% of TCI
Costs of licensing, research and development	0
Allowance for funds used during construction	In detail at Chapter 5.2.2
Total other outlays	
Total capital investment (TCI)	

Table 5.3 Economic assumptions and parameters

Plan for construction	
Construction period (year) (Jan. 2016 - Dec. 2017)	2
Start of commercial operation	Jan. 2018
Parameter for operating	
Economic lifetime for all components except MCFC stack (years)	20
Economic lifetime for MCFC stack (years)	5
Average annual capacity factor (%)	85
Fixed O&M cost (% of PFI) [54, 55, 56]	6.3
Variable O&M cost (% of annual fuel cost) [56]	1
Unit cost of fuel (natural gas, $/MJ-LHV-in 2014) [66]	0.021
Parameter for interest [57]	
Annual inflation rate (%)	2.5
Nominal escalation rate of all services and goods except fuel (%)	2.5
Fuel escalation rate (%)	3
Plan for financing [54, 55, 57]	
Common Equity	
Fraction (%)	35
Required annual return (%)	15
Debt	
Fraction (%)	50
Required annual return (%)	10
Resulting average cost of money (%)	12
Allocation of plant-facilities investment (%)	
Jan. 2016 - Dec. 2016	40
Jan. 2017 - Dec. 2017	60

Parameter for tax [57]	
Tax-related plant lifetime (years)	15
Income tax rate for company (%)	24
Insurance rate and other taxes rate (%)	2

Table 5.4 Release dates for plant expenses

Expense concept	**Release date**
Land	1st of Jan., 2016
40% of PFI	1st of July, 2016
60% of PFI	1st of July, 2017
Startup costs	1st of July, 2017
AFUDC	31th of Dec., 2017
Working capital	31th of Dec., 2017

5.2.3 Total revenue requirement

Total revenue requirement is the sum of carrying charges and expenses. Carrying charges is a kind of investment cost, which can be capitalized. The expenses, however, include fuel cost and operating & maintenance costs, which should be paid immediately from revenue. Thus these costs couldn't be capitalized. Carrying charges contain capital recovery, return on investment, income taxes, other taxes and insurance. These cost should be considered about the depreciation. Therefore, it is assumed that the tax lifetime is 15 years and then the depreciation is concerned by using the modified accelerated cost recovery system (MACRS) method.

In this study, fuel is natural gas, which is approximated as methane. The cost is calculated by using Eqn. 5.13. Unit cost of fuel is 0.021 $/MJ-LHV, which references the IEA reports [66]. The capacity is the annual capacity factor (85 %) in Table 5.3, which means the plant will drive for 7446 h out of annual total load (8760 h).

$$\mathrm{FC} = \text{unit cost} \times \mathrm{LHV} \times \dot{m}_{fuel} \times 8760 h/yr \times capacity \times 3600 s/h \quad (5.13)$$

The operating and maintenance (O&M) costs is composed of fixed costs and variable costs. The fixed costs include the labor cost for the operating and maintenance, marketing cost, administration cost, material cost for O&M, and so on. The variable costs mean catalyst cost, cost of supplies except fuel, like water, and so on. The annual fixed O&M cost is calculated as 6.3 % of PFI, and

the annual variable O&M cost is evaluated as 1 % of annual fuel cost.

5.2.4 Levelized cost of electricity

In previous chapter, the annual total revenue requirement (TRR) was evaluated, but the TRR value is changed year by year due to decreasing carrying charge and increasing fuel, O&M costs. Thus, for the correct comparison of systems, the levelized value should be needed, as shown in Figure 5.2. To calculate the levelized cost, a capital recovery factor (CRF) and a constant-escalation levelization factor (CELF) can be used.

Firstly, the CRF is shown in Eqn. 5.14. *P* is a present value of money, and *A* is levelized to equal-amount money, and the transactions arise at the end of each year. i_{eff} is the annual effective rate of return, which can be calculated according to the financing plan in Table 5.3, as shown in Eqn. 5.16.

$$\mathrm{CRF} = \frac{A}{P} = \frac{i_{eff}(1+i_{eff})^n}{(1+i_{eff})^n - 1} \qquad (5.14)$$

$$\mathrm{A} = CRF \sum_{j=1}^{n} P_j \qquad (5.15)$$

$$\mathrm{i}_{eff} = f_{ce} i_{ce} + f_{ps} i_{ps} + f_d i_d \qquad (5.16)$$

Secondly, the CELF is evaluated with CRF, the escalation rate, as shown in Eqns. 5.17 and 5.18. P_0 means the cost at the beginning of the first year, *A* is the levelized cost, which is returned at the end of each year.

$$CELF = \frac{A}{P_0} = \frac{k(1-k^n)}{1-k} CRF \qquad (5.17)$$

$$\mathrm{k} = \frac{1+r_n}{1+i_{eff}} \qquad (5.18)$$

In this thesis, the levelized TRR value (TRR_L) is calculated by multiplying the sum of the annual TRR with the CRF, where i_{eff} is required annual return and n is plant lifetime. The levelized fuel cost (FC_L) and O&M cost ($O\&M_L$) are evaluated by using CELF formula. For the levelized fuel and O&M costs, r_n are the fuel escalation rate and nominal escalation rate, respectively, shown in Table 5.3. The levelized carrying charge (CC_L) can be derived from the calculated TRR_L, FC_L and $O\&M_L$, shown in Eqn. 5.19.

$$CC_L = TRR_L - FC_L - O\&M_L \qquad (5.19)$$

The main product unit cost (MPUC), which means the levelized cost of electricity, can be evaluated from the TRR_L, shown in Eqn. 5.20. By-product value (BPV) means the levelized cost-benefit of selling steam, which is recovered from waste-heat of the plant in the heat recovery steam generator (HRSG). Main-product quantity is the annual electric energy production (kWh/yr) from the plant.

$$\mathrm{MPUC} = \frac{TRR-BPV}{MPQ} \qquad (5.20)$$

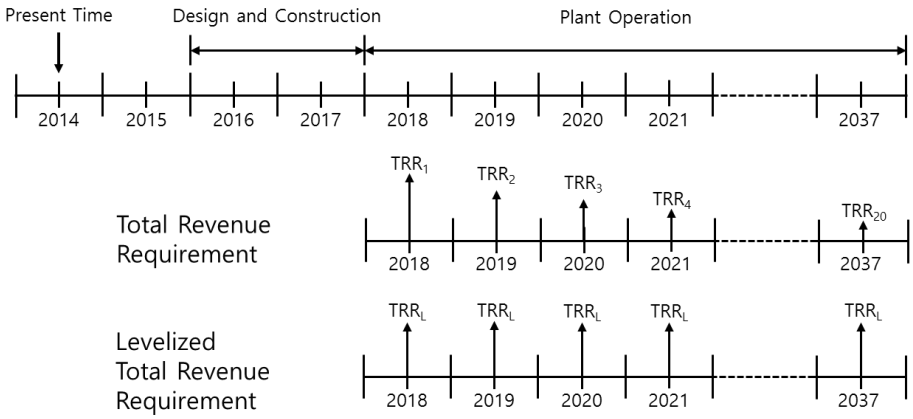

Figure 5.2 The time scale used for calculation of LCOE

5.3 Results of LCOE calculation

By using the TRR method, it can be evaluated for LCOE of MCFC standalone system and MCFC-HCCI engine hybrid system. The LCOE for both systems are calculated by considering various components, i.e. stack, inverter, engine, fuel blower, water pump, air blower, and so on.

The two systems are composed of slightly different components shown in Figures 4.4 and 4.5, thus the LCOE values of the systems can be dissimilar. In following chapters, LCOEs of the standalone system and hybrid system are discussed, and there is sensitivity analysis about some factors.

5.3.1 LCOE of MCFC standalone system

The economic analysis is conducted about the aforementioned standalone system in Chapter 4. The system is composed of MCFC stack, inverter, blowers, pumps, heat exchangers, HRSG, catalytic combustor, and so on. The purchased-equipment costs are calculated by using the functions in Table 5.2. The results are listed in Table 5.5.

It is assumed that the MCFC stack lifetime is 5 years, thus three replacement of stack will be required during the plant lifetime of 20 years. The stack cost includes total four stacks costs in Table 5.5, thus the portion of MCFC stack occupies most of the system cost. The fuel cell system, however, is still developing technology. If the stack lifetime increases 10 years or 20 years that is same with the plant lifetime, the cost of the system will be decreased so much. For the same reason, the PEC and LCOE of the system will be reduced if the

stack cost is down due to the developing technology. Therefore, in this thesis, sensitivity analysis is conducted about the factors that are stack lifetime and stack cost.

The sensitivity about the stack lifetime is analyzed at the lifetime of 5, 10, and 20 years. Figure 5.3 depicts the levelized cost of electricity and system cost, which is total purchased-equipment cost, under the stack lifetime variation. As the stack has the lifetime of 10 years, the LCOE could be reduced to 0.425 $/kWh from 0.504 $/kWh, which is about 15.7 % relative decrease. If the stack lifetime increases to 20 years, the LCOE would be 0.395 $/kWh that is about 21.6 % reduction. System cost also shows similar trend with the LCOE variation.

It is also analyzed at the stack cost of 50-100 %, where the 100 % corresponds to the original stack cost in previous analysis. Figure 5.4 shows the LCOE and the system cost under the stack cost variation. The LCOE and the system cost are definitely reduced as the stack cost is down. If the stack cost can be reduced by 50 % of the original level, the LCOE would be down to 0.374 $/kWh that is a 25.8 % reduction, and the system cost would be also decreased to 2069 $/kW. Because the fuel cell is the developing technology, it is anticipated that the system would be more economical than the current status.

Table 5.5 Purchased-equipment cost of MCFC standalone system

Components	PEC (US$ in mid-2014)	%
MCFC stack	637,483	78.87
Internal reformer	25,339	3.14
Inverter	92,278	11.42
Air blower (for cathode)	10,932	1.35
Air blower (for C/C)	2060	0.25
Fuel blower	1,635	0.20
Water pump	352	0.04
Heat exchangers	17,197	2.13
Heat recovery water pump	2,506	0.31
Heat recovery steam generator	12,774	1.58
Catalytic combustor	5,682	0.70
Total	808,238	100.00
System cost ($/kW)	3416.92 (US $ in mid-2014)	

Table 5.6 LCOE of MCFC standalone system

	Cost (US$ in mid-2014)	%
Fuel cost	410,801	41.79
O&M costs	73,602	7.49
Carrying charge cost	498,614	50.72
Total revenue requirement	983,016	100.00
By-product value	94,710	
LCOE	0.504 $/kWh	

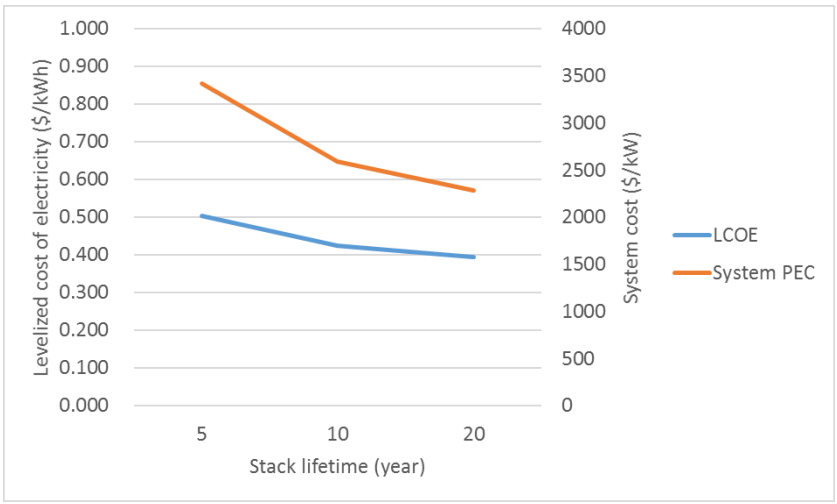

Figure 5.3 LCOE and system cost of standalone system under stack lifetime variation

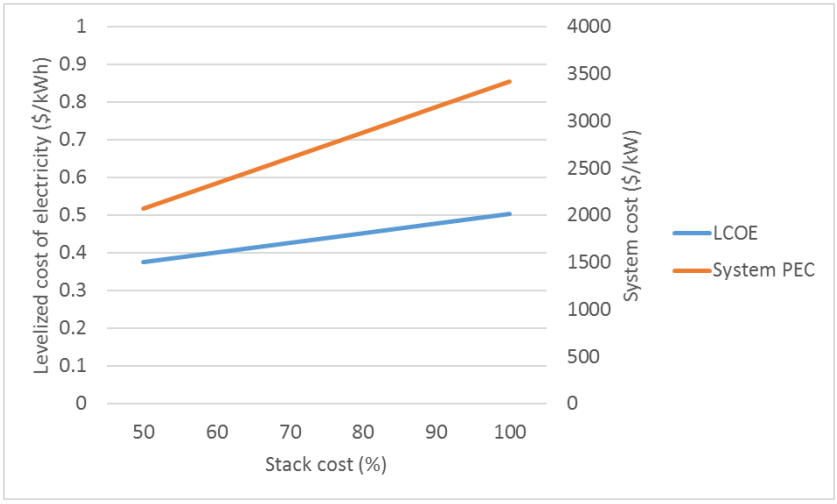

Figure 5.4 LCOE and system cost of standalone system under stack cost variation

5.3.2 LCOE of MCFC-HCCI engine hybrid system

The economic analysis is also conducted for MCFC-HCCI engine hybrid system where the catalytic combustor is replaced by the HCCI engine. Thus, the results of the hybrid system are slightly different with those of the standalone system. Table 5.7 and 5.8 show the results of the economic analysis about the hybrid system. The hybrid system cost, which means total purchased-equipment cost, is 2986 $/kW, and the LCOE is 0.477 $/kWh that is 5.37 % lower than that of the standalone system. The more detail comparison is in next chapter.

The sensitivity about the stack lifetime is also analyzed with the hybrid system. Figure 5.5 shows the LCOE and system cost change under the stack lifetime variation. If the stack lifetime is improved to 10 years and 20 years, the LCOE is reduced by 13.9 % and 18.9 %, respectively.

Figure 5.6 depicts the results of the analysis under the stack cost variation. When the stack cost decreases, the LCOE and the system cost are also reduced likewise the previous results of the standalone system. If the stack cost is half of the cost used in this thesis, the LCOE of the hybrid system can decline to 0.370 $/kWh that is a 22.4 % reduction. The stack cost has a high proportion of the system cost, so if the stack technique is improved more, the hybrid system could be more economical and competitive system.

Table 5.7 Purchased-equipment cost of MCFC-HCCI engine hybrid system

Components	PEC (US$ in mid-2014)	%
MCFC stack	637,483	74.73
Internal reformer	25,339	2.97
Inverter	92,278	10.82
Air blower (for cathode)	10,932	1.28
Air blower (for engine)	2,059	0.24
Fuel blower	1,635	0.19
Water pump	352	0.04
Heat exchangers	35,825	4.20
HCCI engine	47,152	5.53
Total	853,054	100.00
System cost ($/kW)	2986.05 (US $ in mid-2014)	

Table 5.8 LCOE of MCFC-HCCI engine hybrid system

	Cost (US$ in mid-2014)	%
Fuel cost	410,801	40.47
O&M costs	77,465	7.63
Carrying charge cost	526,922	51.90
Total revenue requirement	1,015,188	100.00
LCOE	0.477 $/kWh	

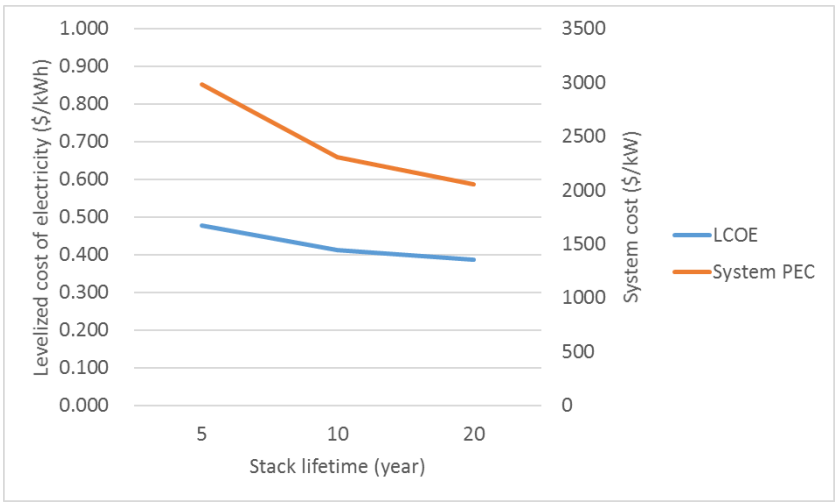

Figure 5.5 LCOE and system cost of hybrid system under stack lifetime variation

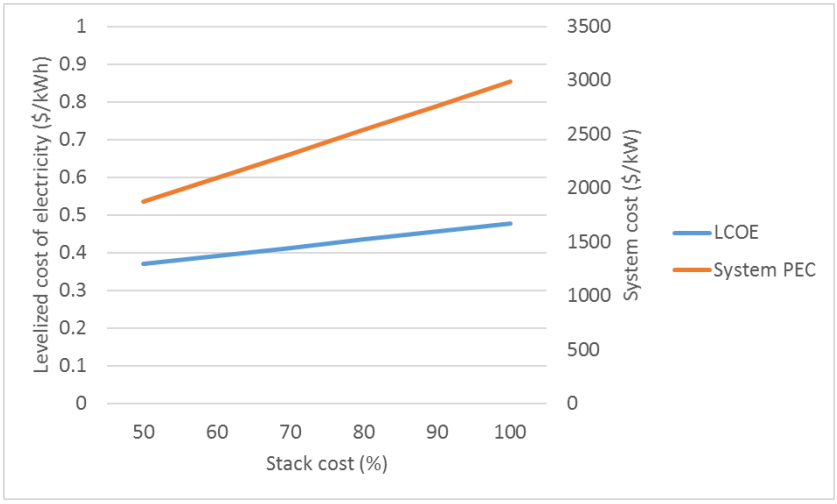

Figure 5.6 LCOE and system cost of hybrid system under stack cost variation

5.3.3 Comparison of the standalone system and hybrid system

The LCOE results of standalone system and hybrid system are shown in Figure 5.7. The standalone system, especially, is divided into two types which are the system with selling steam and without selling steam. In case of hybrid system, the left-over fuel is converted to power output in the engine, thus the system outlet temperature is lower than that of standalone system. So the hybrid system could not recovery the waste-heat of the system. The LCOE is reduced by 8.61 % when it sells the steam in the standalone system. Although the standalone system without selling steam doesn't pay the cost for HRSG, the LCOE is higher than that of the original standalone system due to high effect of selling the steam. The LCOE of the hybrid system can be decreased by 5.4 % and 13.5 % compared with the LCOE of the standalone system selling steam and not, respectively. The hybrid system has the more number of heat exchangers due to the different temperature conditions at the engine inlet and outlet. Thus, the heat exchanger cost is more than that of the standalone system, shown in Tables 5.5 and 5.7. Consequently, the hybrid system cost is higher than that of standalone system due to the HEX cost, adding the HCCI engine and changing other components. The ratio of carrying charge is higher at the hybrid system in the same context. The LCOE of the hybrid system, however, is lower than that of the standalone system due to yielding more power output in the engine.

As shown in earlier, the LCOE of the standalone system is affected by selling the steam or not. That is, the steam cost could also influence the LOCE

of the standalone system. For this reason, the LCOE change is analyzed under the steam cost variation. Figure 5.8 depicts the LCOE under the steam cost variation, where the 100 % point corresponds to the steam cost of earlier analysis. The LCOE rises 0.520 $/kWh at the steam cost ratio of 70 %, and the LCOE is reduced to 0.488 $/kWh at the steam cost ratio of 130 %. That is, the LCOE is changed to ∓3.2 % when the steam cost ratio is changed to ±30 %. It would be estimated that the standalone system is more economical than the hybrid system if the steam cost ratio is over 150 % by extrapolation. But, it is impossible that the steam cost increases that much, thus the hybrid system is still more economical than the standalone system.

In economic analysis of the hybrid system, the engine cost is one of the important factors, because the HCCI engine is not originally included in the fuel cell standalone system. Therefore, it should be known how the price fluctuation of the engine affects to the LCOE. Figure 5.9 shows the LCOE change under the engine cost variation, where the 100 % point is the engine cost in Table 5.7. As the engine costs is 2.5 times higher, the LCOE of the hybrid system is just 0.501 $/kWh that is still under the LCOE of the standalone system. Eventually, if the engine cost doesn't increase abnormally, the hybrid system is still more economical than the standalone system.

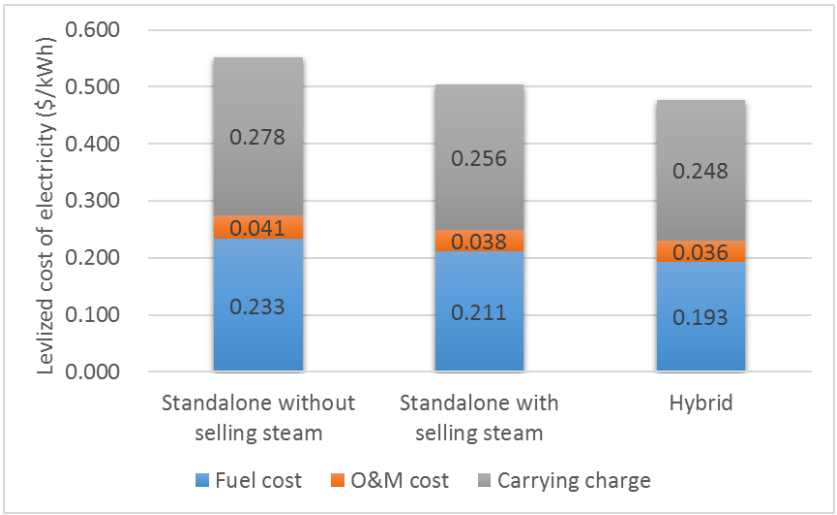

Figure 5.7 Comparison of both standalone and hybrid systems

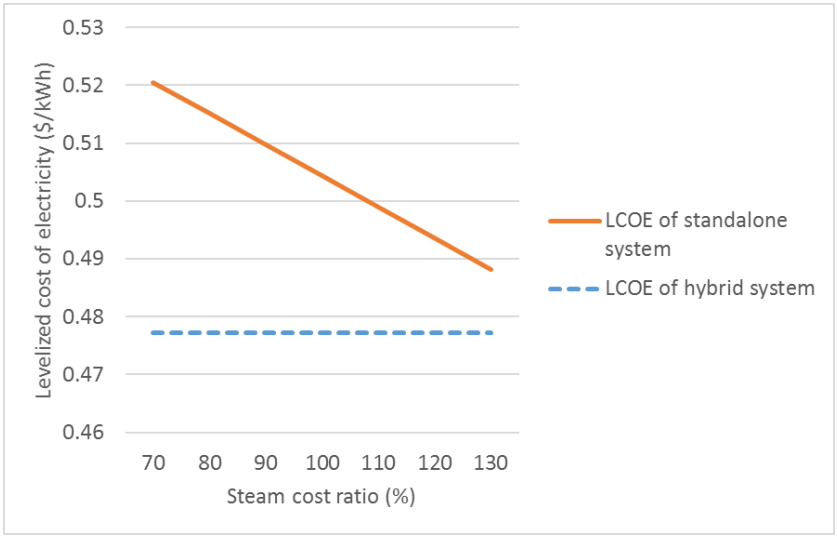

Figure 5.8 LCOE of standalone system under steam cost variation

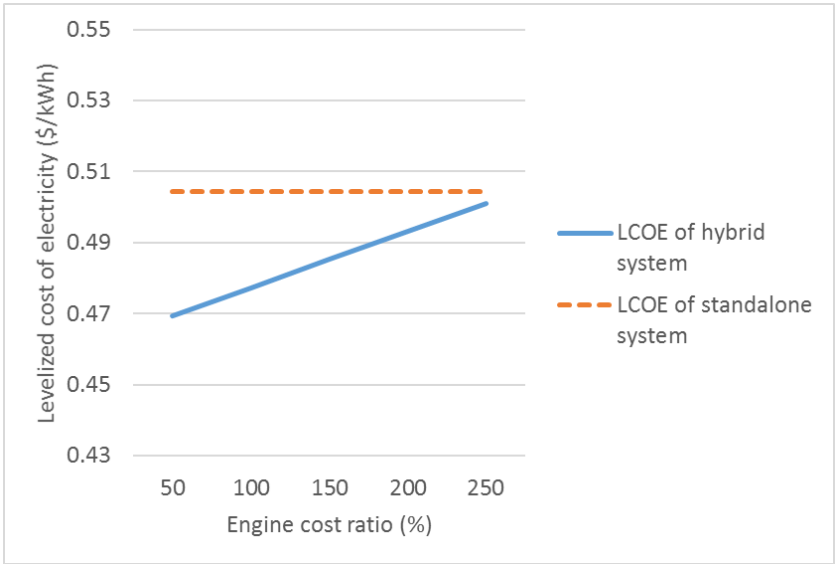

Figure 5.9 LCOE of hybrid system under engine cost variation

5.4 Summary

In this chapter, the economic analysis was conducted for MCFC standalone system and MCFC-HCCI engine hybrid system. For the purpose, TRR method was introduced, and then the levelized cost of electricity (LCOE) of two systems was evaluated by using the method. As a result, the LCOEs of the standalone and hybrid systems are 0.504 $/kWh and 0.477 $/kWh, respectively, thus the hybrid system is more economical than the standalone system.

For two systems, sensitivity analysis of stack cost & lifetime was conducted, and then the LCOEs of the standalone and hybrid system can be reduced by 21.6 % and 18.9 % with the stack lifetime of 20 years, by 25.8 % and 22.4 % with stack cost of 50 %, respectively.

For the standalone system, it was analyzed under the steam cost variation. If the steam cost is increased to 30% relatively, the hybrid system has still lower LCOE value than that of the standalone system. By extrapolation, the steam cost has to increase over 150 % for more economical standalone system. The steam cost, however, might not be increased as much.

For the hybrid system, the LCOE was evaluated under the engine cost variation. Although the engine cost is 2.5 times higher than original cost in Table 5.7, the hybrid system is still more economical than the standalone system.

Chapter 6. Hybrid system feasibility verification

6.1 Introduction

In Chapter 4, the hybrid system performance is evaluated by analyzing the simulation results based on thermodynamic modeling. As a result, the hybrid system efficiency is higher than that of standalone system, and thus the feasibility of the hybrid system is certified. In addition, it is operated the economic analysis for the standalone system and hybrid system in Chapter 5. The LCOE of the hybrid system is lower than that of the standalone system, and thus the hybrid system is more economical. The standalone system saves the cost selling the waste heat from HRSG. In the hybrid system, but the heat recovery is not possible for the lower exhaust temperature of the system, but the engine yields additional power output, and thus the LCOE of the hybrid system is lower than that of the standalone system. We know the feasibility of the hybrid system from the thermodynamic analysis and the economic assessment. In this chapter, the feasibility of the hybrid system would be discussed by experiments. In this thesis, especially, the engine experiment is performed. Based on the various simulation results, the engine experiment is conducted to demonstrate the possibility of the HCCI engine operation in the system. To simulate the thermodynamic state of the anode off-gas, the experimental engine system was developed. Figure 6.1 shows the engine experimental system configuration. This system includes various gas supplies, MFC's, a heater, a static mixer, and a steam generator, an inverter, a motor, a

gas analyzer and so on. The component setup process is explained in Chapter 6.2. In Chapter 6.3, the result of the experiment is discussed, and thus the feasibility of the hybrid system could be certified.

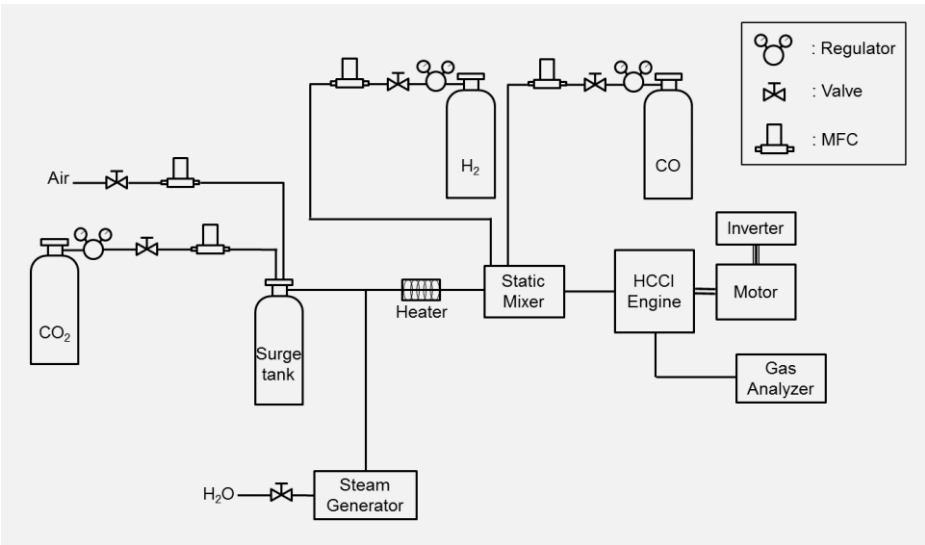

Figure 6.1 Engine system configuration

6.2 Experimental setup

6.2.1 Engine intake system

To simulate the thermodynamic state of the anode off-gas, the intake system is developed. The intake system includes various gas supplies, MFC's, a surge tank, a main heater, a static mixer, a steam generator, which is composed of a pump, a water tank and heaters, and so on. Firstly, to make the gas mixture of air and pseudo anode off-gas, i.e. carbon monoxide, hydrogen, carbon dioxide and steam, relatively stable gases, CO_2, air and steam, are supplied to the surge tank of the system through MFCs and steam generator. And then, the gas mixture is preheated through the main heater. The preheated gas mixture goes to the static mixer, and H_2 and CO are also supplied to the static mixer. After mixing the intake gas mixture, the intake charge enters the intake manifold of the engine. At that time, the intake charge is preheated to the temperature required to achieve the proper HCCI combustion timing.

Gas supplies and surge tank

The pseudo anode off-gas consists of CO_2, H_2, CO, steam, and the engine needs air for combusting the anode off-gas. Thus, these gases are needed to supply to the experimental engine system. Mass flow controllers (Bronkhorst's model) are used to supply the exact amount of the gases mass flow rate. CO_2 and air, which are relatively stable, are firstly supplied to the system through the surge tank. The engine is not stationary component, but pulsating one. The

surge tank is used as a buffer for the stable pressure in the system. H_2 and CO are combustible gases, and thus the gases don't go through surge tank, and are not preheated through the main heater for preventing auto-ignition. The gases are supplied to the system after preheating air and CO_2. The surge tank is modified from a commercial water pump tank. Inlet and outlet line is manufactured by using 1" tubes, there are thermocouple and pressure sensor to measure the temperature and the pressure in the surge tank.

Main heater

The main heater is used to preheat the air, CO_2 and steam to the proper temperature for combusting anode off-gas. It is the type of vessel immersion heater and the capacity is 15kW-class. The power capacity is selected by calculating the amount of heat, which is required to achieve the proper HCCI combustion timing, considering a safety factor. The heater's target temperature is the outlet one. The input of the heater is 0 to 10 Vdc, and the value is controlled by using PID control method with Mathworks Simulink. The heater power is controlled by thyristor power regulator (TPR) method.

Steam generator

The steam is converted from water through the steam generator, which is composed of a water tank, a pump (KNF's Simdos), heaters and heater controller. The flow range of the pump is 1 to 100 ml/min. The heater is 5 kW-

class, and 0.8 kW-class line heater wraps the steam line for preventing steam condensing out.

Figure 6.3 shows the steam generating process. The pump supplies the water to the heater from the water tank, and then the water is heated and converted to the steam. The steam goes to the main heater.

Static mixer

The static mixer is used to mix the intake charge which consists of Air, CO_2, H_2, CO and steam. The component is located between the main heater and the intake manifold. In static mixer, there are elements which play a key role for mixing the gases. The intake charge is mixed due to division of flow, radial mixing and flow reversal by the elements. The static mixer has 6 elements, which is enough to mix the gases. If the number of elements is more, the gases is mixed better. However, the length of the static mixer is longer, the amount of heat loss is more from the heater outlet flow. Then the proper number of element is chosen, which is 6 elements.

Intake manifold

Intake manifold connects the static mixer to the engine. The manifold includes the pressure sensor and 1/16” thermocouple. The thermocouple is located at the closest to the intake valve, and thus measures the temperature of intake charge correctly. And looking the pressure sensor, the intake charge

pressure could be adjusted by controlling the mass flow rate of the intake charge

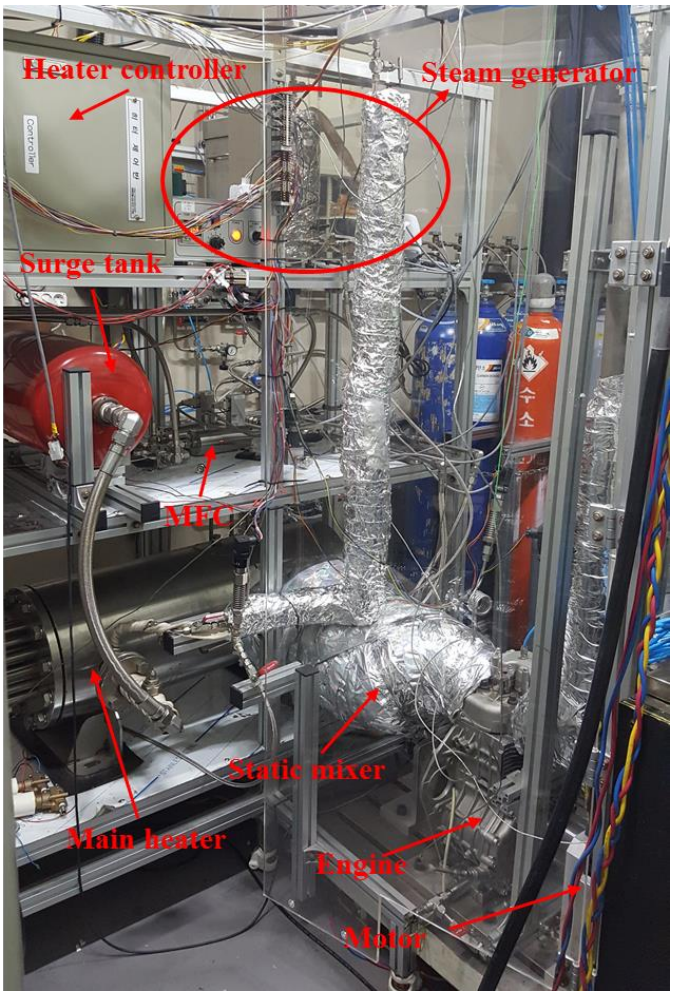

Figure 6.2 Experimental engine system

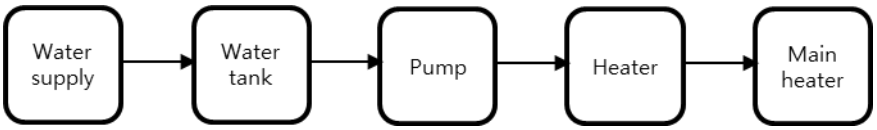

Figure 6.3 Steam generating process

Figure 6.4 Static mixer

6.2.2 HCCI engine

In previous chapter, the intake system, which supplies the pseudo anode off-gas and air mixture to the engine, is introduced. The gas mixture enters the engine, and is combusted in the cylinder, and then goes out through the exhaust manifold.

The experimental engine is originally from a commercial single-cylinder diesel gen-set (Yanmar, YDG-5500N). Table 6.1 shows the engine specifications. The engine compression ratio is 20, and the displacement is 435 cc. Most components of the gen-set, e.g. a starting motor, a fuel supply-line, intake and exhaust manifolds, are disjointed except the engine. The engine is remodeled to perform HCCI operation with the in-cylinder pressure sensor (Kistler, Type 6052C) replacing the direct fuel injector. An adapter, which is shaped like the injector, are made and the in-cylinder pressure sensor with a mounting sleeve is fastened to the adapter. Then the adapter is mounted on the original injector hole. By using in-cylinder pressure and volume information, the engine performance, e.g. indicated power and efficiency, peak pressure, combustion timing, were evaluated.

For controlling the engine speed, the engine system includes a servo drive (Yakawa, SGDV-780A01A), a servo motor (Yaskawa, SGMGV-1EADA21) and a dynamic braking resistor unit (Fullohm, MCRF-STF). The servo drive, which is called inverter, controls the motor speed and supplies power to motor. The engine shaft is mounted on motor shaft, and the motor makes the engine operating with constant RPM. The inverter transfers the engine work to the resistor unit in the form of thermal energy. And the inverter is connected to PC,

and then give some information about motor RPM, torque, position and so on. The inverter and the motor are 15 kW-class.

Table 6.1 Experimental engine specification

Model	**Yanmar L100N**
Bore (mm)	86
Stroke (mm)	75
Connecting rod (mm)	114
Cylinder	1
Displacement (cc)	435
Compression ratio	20
Engine speed (rpm)	1800
Equivalence ratio	1 (Stoichiometric)
IVO	4 ^{o} bTDC
IVC	40 ^{o} aBDC
EVO	30 ^{o} bBDC
EVC	8 ^{o} aTDC

Figure 6.5 Original diesel gen-set

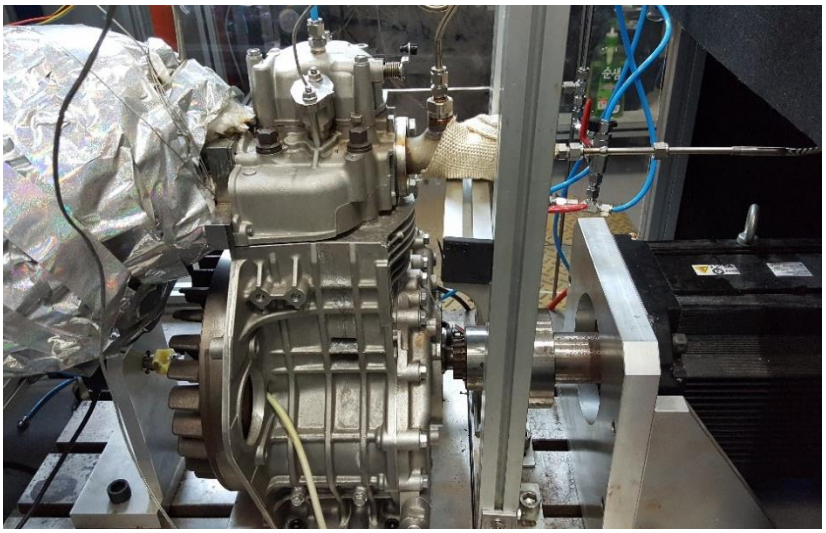

Figure 6.6 Remodeled HCCI engine

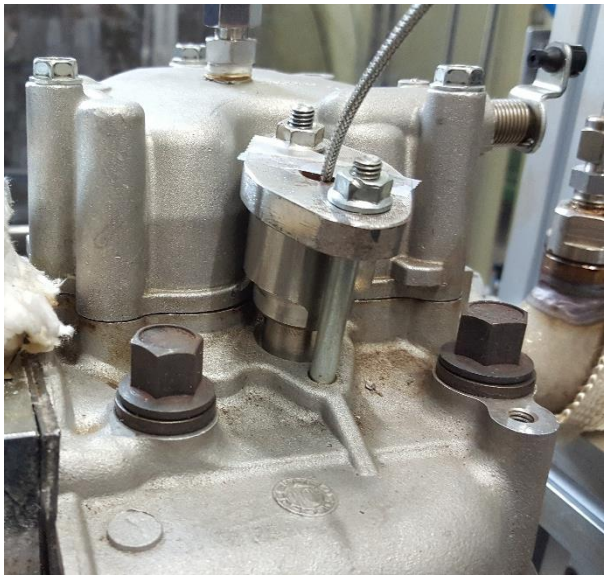

Figure 6.7 In-cylinder pressure sensor

6.2.3 Engine exhaust system and gas analyzer

The engine exhaust gas goes out through the exhaust manifold. The manifold and exhaust line is made for a direct module, and then a pressure sensor and a thermocouple are mounted on the module. The thermocouple is installed at a nearby exhaust valve for measuring the exhaust charge temperature. In case of condensing out the hot exhaust gas, water drain line is installed on the bottom of the exhaust line. And sampling line is also installed on the exhaust line for measuring the exhaust charge composition. The composition is measured by a gas analyzer (Eurotrone, GreenLine MK2). The gas analyzer measures the concentration of O_2, CO, CO_2, NO_X, SO_2, and so on.

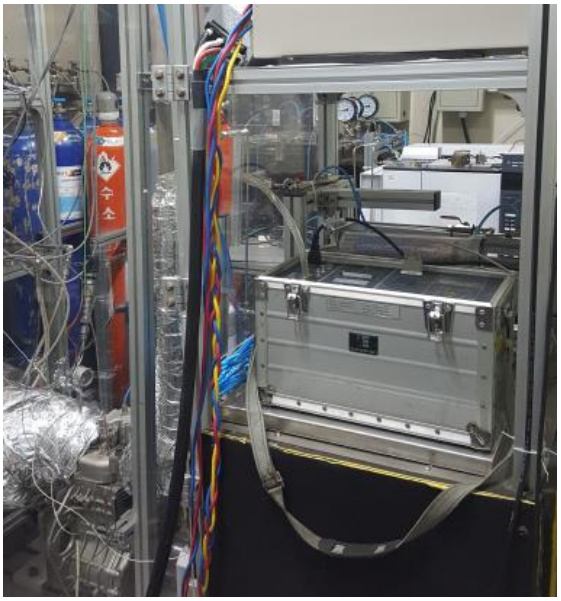

Figure 6.8 Gas analyzer

6.2.4 Data acquisition

Until now, the engine system setup process and each component are explained. The software model is needed for operating the components of the system. Thus, the model is made by using Mathworks Simulink. The data from the components is received to DAQ, thermocouple board, encoder board and serial port, and then transferred to xPC target computer like Figure 6.9. The data is sent to the host computer through the router, and then, shown on the monitor. The data of pressure and motor speed are communicated through the DAQ (NI, PCI-6259), and the thermocouple data is transmitted by thermocouple board (MCC, PCI-DAS-TC). The engine CAD data is transferred from encoder board (MCC, PCI-QUAD04), and mass flow rates of the gases are controlled through rs232 serial communication.

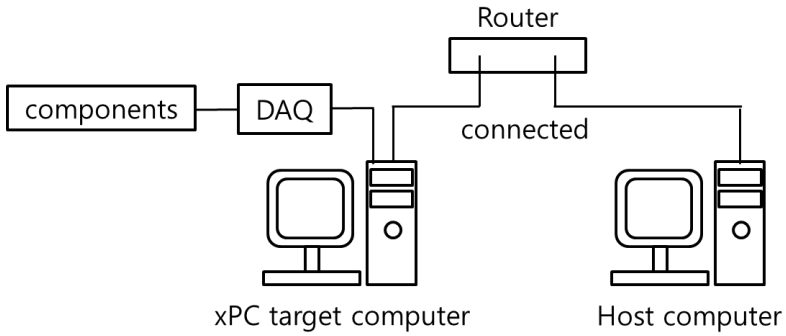

Figure 6.9 System control unit

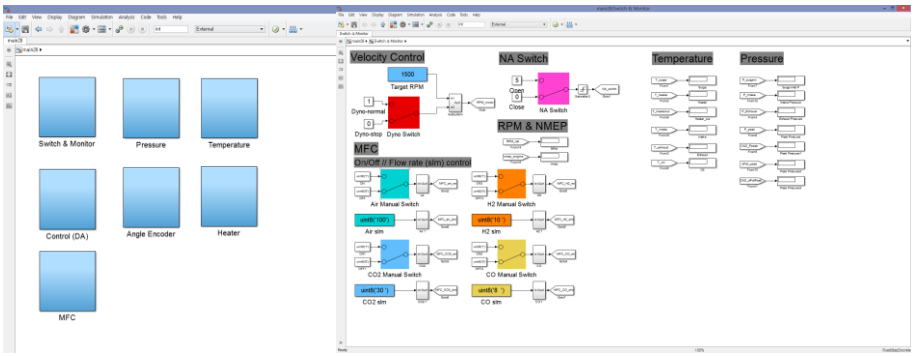

Figure 6.10 Simulink model - controlling and monitoring

6.3 Experimental results

An operability of engine in the hybrid system was confirmed by the thermodynamic analysis under the design point and part-load conditions in Chapter 4.2 and 4.3. To verify the engine operability in real-world system, engine experiments are performed under the design point and part-load condition.

6.3.1 Design point operation

Table 6.2 shows the design point condition which is based on simulation results in Chapter 4.2. At the design point condition, the fuel utilization of the MCFC is 70 %, which means that the engine could only use the left-over fuel that is about 30 % of initial fuel. Moreover, the anode off-gas has much amount of diluent gases which are carbon dioxide and steam. Thus, the engine intake charge has a little amount of real fuel which is composed of hydrogen and carbon monoxide. For the reason, the intake charge temperature should be high for keeping the proper combustion timing. Table 6.2 shows the intake temperature is about 329 ℃, which is much higher than temperature of the typical engine intake charge. The engine RPM is 1800 and the MFC is controlled to match the intake pressure of 1.0 bar. The experimental engine compression ratio is 20 while the compression ratio of simulation is just 15. A diesel block engine is needed due to the harsh operating conditions which mean high intake temperature and high pressure rise rate. But the commercial lab-

scale diesel engine has generally high compression ratio. Thus there is no choice but to choice the experimental engine. However, it is enough to verify the operability of engine in the hybrid system.

Figure 6.11 and 6.12 depict the in-cylinder pressure profile and P-V diagram, respectively, which are the averaged values of ~150 cycles. The peak pressure of the engine is 42.4 bar at 2 ^{o} aTDC. Table 6.3 shows the experimental results. The gross power output is ~950W and the gross indicated efficiency is 22 %. And the NO_X emission is under 10 ppm, which is very low value. NO_X tolerance of the MCFC is about 20 ppm, thus it is expected that the NO_X emission of the HCCI engine in hybrid system doesn't affect the MCFC performance [30]. The COV_{gmep} of engine is under 5, thus the combustion in the cylinder is stable [67].

Table 6.2 Engine operating conditions

Parameter	Value
Utilization (Fuel Cell) (%)	70
Displacement (cc)	435
Compression ratio	20
Intake charge pressure (bar)	1.0
Intake temperature (℃)	329
Equivalence ratio	1.0
Mass flow rate (kg/s)	0.0037
RPM	1800
Intake charge mole fraction	
CO	0.0333
CO_2	0.3162
H_2	0.0692
H_2O	0.3375
N_2	0.1927
O_2	0.0512

Table 6.3 Engine performances

Parameter	Value
Gross power output (W)	947.5
Net power output (W)	588.5
Gross indicated efficiency (%)	21.74
Net indicated efficiency (%)	16.87
GMEP (bar)	1.163
NMEP (bar)	0.9008
NO_X	2.33
COV_{gmep}	4.33

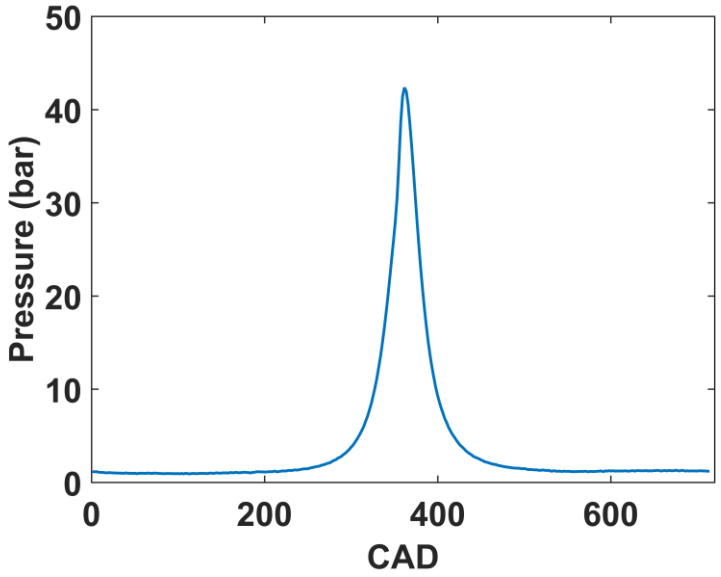

Figure 6.11 In-cylinder pressure profile

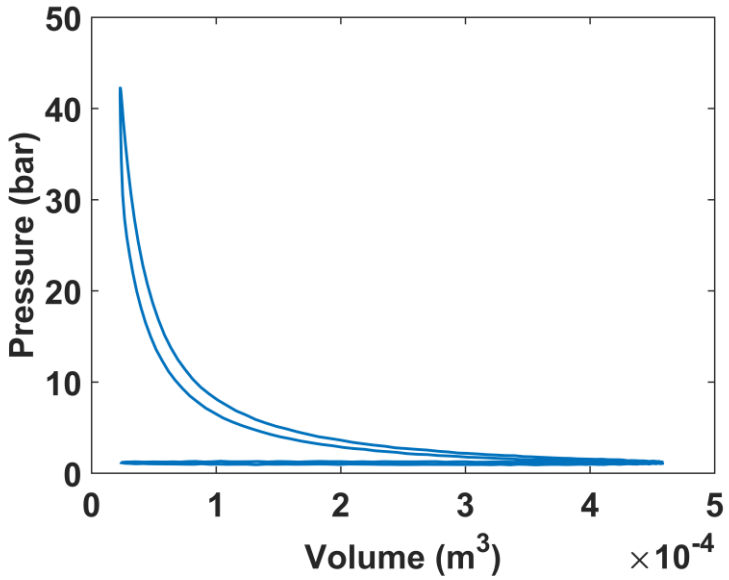

Figure 6.12 P-V diagram

6.3.2 Part-load operation

In Chapter 4.3, the operating strategies for part-load condition was developed and the operability of the HCCI engine in the hybrid system was verified through the thermodynamic analysis. Under the part-load operation, it was shown that the hybrid system could be operated without the loss of efficiency. In this chapter, the engine experiment would be performed under the part-load conditions, which are based on the simulation results. The experiment is conducted at the fueling level of 75-100%. At all the tested conditions, the engine oil temperatures are kept almost the same between 95 and 100 ℃, and the peak pressure timings are kept around 2 ^{o}aTDC. As mentioned in Chapter 4.3, the mass flow rate of the anode off-gas is reduced at the low fueling level. The engine is supplied with more air to compensate for the reduced flow rate of the anode off-gas. Thus the intake charge of the engine is kept almost 1 bar. The intake charge of the engine is composed of more air and less anode off-gas than otherwise, thus the gas has higher specific heat ratio. In a given geometric compression ratio, this higher specific heat ratio can lead to more temperature increase during the main compression stroke of the engine, which achieves the higher temperature with the same initial temperature of the mixture. In other words, the intake charge temperature should be reduced to achieve the similar post-compression temperature and thus proper combustion timing for the low fueling level. Figure 6.13 shows this intake charge temperature trend.

Figure 6.14 shows COV of the engine under fueling level variation. The COV is calculated by using GMEP data of the engine cycle. At the lower fueling

level, it is shown that the COV of the engine is slightly increased, which means that the combustion in the cylinder is a bit unstable. At low fueling level, which means low equivalence ratio, the fueling rate is reduced and the air flow rate is increased. Especially, the equivalence ratio is decreased to 0.36 at the fueling level of 75 %. Thus the MEP of the engine is decreased, as shown in Figure 6.15. This low-load condition is unfavorable for combustion of the engine. Therefore, the COV rises a bit at the low fueling level condition. Likewise, the burned ratio of carbon monoxide (CO) is low, shown in Figure 6.16. At all the tested conditions, GMEP of the engine is around 1 bar, which is extremely low-load operating condition. The heating value of diesel fuel is originally 23.1 kW in the experimental engine. The fuel heating value, however, is just 3.49 kW at the design point operation in the hybrid system. The intake gas mixture is diluted with much amount of carbon dioxide and steam due to the nature of the anode off-gas. For the reason, the CO burned ratio is low and the engine efficiency is also lower than commercial engine efficiency, shown in Figure 6.17.

Figure 6.18 shows emissions in the exhaust gas under the fueling level variation. As mentioned earlier, CO emission is high due to extremely low-load condition. The CO emissions are over 10000 ppm at tested conditions. And at the fueling level of 100 %, CO emission data could not be measured because the emission is over 20000 ppm which is the measuring range limit of the analyzer. At the tested fueling levels, however, oxides of nitrogen (NO_X) emissions are always below 20 ppm which is MCFC tolerance to the NO_X [30]. Thus the NO_X emission would not affect the cathode of stack.

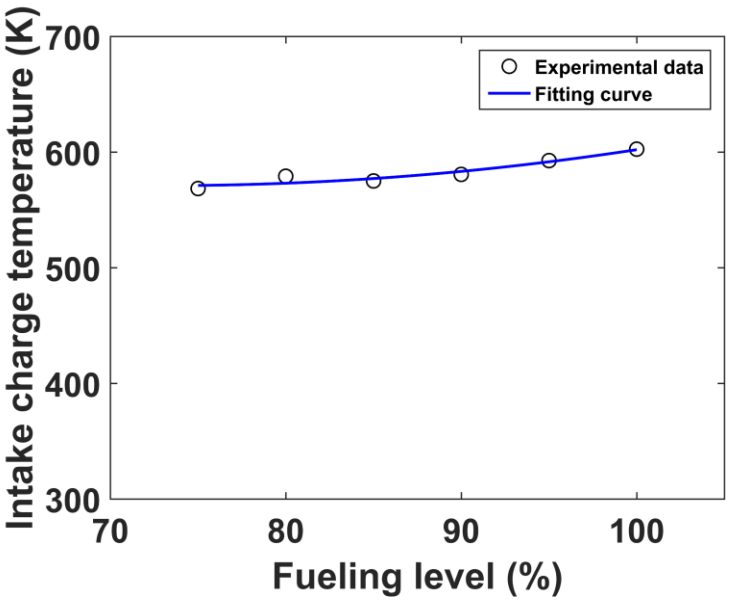

Figure 6.13 Engine intake temperature under fueling level variation

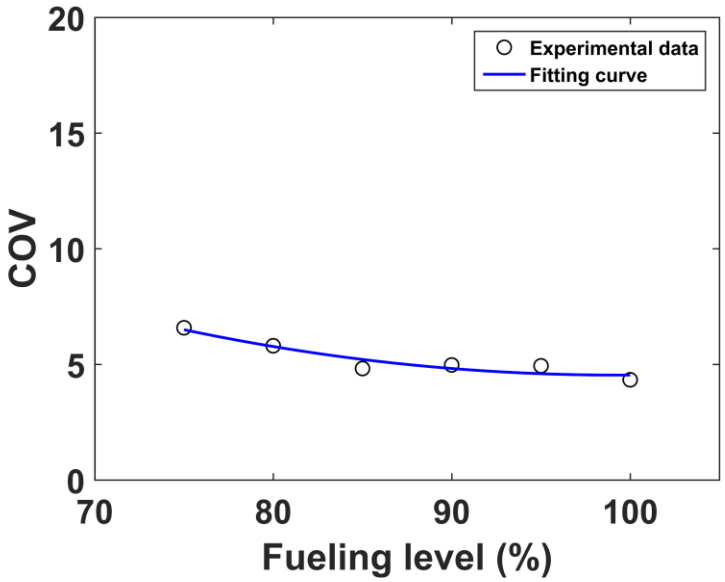

Figure 6.14 COV of engine under fueling level variation

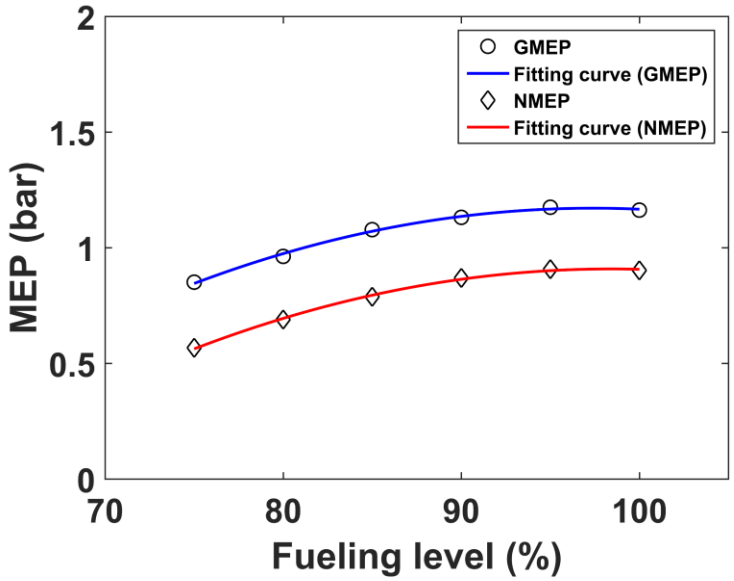

Figure 6.15 Engine mean effective pressure under fueling level variation

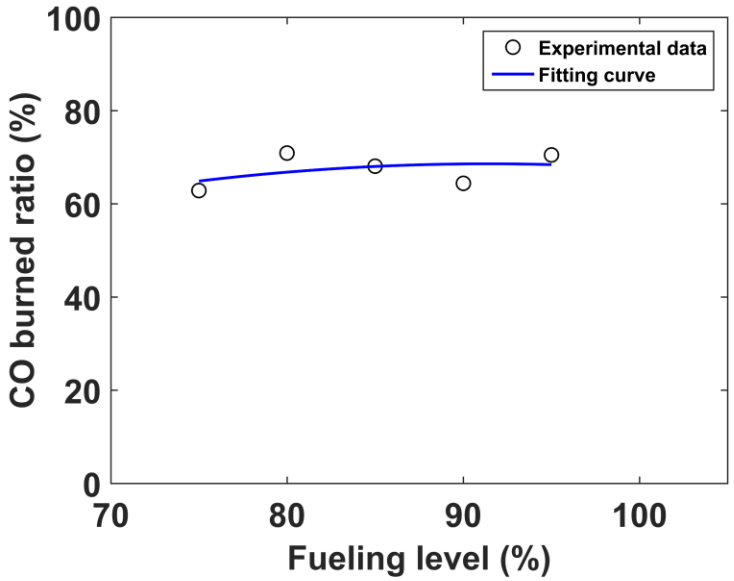

Figure 6.16 CO burned ratio under fueling level variation

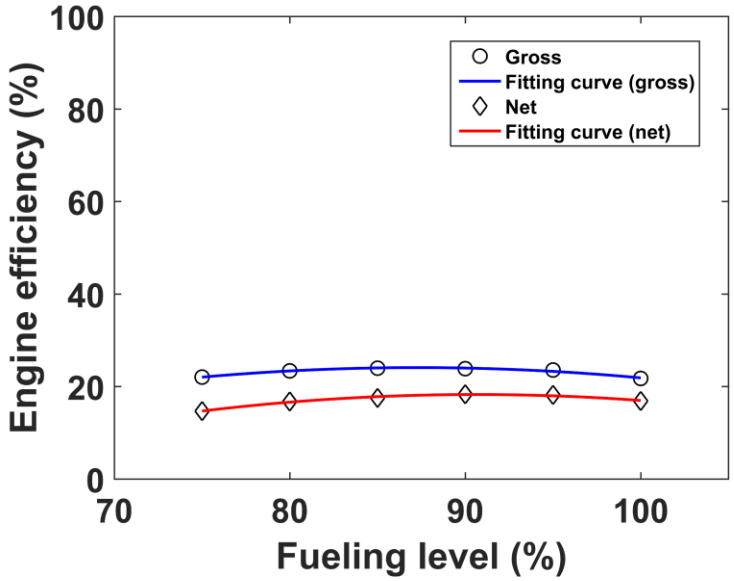

Figure 6.17 Engine efficiency under fueling level variation

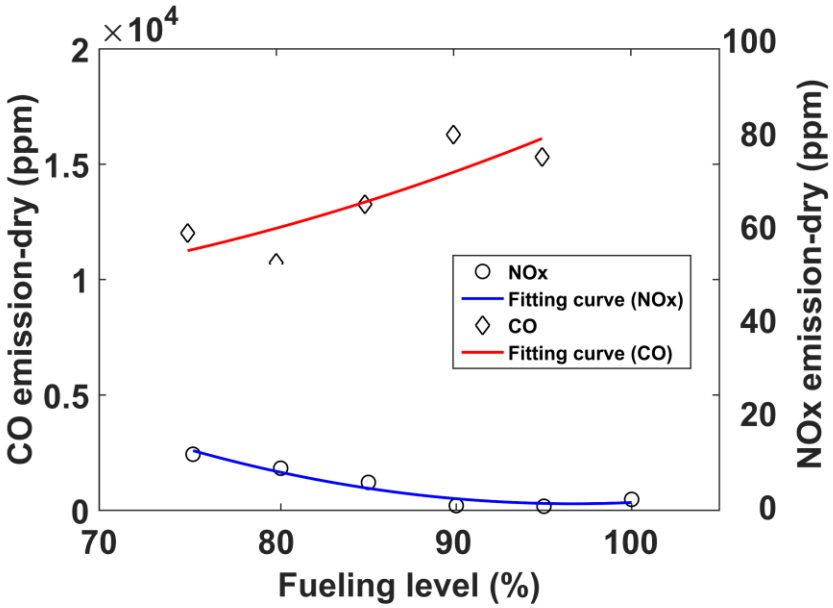

Figure 6.18 Engine emissions under fueling level variation

6.3.3 Comparison between simulation and experimental results

The experimental results show the feasibility of the engine operation in the hybrid system, but the engine performances are not same with the simulation results. Thus, there are overall system analysis with the engine experimental results for comparing between simulation and experimental results and for estimating the hybrid system performances in real-world. Figure 6.19 shows the revised system configuration for the analysis. In previous chapter, the experimental exhaust gas has unburned carbon monoxide and hydrogen for the incomplete combustion. Thus, the small-scale catalytic burner is added to the rear of the engine, and then it is assumed that the unburned gas is completely combusted in the burner.

At this time, the simulation results are not the values in Chapter 4.2, but the newly evaluated values with the engine compression ratio of 20 which is same with the value of the experimental engine Thus the operability of the system is lower due to the aforementioned reason in Chapter 3.2.2. At the fueling level of 100 %, the experimental data of exhaust gas composition is not measured due to the aforementioned reason. Therefore, the simulation and experiment are performed under fueling level of 95 %. In previous simulation, the engine efficiency was calculated by considering the friction loss. The friction loss of the experimental engine, however, could not be measured due to the limit of experimental setup. Thus the engine efficiency and power output would be calculated by considering only compression and expansion strokes for comparing between simulation and experiment with same condition. The

experimental results of the system, i.e. engine power output, system power output and so on., are matched with simulation scale (300 kW-class) by using the engine gross efficiency.

Table 6.4 and 6.5 lists the simulation and experimental results. The engine inlet temperature of simulation is lower and outlet temperature is higher than those of experimental results. It is estimated that these differences between the results of simulation and experiment might be caused by the heat transfer of the engine. For achieving the self-ignition temperature, the intake temperature of experimental engine needs to be higher than that of simulation due to more amount of heat transfer. For the same reason, there is the incomplete combustion in the experimental engine, and thus the exhaust temperature and gross efficiency of the experimental engine are lower than those of the simulation. However, if the unburned gas of the engine could be combusted in the rear-catalytic burner (between state 9 and 9b in Figure 6.19), the exhaust temperature would be higher, and thus the system operability would be higher.

Generally, it is known that the small engine, which has small displacement volume, is relatively un-favorable heat transfer characteristic [68]. The brake specific fuel consumption (bsfc) generally decreases with higher engine size due to reduced heat losses from gas to cylinder wall. It is because the surface to volume ratio is decreased at the large size engine [68]. Figure 6.20 shows the heat loss of the engine under the bore size variations. This graph also depicts that the heat loss is reduced at the large-size engine due to aforementioned reason. The displacement of the experimental engine has just 435cc displacement, which is much smaller than 20.8 L displacement of the engine

for 300 kW-class hybrid system. Therefore, it is expected that the heat loss of the engine would be complemented and the combustion efficiency would be higher if the engine size is larger.

Table 6.4 Engine experimental results

Parameter	Simulation	Experiment
Engine inlet temperature (℃)	245	319
Engine outlet temperature (℃)	415	360 (481*)
Gross efficiency (%)	39.8	23.6
Gross power output (kW)	68.8	40.8** (estimated)

* In experimental results, engine outlet temperature is estimated by assuming that the unburned exhaust components would be combusted at the catalytic burner.

** Engine gross power output is estimated by considering the gross efficiency.

Table 6.5 Performance results of simulation and experiment

Parameter	Hybrid system (sim., CR20)	Hybrid system (exp.)
LHV CH_4 (kW)	475	475 (sim.)
Fuel utilization (%)	0.70	0.70 (sim.)
*MCFC net output(kW)	229	229 (sim.)
MCFC net efficiency (%)	48.3	48.3 (sim.)
Engine gross output (kW)	68.8	40.8 (estimated)
Engine gross efficiency (%)	39.8	23.6 (exp.)
**System power output (kW)	298	270 (estimated)
System electrical efficiency (%)	62.7	56.8 (estimated)

*MCFC net output = MCFC output – BOP power consumption

**System power output = MCFC net output + Engine gross output

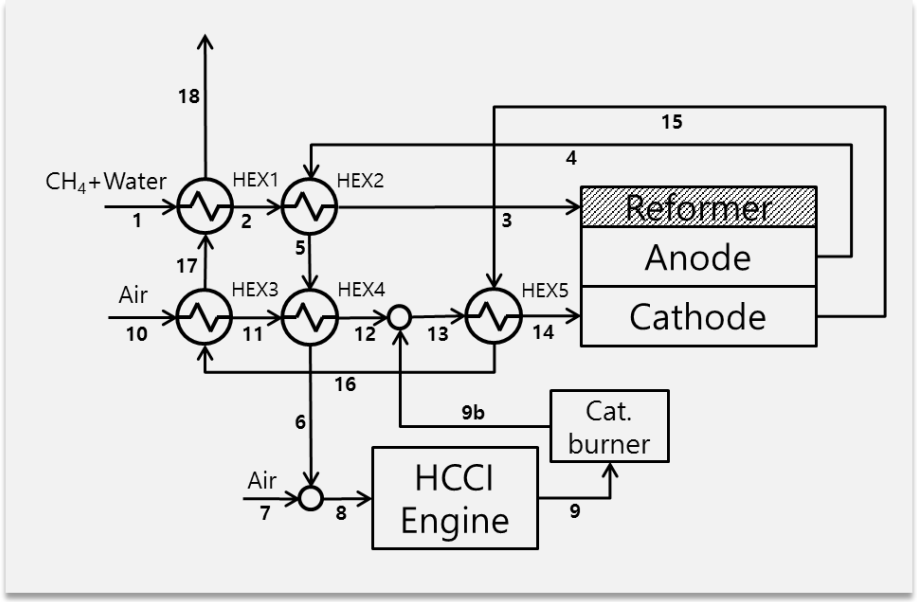

Figure 6.19 Hybrid system configuration
(for simulation with experimental results)

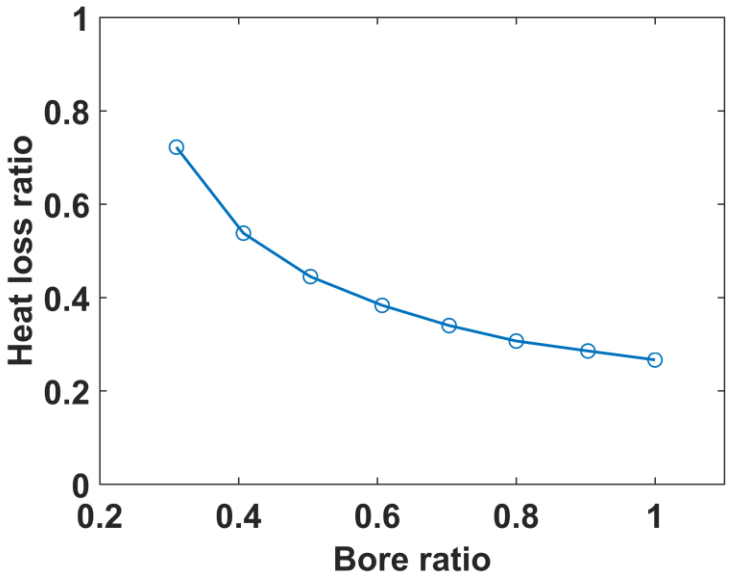

Figure 6.20 Heat loss ratio under bore ratio variation

6.4 Summary

In Chapter 6, the HCCI engine experiment was performed under the design point and part-load conditions. At the design point operation, the HCCI engine performances in hybrid system are shown to be quite promising, considering the small displacement volume of the experimental engine with its relatively un-favorable heat transfer characteristic. The HCCI engine net efficiency is ~17 %, and COV of the cycle is 4.3 under the design point operation, thus it shows that the anode off-gas could be combusted. The NO_X emission is very low level, and then it is anticipated that the emission doesn't affect the MCFC performance. Additionally, it is demonstrated that the HCCI engine can operate under the various load of the fuel cell stack. And it is also shown that the overall system is operable with engine experimental results. Consequently, the feasibility of the hybrid system is confirmed through the engine experiments.

7. Conclusion

In this thesis, a new MCFC hybrid system, which replaces the catalytic combustor with an HCCI engine to generate additional power output, was studied through various approaches. The feasibility of the MCFC-HCCI engine hybrid system, especially, was analyzed in aspect of demonstration for commercialization. For the purpose, there were the thermodynamic analysis, the economic analysis, and the experimental verification in this thesis. The following are the summary of this thesis.

Firstly, the new hybrid system concept was introduced in Chapter 1. In previous author's study, the new hybrid system was proposed, and analyzed preliminary. The hybrid system includes an MCFC and an HCCI engine which increases the system efficiency. The catalytic combustor is replaced with an HCCI engine in bottoming cycle of the system. Thus, the left-over fuel in anode off-gas is combusted in the HCCI engine. For this reason, the HCCI engine yields additional power output, and then the system efficiency could be increased.

Secondly, for the thermodynamic analysis, there are the thermodynamic modeling descriptions about the MCFC stack, the HCCI engine, the blower, the pump, the system integration, and the other components of the system in Chapter 2. The modeling was performed by using the Mathworks MATLAB and Cantera toolbox for calculating chemical reaction kinetics and thermodynamic state. The MCFC stack model can evaluate the power output and efficiency considering the electro-chemical reactions. The HCCI engine

model can show the temperature and the pressure profiles during the engine cycle, and then evaluate the power output and the efficiency. And the blower and pump was modeled for performing the evaluation of power consumption and the economic assessment. Using various components' models, the system integration was conducted, and the system model was used to evaluate the system performances in Chapter 3 and 4.

Thirdly, in Chapter 3, the system design was performed, especially, in aspect of the engine specifications. The HCCI engine is newly added to the original MCFC standalone system, thus the hybrid system needs to adopt the suitable engine specification for the MCFC system capacity. In this thesis, the MCFC system is motivated by DFC300 model (FCE) of which the capacity is about 250 kW. For determining the engine specification at the MCFC system capacity, parametric study was conducted with design options variation that the engine compression ratio, the equivalence ratio, the RPM, and the MCFC fuel utilization. As a result, the engine size could be determined to be 20.4-21.2 L at the compression ratio of 13-16 and the equivalence ratio of unity, shown in Table 3.1. With this engine specification, it is anticipated that the hybrid system would produce low NO_X emission, but still have a high efficiency.

Fourth, in Chapter 4, the hybrid system was analyzed at the design point and off-design point operations, based on the system design determined in Chapter 3. The engine size was decided to be 20.8 L among the range of the suggested engine specification in Chapter 3. With the determined engine specification, the hybrid system was simulated at the design point operation, and the system efficiency could achieve 57.1 %, which is 9.8 % higher than the

standalone system efficiency. The hybrid system was also analyzed at the off-design point operation that is part-load operation in this thesis. Although the heat exchangers needed to operate excessively, the fueling level of the system could be reduced to 75 % of the designed level by using the systematic control strategies, and the system efficiency remains still high. It was known that the feasibility of the hybrid system would be promising through these thermodynamic analyses.

Fifth, the economic assessment was conducted for comparison between the MCFC standalone system and the MCFC-HCCI engine hybrid system in Chapter 5. The analysis was performed by calculating the levelized cost of electricity (LCOE) with the total revenue requirement (TRR) method. As a result, the LCOEs of the standalone system and the hybrid system were 0.504 $/kWh and 0.477 kWh, respectively, thus the hybrid system feasibility of economics was verified. Sensitivity analysis was also performed with the stack cost & lifetime, steam cost, and engine cost variations. In aspect of economics, the hybrid system was still better than the standalone system with the reasonable range of the steam cost and the engine cost. And it was confirmed that the LCOEs of the standalone system and the hybrid system could be reduced with the stack lifetime increase and the stack cost decrease. It is noted that there is a lot of potential in the fuel cell field, thus if the stack cost is lower or the lifetime is longer, the hybrid system is more competitive system.

Finally, the feasibility of the hybrid system was discussed with the engine experiment in Chapter 6. The experiment was conducted at the design point operation that was determined in Chapter 4. The engine is newly added to the

MCFC standalone system. Therefore, it needs to verify that the anode off-gas, which is very diluted gas mixture for the engine, can be combusted well in the engine. To simulate the thermodynamic state of the anode off-gas, the experimental engine system was developed. The experimental system is largely divided into the intake part, the engine part, and the exhaust part. In the intake part, the intake gas mixture, consisting of CO, CO_2, H_2, H_2O (steam), and air, is heated and mixed, and then enters the engine intake manifold. In the engine part, the gas mixture is combusted in the engine cylinder. And the motor and inverter control the engine speed. In the exhaust part, it measures the thermodynamic state of the exhaust gas, and the emissions. The result of the experiment, which is operated at the design point, shows a promising data. The pressure profile in the engine cylinder was measured, and thus the engine net indicated efficiency was calculated to be ~17 % with the pressure information. Considering the small displacement volume of the tested engine with its relatively un-favorable heat transfer characteristic, the engine performances in the hybrid system were shown to be quite promising.

In this thesis, the hybrid system was designed, and the feasibility was certified from three points of view which are the thermodynamic, economic, and experimental analyses. It was known that this hybrid system has better efficiency, and the system is more economical than the fuel cell standalone system. Furthermore, the hybrid system was verified through the engine experiment, thus it is expected that the system would be commercialized in the near future. For the commercialization, however, there are some issues to solve, which is representatively a start-up issue and the heat management in the engine.

The commercial MCFC standalone system has a starting process [69], thus it is expected that the start-up strategy should be newly developed for the hybrid system. The starting scenario for the hybrid system have been studied by research team which author belongs to [70]. According to the scenario, the engine is used for heat source and power generation. A starting process for fuel cell system is generally composed of heat-up and power-up processes. For the heat-up process, the engine is utilized as a substitute for the electric heater. Thus the engine could supply the heat to the fuel cell and yield additional power output. In regards to the heat management of the engine, the experimental results in Chapter 6 show the much amount of heat transfer of the engine. It might be due to the small displacement of the experimental engine. In the lab-scale engine, we have no choice but to select that size of the engine. However, it is expected that the heat transfer characteristics would be more favorable than now if the engine scale is larger, and then it would be easier to manage the heat in the system.

The fuel cell is a prospective technology, so it is possible that the stack cost and the lifetime would be improved. And the issues mentioned earlier can be also solved through the suggested means in future works. Therefore, the MCFC-HCCI engine hybrid system would be one of the best power-generation system with high efficiency and low emissions.

Appendix A. MCFC stack modeling description

In this appendix A, MCFC stack modeling is described more detail. The followings are mostly from previous work of authors [36, 37], and referred to the master degree paper of author [38] and Abid [39]. Thus the followings are almost reproduced from the references [36-39] and some contents are revised in this thesis.

The major assumptions for the MCFC stack model are:

- Cathode and anode streams flow in parallel and assume the same temperature changes along the channels.
- Pressure drop across the fuel cell channel is negligible.
- Heat loss of the fuel cell is negligible.
- In the reforming channel, the fuel mixture is fully reformed and achieves thermodynamic equilibrium at the exit, before it enters the anode channel.
- The water-gas-shift-reaction (WGSR) at the anode channel occurs fast enough to keep anode compositions at equilibrium all the time.
- The overall system operates under steady-state condition.
- Natural gas, a fuel for typical MCFC system, is modeled as pure methane.

There are various reactions in fuel cell. Firstly, methane-steam mixture enters the reforming channel in fuel cell, and then the mixture changes H_2, CO_2, CO, and H_2O by water-gas-shift-reaction (WGSR). The gas after reforming enters the anode channel and O_2 and CO_2 enter the cathode channel. O_2 and CO_2 change to CO_3^{2-}, and then the carbonate ion transfers from the cathode channel

to the anode channel. Hydrogen at anode channel reacts on the carbonate ion moving from the cathode channel. Also, WGSR rebalances the anode gas mixture composition at the same time. Figure A.1 shows species flows in the fuel cell.

The electrochemical reactions occurring in the fuel cell are:

- Reforming channel: $CH_4 + 2H_2O \rightarrow aH_2 + bCO_2 + cCO + dH_2O$
- Water-gas shift reaction: $CO + H_2O \leftrightarrow H_2 + CO_2$
- Anode: $4H_2 + 4{CO_3}^{2-} \rightarrow 4H_2O + 4CO_2 + 8e^-$
- Cathode: $2O_2 + 4CO_2 + 8e^- \rightarrow 4{CO_3}^{2-}$

The fuel cell model is divided into 25 segments in the direction of anode and cathode flows. Figure A.2 (a) shows 25 segments and (b) shows energy and mass flow at each segment. As shown in Figure 2.2, there are isothermal part and non-isothermal part in each segment. At isothermal part, which is state 1 and state 2, electrochemical reactions occur. The current density is determined based on the operating cell voltage and the calculated irreversible losses. WGSR equilibrates the composition of anode gas mixture. At non-isothermal part, which is state 3, the segment temperature is calculated by considering exothermicity $Q_{isothermal,i}$ from isothermal part and heat transfer $Q_{ref,i}$ by reforming process, which is endothermic.

The present model takes a similar approach as described in Ref. [43] by Baranak et al., although the temperature of the fuel cell is not constant. Some of the governing equations have been reproduced here with subsequent modifications or additions.

The operating unit cell voltage V_{opn} is defined as Eqn. A.1

$$V_{opn} = E_{rev,i} - \eta_{Nern,i} - j_i R_{total,i} \quad (A.1)$$

where, for each segment, i, $E_{rev,i}$ is the maximum reversible potential, $\eta_{Nern,i}$ is the Nernst loss, j_i is the current density (A·cm-2), and $R_{total,i}$ (Ω·cm-2) includes overall irreversible losses in the segment i.

The maximum reversible potential is given by Eqn. A.2

$$E_{rev,i} = \frac{\Delta G_i}{2f} \quad (A.2)$$

where ΔGi, given by Eqn. A.3, is the Gibbs free energy change per mol of H_2 reacted for segment i, and f is the Faraday's constant.

$$\Delta G_i = -24200 + 45.8T_i \quad (A.3)$$

where T_i is the isothermal component temperature of each segment *i* in Kelvin (K)

The Nernst loss for each segment $\eta_{Nern,i}$ is calculated by Eqn. A.4 as given in Ref. [71]

$$\eta_{Nern,i} = \frac{RT_i}{2f} ln \left[\frac{P_{H_{2,and}} (P_{O_{2,cat}})^{\frac{1}{2}} P_{CO_{2,cat}}}{P_{H_{2O,and}} P_{CO_{2,and}}} \right] \quad (A.4)$$

where R is the universal gas constant in J/mol-K and P_x is the partial pressure of species x in bar.

$R_{total,i}$ is the sum of all irreversible losses in the segment i and is given by Eqn. A.5

$$R_{total,i} = R_{and,i} + R_{cat,i} + R_{int,i} \quad (A.5)$$

where $R_{and,i}$ and $R_{cat,i}$ are irreversible losses associated with activation energies at anode and cathode, respectively, and $R_{int,i}$ is the ohmic loss

associated with resistance in the electrolyte.

The irreversible losses are then calculated by the following empirical relationships, Eqns. A.6–A.8, as given in Ref. [72]:

$$R_{and,i} = H_a e^{\Delta H_a/RT_i} P_{H_2}^{-0.5} \quad \text{(A. 6)}$$

$$R_{cat,i} = H_{C1} e^{\Delta H_{C1}/RT_i} P_{O_{2,cat}}^{-0.75} P_{CO_{2,cat}}^{0.5} + H_{C2} e^{\Delta H_{C2}/RT_i} M_{CO_{2,cat}}^{-1.0} \quad \text{(A. 7)}$$

$$R_{int,i} = H_{ir} e^{\Delta H_{ir}/RT_i} \quad \text{(A. 8)}$$

where $M_{CO_2,cat}$ is the mole fraction of CO_2 at cathode, H_x values are apparent frequency factors, and ΔH_x values are apparent activation energies in J/mol, both of which are based on Arrhenius plots for Li/K cells. The values for these parameters are directly adopted from Ref. [72] and listed in Table A.1.

Rearranging Eqn. A.1, we can obtain the current density by Eqn. A.9

$$j_i = \frac{E_{rev,i} - V_{opn} - \eta_{Nern,i}}{R_{total,i}} \quad \text{(A. 9)}$$

where V_{opn} is a constant value throughout the unit cell, whereas $E_{rev,i}$, $\eta_{Nern,i}$, $R_{total,i}$ and j_i change from segment to segment.

Once the current density j_i is evaluated, the current in each segment can be obtained by Eqn. A.10

$$i_{seg,i} = j_i A_{seg} \quad \text{(A. 10)}$$

where A_{seg} is the area of each segment, 400 cm^2, which is 1/25th of the total cell area, i.e., 10,000 cm^2, which represents a typical unit cell size.

The amount of current generated in each segment is directly related to the consumption of each reactant species, according to Eqns. A.11–A.15

$$\Delta F_{CO_{2,cat}} = -0.018655 i_{seg} \quad \text{(A.11)}$$

$$\Delta F_{O_{2,cat}} = -0.0093275 i_{seg} \quad \text{(A.12)}$$

$$\Delta F_{H_{2,and}} = -0.018655 i_{seg} \quad \text{(A.13)}$$

$$\Delta F_{H_{2O,and}} = 0.018655 i_{seg} \quad \text{(A.14)}$$

$$\Delta F_{CO_{2,and}} = 0.018655 i_{seg} \quad \text{(A.15)}$$

where $\Delta F_{x,cat}$ and $\Delta F_{x,and}$ are molar flow rate changes of species x at cathode and anode, respectively.

After the electrochemical reaction occurs with consequent compositional change in the anode mixture by Eqns. A.11–A.13, it is assumed that the water-gas-shift-reaction occurs very fast to achieve new equilibrium composition. The equilibrium constant (K_P) for this reaction is given by Eqn. A.16

$$K_P = \frac{P_{CO_2} P_{H_2}}{P_{CO} P_{H_2O}} \quad \text{(A.16)}$$

Here, the partial pressure of species x is defined by Eqn. (A.17)

$$P_x = \frac{F_x}{F_{total}} P_{total} \quad \text{(A.17)}$$

where P_x and F_x are partial pressure and molar flow rate for species *x*, respectively. P_{total} is the total pressure and F_{total} is the total molar flow rate.

The relationship between equilibrium constant and temperature (Eqn. A.18) is obtained from Ref. [72]

$$\ln(K_P) = {}^{4276}/_{T_i} - 3.961 \quad \text{(A.18)}$$

To evaluate the compositional change of each reactant by water-gas-shift-reaction, K_P is defined in terms of conversion degree of *X* and molar flow rate of species, as shown in Eqn. A.19

$$K_P = \frac{(F_{CO_2}+X)(F_{H_2}+X)}{(F_{CO}-X)(F_{H_2O}-X)} \quad \text{(A.19)}$$

Rearranging Eq. 19, we have an equation for *X* (Eqn. A.20). By solving it,

the conversion degree X is determined.

$$(1 - K_P)X^2 + \left[F_{H_2} + F_{CO_2} + K_P\left(F_{CO} + F_{H_2O}\right)\right]X + \left[\left(F_{CO_2}F_{H_2}\right) - \left(F_{CO}F_{H_2O}\right)K_P\right] = 0 \quad \text{(A.20)}$$

Then, the equilibrium molar flow rates at the anode outlet of the isothermal component of each segment can be evaluated by Eqns. A.21–A.24.

$$F_{H_2,after\ WGSR} = F_{H_2} + X \quad \text{(A.21)}$$

$$F_{CO_2,after\ WGSR} = F_{CO_2} + X \quad \text{(A.22)}$$

$$F_{CO,after\ WGSR} = F_{CO} - X \quad \text{(A.23)}$$

$$F_{H_2O,after\ WGSR} = F_{H_2O} - X \quad \text{(A.24)}$$

The work output from each segment is determined by Eqn. A.25.

$$W_{out,i} = V_{opn} i_{seg,i} \quad \text{(A.25)}$$

Using the enthalpies of the flows entering ($H_{in,i}$) and leaving ($H_{mid,i}$) the isothermal component, $Q_{isothermal,i}$ can be evaluated by Eqn. A.26.

$$Q_{isothermal,i} = H_{in,i} - H_{mid,i} - W_{out,i} \quad \text{(A.26)}$$

where $Q_{isothermal,i}$ is the exothermicity from the electrochemical reaction in a segment i.

Finally, this allows us to calculate the enthalpy of the flow exiting the designated segment i ($H_{out,i}$) after the non-isothermal component by Eqn. A.27.

$$H_{out,i} = H_{mid,i} - Q_{isothermal,i} - Q_{ref,i} \quad \text{(A.27)}$$

where $Q_{ref,i}$ is 1/25th of the total energy required for the reforming process that is distributed uniformly through the segments.

It is assumed that the chemical reactions occur only in the isothermal component, and hence there is no change in composition across the non-isothermal component. Only the exit temperature of a segment is calculated by

the outlet enthalpy ($H_{out,i}$) from Eqn. A.27 and the compositions from Eqns. A.14, A.15, A.21–A.24.

After determining the thermodynamic state at each segment exit, the above processes are repeated for the next segment. Once the calculation is completed for 25 segments, the total fuel cell current is evaluated as the sum of the currents from all the segments (Eqn. A.28).

$$i_{unit\ \ cell} = \sum i_{seg,i} \qquad \text{(A.28)}$$

This corresponds to the current from a single unit cell. To find total current in the fuel cell stack, it is then multiplied by the number of unit cells in a stack.

$$i_{stack} = i_{unit\ \ cell} \times Number\ \ of\ \ unit\ \ cells \qquad \text{(A.29)}$$

where Number of unit cells are assumed to be 250 for this study. Total work output from the fuel cell stack can be determined by Eqn. A.30.

$$W_{out} = V_{opn} i_{stack} \qquad \text{(A.30)}$$

To prevent the fuel cell from fuel starvation, a certain level of excess fuel should be supplied, which is quantified as fuel utilization factor (U_f) and the calculation is based on Eqn. A.31.

$$U_f = 1 - \frac{F_{H_2,an,out} + F_{CO,an,out}}{F_{H_2,an,in} + F_{CO,an,in}} \qquad \text{(A.31)}$$

The fuel utilization factor is defined by the amount of H_2 and CO consumption in the fuel cell.

Table A.1 Parameters for Irreversible Losses [72]

Parameter	Value
H_{C1}	1.97×10^{-6}
H_{C2}	2.2×10^{-3}
H_a	1.39×10^{-6}
H_{ir}	0.0128
ΔH_{C1} $(j \cdot mol^{-1})$	83,400
ΔH_{C2} $(j \cdot mol^{-1})$	22,800
ΔH_a $(j \cdot mol^{-1})$	77,800
ΔH_{ir} $(j \cdot mol^{-1})$	25,200

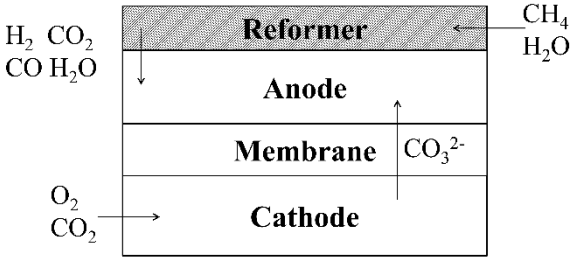

Figure A.1 Species flows in MCFC stack (N2 and H2O omitted at cathode) [36]

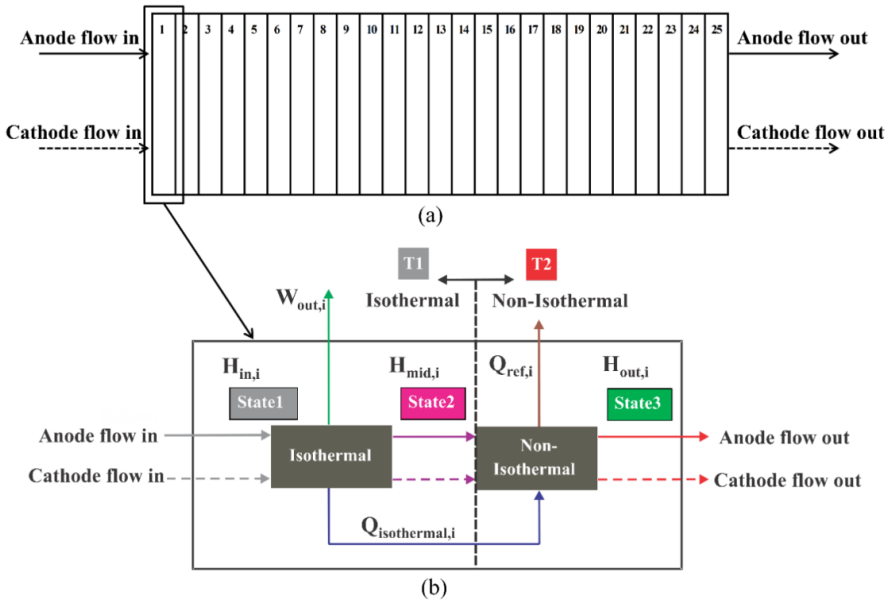

Figure A.2 MCFC stack modeling schematic (a) Parallel flows with 25 segments and (b) Energy flows within each segment [36]

Appendix B. HCCI engine modeling description

In this appendix B, modeling process of an HCCI engine is discussed in details. The original contents are from the previous work [46] and some of the major equations are reproduced here.

The present model assumes a homogeneous thermodynamic state for in-cylinder mixture and only includes compression and expansion strokes without gas exchange. A series of ordinary differential equations are solved for the state variables–crank angle, cylinder volume, temperature, and mass of species–by using an ode solver provided by the Mathworks MATLAB.

The engine is running at a constant speed of n RPM, and the piston location is given by crank angle θ

$$\dot{\theta} = n \qquad \text{(B.1)}$$

The instantaneous cylinder volume (V) is updated by a slider–crank relationship from Heywood [49]

$$\dot{V} = \frac{\pi}{4} B^2 a \dot{\theta} \left(\sin\theta + \frac{a \sin\theta \cos\theta}{\sqrt{l^2 - a^2 \sin^2\theta}} \right) \qquad \text{(B.2)}$$

where B is the bore, a is the crank radius, and l is the connecting rod length. The energy equation is solved for the instantaneous cylinder temperature T. By using the first law of thermodynamics for a closed, reacting system, it is possible to write

$$\dot{U} = -P\dot{V} - \dot{Q} \qquad \text{(B.3)}$$

$$mC_v\dot{T} + \sum_i \dot{m}_i u_i + P\dot{V} + \dot{Q} = 0 \qquad \text{(B.4)}$$

$$\rightarrow \dot{T} = -\frac{1}{mC_v}\left(\sum_i \dot{m}_i u_i + P\dot{V} + \dot{Q}\right) \qquad \text{(B.5)}$$

where U is the total (extensive) internal energy, m is the total mixture mass, C_v is the specific heat at constant volume for the total mixture, m_i and u_i are the mass and internal energy of the i-th species, respectively, P is the instantaneous cylinder pressure, Q is the heat transfer amount. Here, the production (or destruction) rate of species mass m_i by chemical reactions is evaluated by using a function from the Cantera toolbox, which refers to GRI-Mech 3.0 mechanisms [48]. Finally, the instantaneous cylinder pressure P is evaluated by using the ideal gas law

$$P = \frac{mRT}{V} \qquad \text{(B.6)}$$

where R is the mass-based gas constant.

References

1. International Energy Agency. (2015). Energy and Climate Change. World Energy Outlook Special Report.
2. International Renewable Energy Agency. (2015). Rethinking Energy. IRENA.
3. Rogelj, J., Den Elzen, M., Höhne, N., Fransen, T., Fekete, H., Winkler, H., ... & Meinshausen, M. (2016). Paris Agreement climate proposals need a boost to keep warming well below 2 C. Nature, 534(7609), 631-639.
4. James, R. (1999). Fuel Cell Technology: An Alternative Energy System for the Future. U.S. Department of Energy. Federal Energy Technology Center, Morgantown, WV.
5. Ellis, M. W., & Gunes, M. B. (2002). Status of fuel cell systems for combined heat and power applications in buildings/Discussion. ASHRAE transactions, 108, 1032.
6. Tomczyk, P. (2006). MCFC versus other fuel cells-Characteristics, technologies and prospects. Journal of Power sources, 160(2), 858-862.
7. McPhail, S. J., Aarva, A., Devianto, H., Bove, R., & Moreno, A. (2011). SOFC and MCFC: Commonalities and opportunities for integrated research. International journal of hydrogen energy, 36(16), 10337-10345.

8. Wee, J. H. (2011). Molten carbonate fuel cell and gas turbine hybrid systems as distributed energy resources. Applied Energy, 88(12), 4252-4263.
9. Oh, K. S., & Kim, T. S. (2006). Performance analysis on various system layouts for the combination of an ambient pressure molten carbonate fuel cell and a gas turbine. Journal of power sources, 158(1), 455-463.
10. El-Emam, R. S., & Dincer, I. (2011). Energy and exergy analyses of a combined molten carbonate fuel cell-gas turbine system. International journal of hydrogen energy, 36(15), 8927-8935.
11. Lunghi, P., Bove, R., & Desideri, U. (2003). Analysis and optimization of hybrid MCFC gas turbines plants. Journal of Power Sources, 118(1), 108-117.
12. Kimijima, S., & Kasagi, N. (2005). Cycle analysis of micro gas turbine-molten carbonate fuel cell hybrid system. JSME International Journal Series B Fluids and Thermal Engineering, 48(1), 65-74.
13. Liu, A., & Weng, Y. (2010). Performance analysis of a pressurized molten carbonate fuel cell/micro-gas turbine hybrid system. Journal of Power Sources, 195(1), 204-213.

14. Leto, L., Dispenza, C., Moreno, A., & Calabrò, A. (2011). Simulation model of a molten carbonate fuel cell-microturbine hybrid system. Applied Thermal Engineering, 31(6), 1263-1271.
15. Milewski, J., Świercz, T., Badyda, K., Miller, A., Dmowski, A., & Biczel, P. (2010). The control strategy for a molten carbonate fuel cell hybrid system. international journal of hydrogen energy, 35(7), 2997-3000.
16. Zhang, X., Liu, H., Ni, M., & Chen, J. (2015). Performance evaluation and parametric optimum design of a syngas molten carbonate fuel cell and gas turbine hybrid system. Renewable Energy, 80, 407-414.
17. De Lorenzo, G., & Fragiacomo, P. (2012). A methodology for improving the performance of molten carbonate fuel cell/gas turbine hybrid systems. International Journal of Energy Research, 36(1), 96-110.
18. Huang, H., Li, J., He, Z., Zeng, T., Kobayashi, N., & Kubota, M. (2015). Performance analysis of a MCFC/MGT hybrid power system bi-fueled by city gas and biogas. Energies, 8(6), 5661-5677.
19. Angelino, G., & Di Paliano, P. C. (2000). Organic Rankine cycles (ORCs) for energy recovery from molten carbonate fuel cells. In Energy Conversion Engineering Conference and Exhibit, 2000.(IECEC) 35th Intersociety (Vol. 2, pp. 1400-1409). IEEE.

20. Vatani, A., Khazaeli, A., Roshandel, R., & Panjeshahi, M. H. (2013). Thermodynamic analysis of application of organic Rankine cycle for heat recovery from an integrated DIR-MCFC with pre-reformer. Energy Conversion and Management, 67, 197-207.
21. Mamaghani, A. H., Najafi, B., Shirazi, A., & Rinaldi, F. (2015). 4E analysis and multi-objective optimization of an integrated MCFC (molten carbonate fuel cell) and ORC (organic Rankine cycle) system. Energy, 82, 650-663.
22. Sanchez, D., Chacartegui, R., Torres, M., & Sanchez, T. (2009). Stirling based fuel cell hybrid systems: an alternative for molten carbonate fuel cells. Journal of power sources, 192(1), 84-93.
23. De Escalona, J. M., Sanchez, D., Chacartegui, R., & Sanchez, T. (2013). Performance analysis of hybrid systems incorporating high temperature fuel cells and closed cycle heat engines at part-load operation. International Journal of Hydrogen Energy, 38(1), 570-578.
24. Chen, L., Zhang, H., Gao, S., & Yan, H. (2014). Performance optimum analysis of an irreversible molten carbonate fuel cell-Stirling heat engine hybrid system. Energy, 64, 923-930.
25. http://www.fuelcellenergy.com/ [last accessed: January 2017]

26. Farooque, M., & Maru, H. C. (2006). Carbonate fuel cells: Milliwatts to megawatts. Journal of Power Sources, 160(2), 827-834.
27. Ghezel-Ayagh, H., Walzak, J., Junker, S. T., Patel, D., Michelson, F., & Adriani, A. (2008). DFC/T® power plant: from sub-megawatt demonstration to multi-megawatt design. ECS Transactions, 12(1), 713-717.
28. Ghezel-Ayagh, H. (2004). Direct FuelCell/Turbine Power Plant. FCE technical report.
29. Ghezel-Ayagh, H. (2008). Direct FuelCell/Turbine Power Plant. FCE technical report.
30. McPhail, S., Moreno, A., Bove, R. (2009). International Status of Molten Carbonate Fuel Cell (MCFC) Technology. ENEA.
31. Samuelsen, S. (2004). Fuel Cell/Gas Turbine Hybrid Systems. 2004 ASME International Gas Turbine Institute.
32. Brouwer, J. (2006). Hybrid gas turbine fuel cell systems.
33. Ando, Y., Oozawa, H., Mihara, M., Irie, H., Urashita, Y., & Ikegami T. (2015). Demonstration of SOFC-Micro Gas Turbine (MGT) Hybrid Systems for Commercialization. Mitsubishi Heavy Industries Technical Review, 52(4).

34. Kitagawa, Y., Tomida, K., Nishiura, M., Hiwatashi, K., Kishizawa, H., Oozawa, H., Kobayashi, Y., Takeuchi, Y., & Mihara, M. (2015). Development of High Efficiency SOFC Power Generation at MHPS. Fuel Cell Seminar and Energy Exposition.
35. McPhail, S. J., Leto, L., & Boigues-Muñoz, C. (2013). The Yellow Pages of SOFC Technology-International Status of SOFC Deployment 2012-2013. ENEA, Rome.
36. Kim, S., Abid, A. R., Jang, J. J., Song, H. H., Song, S. J., Ahn, K. Y., ... & Kang, S. G. (2013). Development of a hybrid system of molten carbonate fuel cell and homogeneous charge compression ignition engine for distributed power generation. Journal of Fuel Cell Science and Technology, 10(6), 061002.
37. Kim, S., Jung, J. Y., Song, H. H., Song, S. J., Ahn, K. Y., Lee, S. M., ... & Kang, S. (2014). Optimization of molten carbonate fuel cell (MCFC) and homogeneous charge compression ignition (HCCI) engine hybrid system for distributed power generation. International Journal of Hydrogen Energy, 39(4), 1826-1840.
38. Kim, S. (2013). Optimization of Molten Carbonate Fuel Cell (MCFC) and Homogeneous Charge Compression Ignition (HCCI) Engine Hybrid System for Distributed Power Generation.

39. Abid, A. (2012). (A) Novel Fuel Cell-IC Engine Hybrid System for Distributed Power Generation.

40. Ahn, K. Y., Lee, Y. D., Kang, S. G., Lee, S. M., Kim, H. S., Cho, J. H., ... & Song, H. H. (2012). Korea Patent No.10-1115333.

41. Ahn, K. Y., Lee, Y. D., Kang, S. G., Lee, S. M., Kim, H. S., Cho, J. H., ... & Song, H. H. (2015). U.S. Patent No. 9,038,579. Washington, DC: U.S. Patent and Trademark Office.

42. Caton, P. A., Song, H. H., Kaahaaina, N. B., & Edwards, C. F. (2005). Residual-effected homogeneous charge compression ignition with delayed intake-valve closing at elevated compression ratio. International journal of engine research, 6(4), 399-419.

43. Baranak, M., & Atakül, H. (2007). A basic model for analysis of molten carbonate fuel cell behavior. Journal of Power Sources, 172(2), 831-839.

44. Verda, V., & Nicolin, F. (2010). Thermodynamic and economic optimization of a MCFC-based hybrid system for the combined production of electricity and hydrogen. International journal of hydrogen energy, 35(2), 794-806.

45. Daly, J., Jahnke, F., & Patel, P. (2011). Combined Heat, Hydrogen and Power from DFC® Fuel Cell. FCE Information Towards Design: Hydrogen Education Foundation's 2011-2012 CHHP Contest.

46. Song, H. H., & Edwards, C. F. (2009). Understanding chemical effects in low-load-limit extension of homogeneous charge compression ignition engines via recompression reaction. International Journal of Engine Research, 10(4), 231-250.
47. Song, H. H., Padmanabhan, A., Kaahaaina, N. B., & Edwards, C. F. (2009). Experimental study of recompression reaction for low-load operation in direct-injection homogeneous charge compression ignition engines with n-heptane and i-octane fuels. International Journal of Engine Research, 10(4), 215-229.
48. GRI-Mech™ [Internet]. Chicago: Gas Research Institute; c2000. Available from: http://www.me.berkeley.edu/gri-mech/. [last accessed: January 2017].
49. Heywood, J. (1988). Internal combustion engine fundamentals. New York: McGraw-Hill.
50. Chen, S. K., & Flynn, P. F. (1965). Development of a single cylinder compression ignition research engine (No. 650733). SAE Technical Paper.
51. Ukidave, S. S. (2011). Development of a technique for achieving an optimum BSFC for LAF engine.
52. Bejan, A., & Tsatsaronis, G. (1996). Thermal design and optimization. John Wiley & Sons.

53. Xicoy Almirall, B. (2008). Introduction to Wet Sulfuric Acid Plants Optimization Through Exergoeconomics.

54. Lee, Y. D. (2015). Thermodynamic, economic and environmental evaluation of solid-oxide fuel-cell hybrid power-generation systems (Doctoral dissertation, Technische Universit?t Berlin).

55. Lee, Y. D., Ahn, K. Y., Morosuk, T., & Tsatsaronis, G. (2014). Exergetic and exergoeconomic evaluation of a solid-oxide fuel-cell-based combined heat and power generation system. Energy Conversion and Management, 85, 154-164.

56. Park, S. H. (2013). Thermo-economic evaluation of solid oxide fuel cell (SOFC)-homogeneous charge compression ignition (HCCI) engine hybrid system.

57. Park, S. H., Lee, Y. D., & Ahn, K. Y. (2014). Performance analysis of an SOFC/HCCI engine hybrid system: system simulation and thermo-economic comparison. International Journal of Hydrogen Energy, 39(4), 1799-1810.

58. Steward, D., Penev, M., Saur, G., Becker, W., & Zuboy, J. (2013). Fuel Cell Power Model Version 2: Startup Guide, System Designs, and Case Studies. Modeling Electricity, Heat, and Hydrogen Generation from Fuel

Cell-Based Distributed Energy Systems (No. NREL/TP-5600-57457). National Renewable Energy Laboratory (NREL), Golden, CO..

59. Körner, A., Tam, C., Bennett, S., & Gagné, J. F. (2015). Technology roadmap-hydrogen and fuel cells. International Energy Agency (IEA).
60. Calise, F., d'Accadia, M. D., Vanoli, L., & Von Spakovsky, M. R. (2006). Single-level optimization of a hybrid SOFC-GT power plant. Journal of Power Sources, 159(2), 1169-1185.
61. Oyarzabal, B. (2001). Application of a decomposition strategy to the optimal synthesis/design of a fuel cell sub-system.
62. Chan, S. H., Low, C. F., & Ding, O. L. (2002). Energy and exergy analysis of simple solid-oxide fuel-cell power systems. Journal of Power Sources, 103(2), 188-200.
63. Chiesa, P., Consonni, S., Kreutz, T. G., & Williams, R. H. (2003, May). Co-production of hydrogen, electricity and CO2 from coal using commercially-ready technology. In Second Annual Conference on Carbon Sequestration, Washington, DC, May (pp. 5-8).
64. Frangopoulos, C. A. (1991). Optimization of synthesis-design-operation of a cogeneration system by the intelligent functional approach. International Journal of Energy-Environment-Economics;(United States), 1(4).

65. Nikhil, D., Rajesh, A., Vijay, M., Sandeep, K., Satyapal, M., & Pardeep, K. (2012). Economic and performance analysis of thermal system. Research Journal of Recent Sciences, 1(4), 57-59.
66. International Energy Agency. (2015). Key world energy statistics. International Energy Agency.
67. Yamasaki, Y., Tomatsu, G., Nagata, Y., & Kaneko, S. (2007). Development of a small size gas engine system with biomass gas (combustion characteristics of the wood chip pyrolysis gas) (No. 2007-01-3612). SAE Technical Paper.
68. Saha, U. K. (2006). Internal Combustion Engines - Engine Efficiencies. Indian Institute of Technology Guwahati.
69. Ministry of Commerce, Industry and Energy. (1999). Development of a 100kW Externally Reforming Molten Carbonate Fuel Cell System (Phase I: 25kW Class). Republic of Korea. pp. 397-406.
70. Jung, J. (2013). A Start-Up Strategy of Molten Carbonate Fuel Cell and Internal Combustion Engine Hybrid System for Distributed Power Generation.
71. Kordesch, K., & Simader, G. R. (1996). Fuel cells and their applications.
72. Morita, H., Komoda, M., Mugikura, Y., Izaki, Y., Watanabe, T., Masuda, Y., & Matsuyama, T. (2002). Performance analysis of molten carbonate

fuel cell using a Li/Na electrolyte. Journal of Power Sources, 112(2), 509-518.

국 문 초 록

각종 환경문제와 에너지 자원 고갈에 대한 우려가 높아지고 있는 요즘 신재생에너지에 대한 수요는 나날이 증가하고 있다. 이러한 신재생에너지 중 특히 연료전지는 높은 효율과 오염물질을 적게 배출한다는 점에서 각광 받고 있다. 이러한 연료전지 시스템에는 효율을 높이기 위해 다양한 하이브리드 시스템이 연구되고 있는데, 대표적으로 가스터빈과 ORC를 결합한 하이브리드 시스템이 있다. 그러나 가스터빈의 경우 가격이 높고 유지보수가 어렵다는 단점이 있으며 ORC의 경우 효율 상승 측면에서 가스터빈보다 다소 낮다는 단점이 있다. 그러나 엔진의 경우 가스터빈보다 cost적인 측면에서 유리하며 소규모 분산발전 시스템에서는 효율 또한 우수하다는 장점이 있다. 그리하여 지난 연구에서 고온형 연료전지인 용융탄산염 연료전지(MCFC)와 예혼합압축착화(HCCI) 엔진을 결합한 분산발전용 하이브리드 시스템을 개발했었다.

본 연구에서는 이러한 시스템에 대해 주어진 연료전지 사이즈에 알맞은 엔진 설계 사양을 선정하였다. 이를 위해 열역학적 모델링을 통해 시뮬레이션 분석을 수행하였다. 선정한 엔진 파라미터를 바탕으로 설계점에서 시뮬레이션 분석을 수행한 결과 기존 연료전지 시스템에 비해 효율이 증가하였으며 약 57% 이상의 효율을 보여주었다. 또한 MCFC-HCCI 엔진 하이브리드 시스템에 대해 설계점 이외의 넓은 구동 범위에서 작동 가능성을 알아보기 위해 다양한 연료량 범위 내에서 시스템이 구동 가능 한지 알아보았다. 75%-100%

의 연료량 범위 내에서 부분 부하 운전에 대한 가능성을 알아보았으며 높은 효율이 유지되는 것을 확인할 수 있었다.

이외에도 실제 시스템의 상용화를 위해서는 비용적인 측면도 매우 중요하다. 따라서 연료전지 단독 시스템 및 하이브리드 시스템에 대한 경제성 분석을 수행하기 위해 TRR method를 바탕으로 levelized cost of electricity (LCOE) 분석을 수행하였다. 그 결과 연료전지 단독 시스템 대비 새롭게 개발한 하이브리드 시스템의 LCOE 값은 4.7% 가량 낮게 나오는 것을 알 수 있어, 하이브리드 시스템이 경제성 측면에서도 우수하다는 것을 확인할 수 있었다.

이렇게 개발한 하이브리드 시스템의 실제 구동 가능성을 알기 위해선 최종적으로 실험적 입증을 하는 것도 중요하다. 기존의 연료전지 시스템에 새로운 컴포넌트인 엔진이 추가되어 다양한 문제가 발생할 수도 있다. 따라서 그 동안의 시뮬레이션 결과를 바탕으로 엔진 실험 시스템을 구축한 후 시뮬레이션 결과를 검증하여 하이브리드 시스템의 구동가능성에 대해 알아보고자 하였다. 엔진 및 모터, 인버터 등을 바탕으로 엔진 실험 시스템을 구축하고 xPC 및 Simulink 등을 이용해 장비 구동 모델을 개발하였다. 이를 통해 실험해 본 결과, 비록 연료전지의 anode off-gas가 엔진에게는 매우 dilution되어있는 연료임에도 불구하고, HCCI 엔진 내에서 충분히 연소시킬 수 있어 시스템의 구동 가능성에 대해 확인할 수 있었다. 본 연구를 통해 얻은 결과들이 새로운 분산발전용 MCFC-HCCI 엔진 하이브리드 발전 시스템의 도입을 앞당기는데 기여할 수 있기를 기대한다.

주요어: 용융탄산염 연료전지, 예혼합압축착화 엔진, 하이브리드 시스템 설계, 효율, 경제성 분석, 엔진 실험

학 번: 2013-30945